



Search in diphoton and dielectron final states for displaced production of Higgs or Z bosons with the ATLAS detector in $\sqrt{s} = 13$ TeV pp collisions

The ATLAS Collaboration

A search is presented for displaced production of Higgs bosons or Z bosons, originating from the decay of a neutral long-lived particle (LLP) and reconstructed in the decay modes $H \rightarrow \gamma\gamma$ and $Z \rightarrow ee$. The analysis uses the full Run 2 data set of proton–proton collisions delivered by the LHC at an energy of $\sqrt{s} = 13$ TeV between 2015 and 2018 and recorded by the ATLAS detector, corresponding to an integrated luminosity of 139 fb^{-1} . Exploiting the capabilities of the ATLAS liquid argon calorimeter to precisely measure the arrival times and trajectories of electromagnetic objects, the analysis searches for the signature of pairs of photons or electrons which arise from a common displaced vertex and which arrive after some delay at the calorimeter. The results are interpreted in a gauge-mediated supersymmetry breaking model with pair-produced higgsinos that decay to LLPs, and each LLP subsequently decays into either a Higgs boson or a Z boson. The final state includes at least two particles that escape direct detection, giving rise to missing transverse momentum. No significant excess is observed above the background expectation. The results are used to set upper limits on the cross section for higgsino pair production, up to a $\tilde{\chi}_1^0$ mass of 369 (704) GeV for decays with 100% branching ratio of $\tilde{\chi}_1^0$ to Higgs (Z) bosons for a $\tilde{\chi}_1^0$ lifetime of 2 ns. A model-independent limit is also set on the production of pairs of photons or electrons with a significant delay in arrival at the calorimeter.

1 Introduction

The Standard Model (SM) of particle physics is a renormalizable quantum field theory that provides a framework for understanding fundamental particles and their interactions. Predictions of the SM have been substantiated by experimental results over decades, one highlight being the 2012 discovery of the Higgs boson by the ATLAS and CMS experiments [1, 2] at the Large Hadron Collider (LHC) at CERN. However, the SM does not describe gravity, does not contain a dark matter candidate, or provide a solution to the hierarchy problem, pointing to the need for new fundamental physics.

Supersymmetry (SUSY) [3–9] is a well-motivated theoretical extension to the SM that offers possible answers to many of these questions. The theory predicts the existence of SUSY partners (sparticles) for particles in the SM. Each sparticle has identical quantum numbers to its SM partner, differing only by half a unit of spin. A new symmetry called R-parity acts on supersymmetric fields, and assigns a quantum number of +1 to all SM particles and -1 to sparticles. In R-parity-conserving SUSY models [10–14], the lightest SUSY particle (LSP) is stable. At colliders, sparticles would be produced in pairs, which would then decay in cascades involving other sparticles and SM particles until two final state LSPs are produced.

The weak eigenstates of the SUSY partners of the Higgs and gauge bosons mix to form mass eigenstates called electroweakinos that can be electrically neutral or charged fermions. These are respectively referred to as neutralinos ($\tilde{\chi}_1^0, \tilde{\chi}_2^0, \tilde{\chi}_3^0, \tilde{\chi}_4^0$) and charginos ($\tilde{\chi}_1^\pm, \tilde{\chi}_2^\pm$), with the subscripts indicating increasing mass. These mass eigenstates are model-dependent combinations of the individual electroweakino degrees of freedom. Of the many new particles predicted in SUSY, existing exclusions from the LHC are generally weaker for these electroweak sparticles as compared to sparticles produced via strong interactions, due in part to the low electroweak process cross sections in pp collisions [15–20].

In gauge-mediated SUSY breaking (GMSB) models [21–26], the superpartner of the graviton called the gravitino (\tilde{G}) is the LSP for typical model parameter values. The weak coupling of the next-to-lightest SUSY particle (NLSP) to the gravitino LSP could generate a lifetime of the NLSP that is non-negligible on the detector length scale, leading to displaced NLSP decay vertices [25]. In GMSB models, the lightest neutralino $\tilde{\chi}_1^0$ is often the NLSP. If the combination of weak eigenstates in the $\tilde{\chi}_1^0$ mass eigenstate is mostly composed of the supersymmetric Higgs eigenstate (higgsino), then the most likely decay modes will be $\tilde{\chi}_1^0 \rightarrow H/Z + \tilde{G}$.

This search considers GMSB models with the $\tilde{\chi}_1^\pm, \tilde{\chi}_2^0$ and $\tilde{\chi}_1^0$ forming an almost degenerate triplet of SUSY partners of the SM electroweak bosons, and with the heavier charginos and neutralinos sufficiently massive to be essentially decoupled. As shown in the example Feynman diagrams in Figure 1, the search focuses on direct pair production of members of the nearly degenerate triplet. Each $\tilde{\chi}_2^0$ and $\tilde{\chi}_1^\pm$ that is produced decays to the NLSP plus two light SM fermions (denoted by x), followed by the subsequent NLSP decay via $\tilde{\chi}_1^0 \rightarrow H/Z + \tilde{G}$. The small mass splitting between electroweakinos results in final state SM fermions with very low p_T , making them challenging to reconstruct and thus not useful for event selection. The Feynman diagrams shown include both $H \rightarrow \gamma\gamma$ and $Z \rightarrow ee$ final states.

The analysis exploits the precision spatial and timing capabilities of the ATLAS liquid argon (LAr) electromagnetic (EM) calorimeter to achieve sensitivity to the displaced production of the SM Higgs or Z boson by reconstructing the resultant $H \rightarrow \gamma\gamma$ or $Z \rightarrow ee$ decays. The main characteristic of such events is the presence of two electromagnetic (EM) objects, either photons or electrons, that originate from the decay of the same LLP parent. The EM objects are reconstructed using only EM calorimeter information, so no attempt is made to separate between the diphoton and dielectron final states. These EM objects are

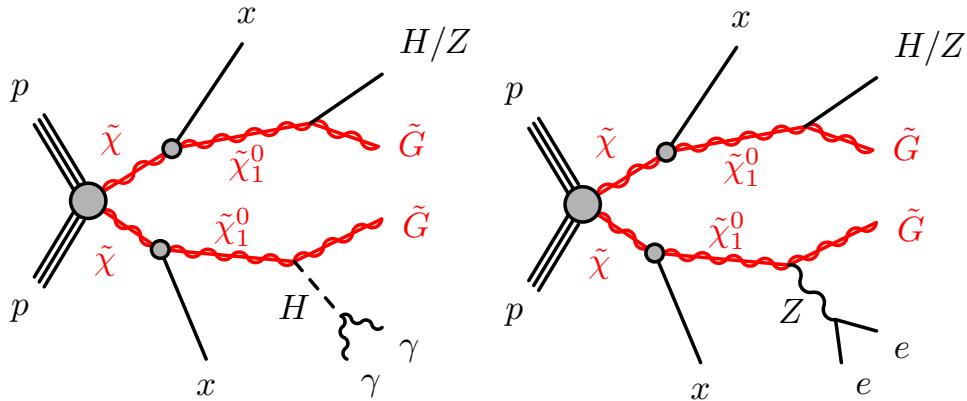


Figure 1: Feynman diagrams of the signal process considered, targeting pair production of electroweak sparticles decaying to two light SM fermions x (including all leptons and quarks except top and bottom) and a $\tilde{\chi}_1^0$ particle, which then decays to either a Z or Higgs boson along with a \tilde{G} . Each of the $\tilde{\chi}_1^0$ particles is required to decay to a Higgs (Z) boson as shown on the left (right) which decays to a diphoton (dielectron) final state. The other $\tilde{\chi}_1^0$ is not used in the analysis, and the Higgs/Z boson decays with its Standard Model branching ratio.

detected with some delay compared to prompt objects in the final state. Given the size of the ATLAS detector and the LAr timing resolution, the requirement of LAr calorimeter measurements of the delayed EM objects restricts the sensitivity of the analysis to NLSP lifetimes of $\mathcal{O}(\text{ns})$. In addition, due to the opening angle between the H/Z boson and the gravitino LSP produced in the NLSP decay, the EM objects would have flight paths that are inconsistent with originating from the primary vertex (PV), and hence are called non-pointing. Hereafter, the daughter particles will be referred to as photons, and the signature as a *displaced diphoton vertex* (DDV), covering both electron and photon final states. Precise LAr timing and spatial information is used to enhance sensitivity to this signature, and this result represents the first application of a new method to localize a displaced decay vertex position using only LAr measurements.

This analysis utilizes the full Run 2 ATLAS dataset of 13 TeV pp collisions and is the first LHC search optimized for the DDV signature. Previous ATLAS analyses searched for non-pointing and delayed photons produced in long-lived NLSP decays in the datasets of pp collisions collected at center-of-mass energies of 13 TeV [27] during Run 2 of the LHC, and at both 7 [28] and 8 TeV [29] during Run 1. No search found an excess above the SM background expectation, and results were interpreted in the context of a particular set of GMSB SUSY models. A recent Run 2 CMS result searching for such models also found data agreeing with the SM prediction [30]. These previous searches provide generic sensitivity to events containing one or more non-prompt photons that do not necessarily originate from a common vertex, making this result the first to exploit the correlation between e/γ measurements expected from the GMSB delayed higgsino signal.

The analysis considers a simplified model for signals, where the mass and lifetime of the NLSP are treated as independent parameters. A branching ratio (BR) of unity is considered for the combination of the two NLSP decay modes considered, namely $\tilde{\chi}_1^0 \rightarrow H/Z + \tilde{G}$, though the relative probability of the two modes is considered a free parameter. The H and Z are assumed to have their Standard Model branching ratios. Both $H \rightarrow \gamma\gamma$ and $Z \rightarrow ee$ signals are reconstructed as final state photons, as electrons and photons have the same EM shower shape and thus the same EM calorimeter reconstruction. Furthermore, both prompt and displaced track reconstruction efficiencies are low for highly displaced electrons, and the application of calorimeter-based selection can recover sensitivity to these signatures. The photons should have a delay

compared to prompt objects, and as $t = 0$ is defined as the expected value for a prompt photon from the PV of the hard collision, the photons are required to have $t > 0$. Measurements of the trajectories of the two photons, as determined by their EM shower shapes, are used to determine a common origin. The separation distance between this secondary vertex candidate and the PV is calculated in the (R, z) plane, and used to categorize the events according to the degree of displacement. This procedure is shown diagrammatically in Figure 2 and described in detail in Section 4.2.

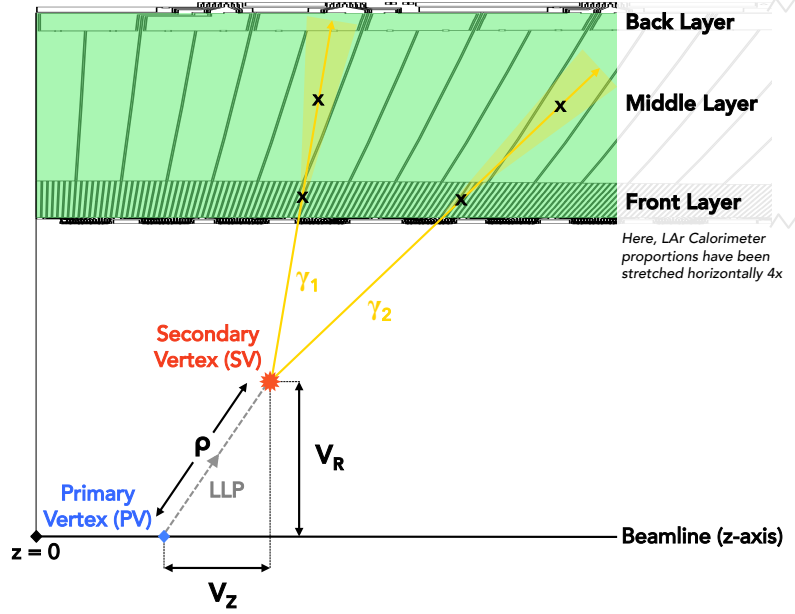


Figure 2: Illustration of the two-dimensional calo-vertexing procedure to calculate the V_R and V_z discriminating variables used in the analysis, with R on the y -axis and z on the x -axis. The three layers of the LAr calorimeter are highlighted, along with the energy deposits left by the passage of the two daughter photons γ_1 and γ_2 of the LLP. The location of the secondary vertex (SV) is determined by the pointing measurements of the two photons. V_R is defined as the distance in R from the SV to the beamline, and V_z as the distance in z from the SV to the PV.

The signal region (SR) is defined by the presence of at least two photons, as well as a high value of missing transverse momentum (E_T^{miss}) resulting from the escaping gravitinos. In addition, a few optimized kinematic selections, designed to enhance the signal-to-background ratio, are applied. The events in the SR were kept blinded until the analysis design was finalized. The background estimation procedure assesses the contribution of SM processes that populate the SR selection and is fully data-driven due to non-Gaussian tails in the timing and vertexing LAr measurements. The predicted background is determined using a control region (CR) with low values of E_T^{miss} , which is validated using two different orthogonal validation regions (VR). The first VR requires intermediate values of E_T^{miss} and is denoted $\text{VR}(E_T^{\text{miss}})$, while the second, denoted $\text{VR}(t)$, imposes the same E_T^{miss} requirement as the SR but reverses the photon timing requirements by requiring $t_\gamma < 0$ for each photon. By construction the various analysis regions are orthogonal, and any signal contamination in the CR, $\text{VR}(E_T^{\text{miss}})$, or $\text{VR}(t)$ was found to be negligible. The development of the background modeling using the CR, and its validation using the VRs, were finalized before analyzing the data in the SR. A simultaneous likelihood fit of the background model to SR data is performed using the average photon timing distribution in categories of the photon secondary vertex displacement.

2 ATLAS detector

The ATLAS detector [31] at the LHC covers nearly the entire solid angle around the collision point.¹ It consists of an inner tracking detector surrounded by a thin superconducting solenoid, electromagnetic and hadron calorimeters, and a muon spectrometer incorporating three large superconducting air-core toroidal magnets.

The inner detector system is immersed in a 2 T axial magnetic field and provides charged-particle tracking in the range $|\eta| < 2.5$. The high-granularity silicon pixel detector covers the vertex region and typically provides four measurements per track, the first hit normally being in the insertable B-layer (IBL) installed before Run 2 [32, 33]. It is followed by the silicon microstrip tracker (SCT), which provides typically eight measurements per track. These silicon detectors are complemented by the transition radiation tracker (TRT), which enables radially extended track reconstruction up to $|\eta| = 2.0$. The TRT also provides electron identification information based on the fraction of hits (typically 30 in total) above a higher energy-deposit threshold corresponding to transition radiation.

The calorimeter system covers the pseudorapidity range $|\eta| < 4.9$. Within the region $|\eta| < 3.2$, electromagnetic (EM) calorimetry is provided by barrel (EMB) and endcap (EMEC) high-granularity lead/liquid-argon (LAr) calorimeters, with an additional thin LAr presampler covering $|\eta| < 1.8$ to correct for energy loss in material upstream of the calorimeters. For $|\eta| < 2.5$, the LAr EM calorimeter is segmented into three layers in depth that can be used to measure the longitudinal profile of the shower. The first layer uses highly granular “strips” segmented in the η direction, with a typical transverse segmentation of $\Delta\eta \times \Delta\phi = 0.003 \times 0.1$ in the barrel, allowing for efficient discrimination between single photon showers and two overlapping showers from the decay of a π^0 meson. The second layer has a typical transverse segmentation of $\Delta\eta \times \Delta\phi = 0.025 \times 0.025$, and collects most of the energy deposited in the calorimeter by EM showers initiated by electrons or photons. Very high energy EM showers can leave significant energy deposits in the third layer, which can also be used to correct for energy leakage beyond the EM calorimeter. These features of the LAr calorimeter allow it to make precise measurements of photon direction and timing, which are used to build key discriminants in the analysis as described in Section 4. Hadron calorimetry is provided by the steel/scintillator-tile calorimeter, segmented into three barrel structures within $|\eta| < 1.7$, and two copper/LAr hadron endcap calorimeters. The solid angle coverage is completed with forward copper/LAr and tungsten/LAr calorimeter modules, optimised for electromagnetic and hadronic energy measurements respectively.

The muon spectrometer (MS) comprises separate trigger and high-precision tracking chambers measuring the deflection of muons in a magnetic field generated by the superconducting air-core toroidal magnets. The field integral of the toroids ranges between 2.0 and 6.0 T m across most of the detector. Three layers of precision chambers, each consisting of layers of monitored drift tubes, covers the region $|\eta| < 2.7$, complemented by cathode-strip chambers in the forward region, where the background is highest. The muon trigger system covers the range $|\eta| < 2.4$ with resistive-plate chambers in the barrel, and thin-gap chambers in the endcap regions.

¹ ATLAS uses a right-handed coordinate system with its origin at the nominal interaction point (IP) in the centre of the detector and the z -axis along the beam pipe. The x -axis points from the IP to the centre of the LHC ring, and the y -axis points upwards. Cylindrical coordinates (r, ϕ) are used in the transverse plane, ϕ being the azimuthal angle around the z -axis. The pseudorapidity is defined in terms of the polar angle θ as $\eta = -\ln \tan(\theta/2)$. Angular distance is measured in units of $\Delta R \equiv \sqrt{(\Delta\eta)^2 + (\Delta\phi)^2}$.

The ATLAS trigger and data acquisition system [34] consists of a hardware-based first-level (L1) trigger followed by a software-based high-level trigger (HLT) that reduces the rate of events selected for offline storage to 1 kHz. An extensive software suite [35] is used in the reconstruction and analysis of real and simulated data, monitoring the detector during operation, and the trigger and data acquisition systems of the experiment.

3 Data and Monte Carlo samples

This search was performed with the full Run 2 LHC dataset, collected by the ATLAS detector between 2015 and 2018. After the application of data quality requirements [36] that ensure good working condition of all detector components, the dataset corresponds to an integrated luminosity of $139.0 \pm 2.4 \text{ fb}^{-1}$ [37, 38]. The recording of events used for this search was triggered by the presence of two high- p_T photons, where the full-rate trigger with the lowest available p_T threshold is used across data-taking years [34, 39]. For 2015 and 2016, the trigger used requires the two photons to pass LOOSE identification (ID) selection, defined in Section 5.1. A trigger based on MEDIUM ID photons became available in 2017 and 2018, and is thus used here for the data collected in those years due to its lower p_T threshold. Kinematic selections were imposed on the photons to ensure that the selected events lie in the fully efficient regime of the trigger, namely for the leading (subleading) photon p_T to be greater than 40 (30) GeV.

Monte Carlo event generators were used to simulate the signal targeted by this search. Signal matrix elements were generated at leading order (LO) using MADGRAPH 2.7.3 [40] with showering and hadronization performed by PYTHIA 8 [41]. The A14 tune [42] and the NNPDF2.3LO PDF set [43] were used in the event generation. Each event has two long-lived NLSPs and two final state H/Z bosons. Events were filtered such that only one H/Z is required to decay to the desired di- γ/e resonance, and the other takes its SM branching ratios. Therefore, four separate processes are simulated: $H \rightarrow \gamma\gamma + H \rightarrow \text{SM}$, $Z \rightarrow ee + H \rightarrow \text{SM}$, $H \rightarrow \gamma\gamma + Z \rightarrow \text{SM}$, and $Z \rightarrow ee + Z \rightarrow \text{SM}$. The generated signals are parameterized by the mass of the NLSP, which ranges from 100 GeV to 725 GeV, and its lifetime. The mass of the gravitino LSP is set at 1 MeV, and the lightest chargino and next-to-lightest neutralino have the same mass which is set to be 1 GeV heavier than the lightest neutralino.

For each NLSP mass value, at least two different NLSP lifetimes, typically 2 ns and 10 ns, were simulated. Since the distribution of particle decays follows an exponential decay curve, it is possible to reweight the shape of that curve and thus generalize to other lifetime values. Each event was assigned a weight according to a source signal lifetime, target signal lifetime, and the decay of the event in question. Weights for target lifetimes between 0.25 and 1000 ns were calculated using the generated signal point with the closest lifetime as the source distribution. The signal model MC events were passed through a GEANT4 [44] simulation of the ATLAS detector [45] and reconstructed with the same software [35] as used for the data. The generation of the simulated event samples includes the effect of multiple pp interactions in the same or neighboring bunch crossings (pileup). The effect is assessed with the inclusion of overlaid minimum-bias events, as well as the effect on the detector response due to interactions from bunch crossings before or after the one containing the hard interaction. Events in the simulation were weighted in order to reproduce the amount of pileup observed in the Run 2 data-taking period.

As the background estimation is fully data-driven, no simulation is required of the background processes. Prompt SM $Z \rightarrow ee$ Monte Carlo was used to study the modeling of the specialized e/γ variables described in Section 4. These samples were generated using POWHEG_V1 [46] interfaced to PYTHIA 8 with the AZNLOCTEQ6L1 PDF/tune [47, 48].

4 Photon variables

The capability of the ATLAS LAr calorimeter to provide precision spatial and timing information for EM objects is essential for the reconstruction of and sensitivity to DDV events. In addition to standard four-vector information, two key variables are used to characterize photons: the timing of the photon signal, and the pointing of its trajectory back to the beamline. These measurements are almost completely uncorrelated for prompt backgrounds, but the signal is expected to populate higher values of both quantities than the SM expectation, making them excellent variables to discriminate between signal and prompt backgrounds. Since the targeted final state has two photons that share a common secondary vertex, the two pointing measurements are algorithmically combined into two novel vertexing variables, which describe the position of the diphoton vertex in the two-dimensional (R, z) plane. Details of the timing and vertexing calculations and their use in the analysis are provided below. The photons and electrons used in this section are selected with the criteria enumerated in Section 5.1.

4.1 Timing

Photons from long-lived NLSP decays reach the LAr calorimeter with a slight delay compared to prompt photons produced directly in the hard scattering. This delay results mostly from the flight time of the heavy NLSP, which would have a relativistic speed ($\beta = v/c$) that is less than 1. In addition, the opening angle in the NLSP decay, which causes the photon to be non-pointing, results in the geometrical path to the calorimeter being longer than that for a prompt photon from the PV.

The LAr calorimeter has an accordion geometry and excellent timing resolution, with a readout which incorporates fast shaping, and a clock jitter on the readout board that is less than 20 ps. The energy deposited by an EM object in the LAr calorimeter is measured using samples read out from the calorimeter channel at 25 ns intervals. The arrival time is determined using the energy deposit from the second-layer calorimeter cell with the maximum energy deposit among cells in the associated EM cluster (E_{cell}). For the EM shower of an electron or photon with an energy in the range of interest, this cell typically contains about 20%–50% of the total energy deposited in the EM shower. The energy and timing for each cell are reconstructed by applying the optimal filtering coefficient (OFC) algorithm [49] to four samples of the signal shape.

The time resolution $\sigma(t)$ improves as the E_{cell} increases, reaching a lower plateau at $O(10)$ GeV above which the resolution is flat at approximately 200 ps. More specifically, it follows the form $\sigma(t) = p_0/E_{\text{cell}} \oplus p_1$, where E_{cell} is the cell energy, \oplus denotes addition in quadrature, and parameters p_0 and p_1 are the coefficients of the so-called noise term and constant term, respectively, determined by a fit to data. The time measurements are observed to include a correlated contribution of ≈ 190 ps, which agrees well with the expected spread of times from a single vertex due to their spatial distribution along the beamline.

An offline calibration procedure is necessary to obtain the best possible resolution on each timing measurement. Offline corrections are determined for each interval of validity of the LAr online calibrations, of which there are 13 in the Run 2 dataset. Timing calibration corrections are determined with a dedicated procedure that uses a large sample of $W \rightarrow e\nu$ data. This procedure defines a time of zero as the expected measurement from a prompt photon originating at the PV, and includes corrections for offsets between channels, energy dependence, electronic crosstalk, and the position of the PV. The calibration is validated over an independent sample of $Z \rightarrow ee$ events, which also provide a measurement of the expected resolution that is obtained by performing Gaussian fits to the time distributions in bins of cell energy. Application of

the calibration constants offline achieves a final resolution of $O(100)$ ps in response to high-energy e/γ objects [27].

A source of early and delayed photons in data emerges through satellite bunches of protons that, due to the radio-frequency structure of the LHC accelerator and injection complex, are present in the LHC beams but separated from the main bunches by multiples of ± 5 ns. These contribute as a background process to the signal region of interest, while also allowing for an assessment of the OFC reconstruction method in data that more closely matches the expected timing distribution of the signal. The typical population of a satellite bunch is about a factor of one thousand lower than that of the nearby nominal bunch, so collisions between two satellite bunches are suppressed by roughly a factor of a million. Despite their low rate, such satellite collisions are nonetheless observable in the ATLAS data. Figure 3 shows the timing distribution of the electrons with the highest (e_1) and second highest (e_2) p_T in data events that are subject to a selection, defined in Section 5.2, that isolates the prompt $Z \rightarrow ee$ process. In addition to the bulk of events clustered around times of zero, satellite collisions are seen with both electron times around ± 5 ns and also at +10 ns. Known features of the LHC bunch structure cause a slight asymmetry between the positive and negative populations.

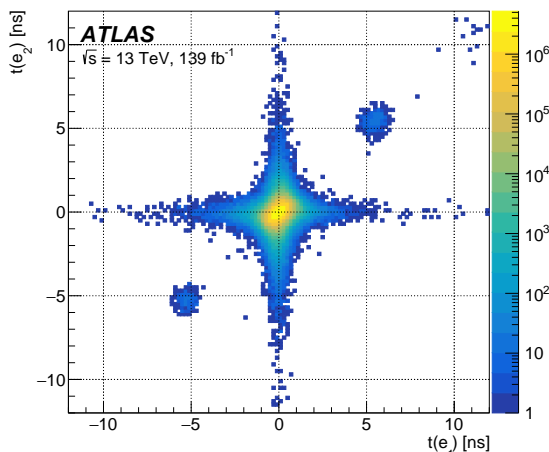


Figure 3: Distribution of leading versus subleading electron LAr timing values for a $Z \rightarrow ee$ analysis selection where at least two electrons are required that have $68 \text{ GeV} < m_{ee} < 108 \text{ GeV}$ and $|\Delta\eta(e_1, e_2)| > 0.1$. Populations of electrons from satellite collisions are visible at ± 5 ns and +10 ns.

The shape of the signal timing distribution is constructed using the timing variable of the simulated signal samples. The photon time resolution is not modeled precisely in the MC simulation, which underestimates the time resolution observed in data. Additional resolution uncertainties are assigned to cover the observed discrepancy between radiative $Z \rightarrow \ell\ell\gamma$ events in data and those from MC simulation. In addition to a contribution applied independently to each photon, the additional smearing includes a correlated event-level contribution to account for the impact of the spread of the actual time of the pp collision, which results from the longitudinal profiles of the proton bunches along the LHC beamline. The combined smearing contributions are tuned to match the time performance observed in data using electrons since, due to their similar EM shower developments, electrons have the same timing performance as photons. The correlated and uncorrelated contributions to the time measurement are de-convolved by studying the times of electron-positron pairs in events from the $Z \rightarrow ee$ selection.

In order to exploit the correlation of the timing between two photons produced in the same parent decay, the final analysis variable is the average of the times of the two leading photons (γ_1 and γ_2), defined as $t_{\text{avg}} = (t_{\gamma_1} + t_{\gamma_2})/2$. The distribution of t_{avg} that is expected in the signal region as defined in Section 5, for data and several representative simulated signals, is shown in Figure 4. The H decay channels have longer timing tails due to the $m_{\gamma\gamma}$ window discussed in Section 5.2. Because the calculation of $m_{\gamma\gamma}$ is dependent on the opening angle between the photons and thus highly displaced signals have underestimated values of the reconstructed $m_{\gamma\gamma}$, the Z signals with a lower truth $m_{\gamma\gamma}$ are more likely to be cut away by the lower bound.

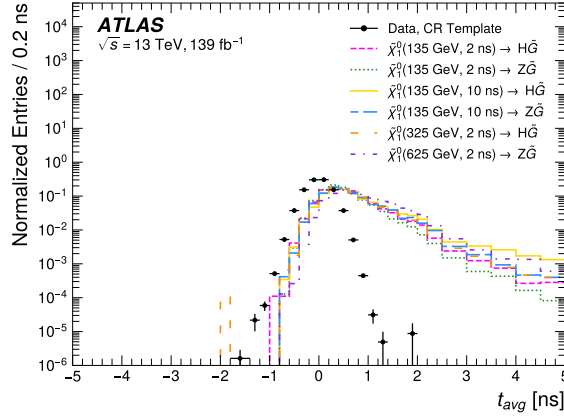


Figure 4: Distribution of the average timing (t_{avg}) for the expected background in the signal region, obtained by transforming data templates from the CR according to the background estimation procedure. Superimposed are the expected distributions for representative signal models in the SR, labeled by the $\tilde{\chi}_1^0$ mass (in GeV) and lifetime (in ns), as well as the decay channel to H or Z .

4.2 Displaced Vertex Finding

The precise spatial resolution and segmentation of the LAr calorimeter provides geometrical information about the origin and direction of travel of EM objects. In contrast to standard displaced vertex finding methods which rely on tracking information from charged particles passing through the inner detector, this analysis uses a novel method called *calo-vertexing*, where the di- e/γ production vertex is localized using only information from the LAr calorimeter. Calo-vertexing is the only way that unconverted photons can be vertexed, while also providing enhanced acceptance for highly displaced electrons that do not have associated tracks.

The calo-vertexing method developed for this search uses well-established pointing variables to localize the DDV in two dimensions. The granularity of the LAr calorimeter in ϕ is insufficient for unambiguous localization in this dimension, so the algorithm first rotates all photon measurements onto $\phi=0$. It then finds each photon's pointing value, defined as the position on the beamline ($x=y=0$) with respect to the PV that its trajectory "points" back to. Pointing is determined using the signals in the first two calorimeter layers, each of which has an associated distance from the beamline R and η . A line can be drawn through the measurements from the first two calorimeter layers, (R_1, η_1) and (R_2, η_2) , and extrapolated back to the beamline to determine the origin of the photon in z . The resolution on the pointing measurement is ≈ 15 mm for a photon with energy of ≈ 50 -100 GeV in the barrel, with good agreement between simulation

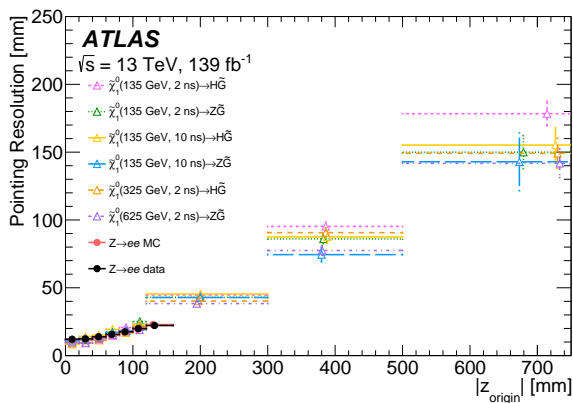


Figure 5: Resolution of the photon pointing variable $|z_{\text{origin}}|$ as a function of $|z_{\text{origin}}|$ in units of mm. Shown are prompt $Z \rightarrow ee$ data and simulation in a selection of events with at least two electrons that have $68 \text{ GeV} < m_{ee} < 108 \text{ GeV}$, and $|\Delta\eta(e_1, e_2)| > 0.1$. Overlaid for comparison are representative signals in the SR selection, labeled by the $\tilde{\chi}_1^0$ mass in GeV, the $\tilde{\chi}_1^0$ lifetime in ns, and the decay channel to H or Z .

and data over the observable pointing distribution [27]. Figure 5 shows the resolution of the pointing variable $|z_{\text{origin}}|$ as a function of $|z_{\text{origin}}|$, comparing $Z \rightarrow ee$ -selected data, $Z \rightarrow ee$ simulation, and signal simulation for several benchmark points. The resolution of the predicted signal, $Z \rightarrow ee$ MC, and $Z \rightarrow ee$ data agrees well over the range that is well-populated with events from prompt data, confirming that data and simulation are similarly modeled. Further, the agreement of the signal and $Z \rightarrow ee$ MC across higher pointing values confirms the use of the pointing variable to describe both signal and background processes.

The intersection of the two photon paths as determined by the pointing procedure then defines the location of the reconstructed secondary vertex candidate. The variables V_R and V_z refer to the location of the vertex along the R and z axis respectively, measured with respect to the PV of the event. Figure 2 diagrammatically illustrates an LLP that is produced at the PV and decays after some travel distance into two photons, whose pointing measurements are used to reconstruct the SV location and thus the two vertexing variables.

As the pointing value will tend to be larger for photons that are produced in the decay of an LLP, and the pointing for two photons that share a common vertex will be correlated, the V_R and V_z measurements are highly discriminating against prompt background. Furthermore, the correlation between V_R and V_z can be exploited by summing them in quadrature, generating the variable $\rho = \sqrt{V_R^2 + V_z^2}$ that is used in the analysis. The distribution of ρ that is expected in the signal region for data and several representative simulated signals is shown in Figure 6.

² The reconstruction of the invariant mass of the di- e/γ system is biased by displacement, as the calculation of the opening angle between the two objects assumes they originate at the beamline. Decays with larger displacement leads to a greater underestimation of the $m_{\gamma\gamma}$ value, leading to a population of events reconstructed below the truth boson mass. As the Z boson mass is lower than the Higgs boson mass, more mis-reconstructed Z boson invariant masses are removed by the 60 GeV lower bound.

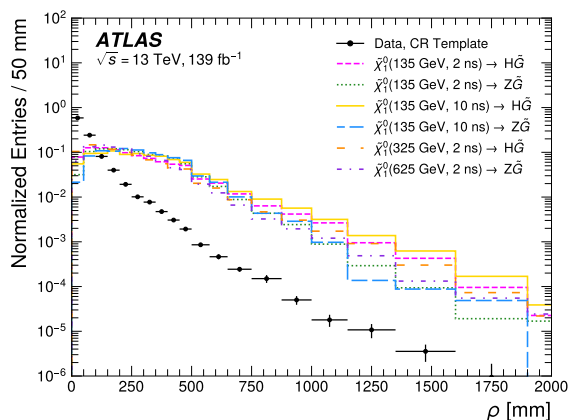


Figure 6: Distribution of the displacement ρ for the expected background in the signal region, obtained by transforming data templates from the CR according to the background estimation procedure. Superimposed are the expected distributions for representative signal models in the SR, labeled by the $\tilde{\chi}_1^0$ mass (in GeV) and lifetime (in ns), as well as the decay channel to H or Z . Signals with an H decay have a slightly broader distribution due to sculpting of the ρ distribution by the lower bound of $m_{\gamma\gamma}$ imposed at 60 GeV^2 .

5 Event selection

Events are selected based on object quality requirements, event-level features and kinematics, as well as the timing and displacement of the two photon objects. The selection criteria are defined based on optimization procedures that maximize signal sensitivity.

5.1 Object Selection

Electrons and photons are reconstructed from calorimeter signals using a dynamical, topological cell clustering-based algorithm [50]. While the signal is reconstructed only with photons, prompt electron objects are used to define the prompt $Z \rightarrow ee$ selection.

Photons are required to satisfy $p_T > 10 \text{ GeV}$ and $|\eta| < 2.37$, excluding the region $1.37 < |\eta| < 1.52$ which corresponds to the transition region between the EM barrel and endcap calorimeters. To reduce the background of jets misreconstructed as photons, they are also subject to track- and calorimeter-based isolation requirements. The calorimeter isolation variable is defined as the energy of calorimeter clusters around the photon candidate in the EM calorimeter in a radius of $\Delta R < 0.2$. Additional corrections based on the leakage of photon energy outside this window, pileup, and the underlying event contribution are applied [50]. The track-based isolation variable is defined as the scalar sum of the p_T of all tracks with $p_T > 1 \text{ GeV}$ within $\Delta R < 0.2$ of the photon candidate. The calorimeter (track) isolation is required to be less than 6.5% (5%) of the photon transverse energy.

A set of photon ID selections uses shower shape variables that describe the energy profiles of the EM showers in the calorimeter, and further enhance the photon efficiency while providing rejection against the background. Three working points are employed in this analysis. Loose ID uses only variables pertaining to the second layer of the EM calorimeter and leakage into the hadronic calorimeter, which minimizes its bias against the identification of non-pointing photons. It is applied to all baseline photon objects, including those used to calculate the E_T^{miss} , and in an overlap removal procedure that prohibits the double-counting of

overlapping objects in an event. The second working point, Medium ID, shares all Loose requirements with the addition of an η -dependent selection on a first-layer shower shape variable E_{ratio} . While this selection decreases signal efficiency by a few percent across the expected range of displacement values, it also offers a lower p_T threshold by way of the Medium ID-based diphoton triggers, which was found to enhance the signal-to-background ratio overall. Therefore, photons that are considered as potential signal objects are required to pass Medium ID. The discrepancy between data and simulation related to the Medium identification selection is found to be negligible across displacement values, thus no systematic uncertainty on the efficiency is added. Finally, Tight ID is used to define the photon-enriched background template described in Section 6. It includes a variety of additional selections to ensure good rejection of fake photons. All ID working points are defined in Ref. [50].

Electron candidates must pass the same isolation and identification criteria as the photons (where the electron track is excluded from the track isolation calculation.) The reconstructed track associated to the electron candidate must be consistent with originating at the PV, in that its longitudinal impact parameter z_0 and transverse impact parameter d_0 must satisfy $|z_0 \cdot \sin \theta| < 0.5$ mm and $|d_0|/\sigma_{d_0} < 5$, respectively. Finally, electron objects are required to have $p_T > 10$ GeV and $|\eta| < 2.47$, excluding the crack region ($1.37 < |\eta| < 1.52$).

Muons and jets only enter the analysis via overlap removal and contributions to the calculation of the missing transverse momentum E_T^{miss} . Muons are reconstructed by matching tracks from the inner detector and MS subsystems. Muons without an inner detector track in the range $2.5 < |\eta| < 2.7$ but with a MS track that is compatible with the interaction point are also considered. Muon candidates are required to have $p_T > 10$ GeV and $|\eta| < 2.7$, and must satisfy Medium muon identification requirements [51]. Muons are further required to satisfy calorimeter- and track-based isolation requirements [51] that are 95%–97% efficient for muons with $p_T \in [10, 60]$ GeV and 99% efficient for $p_T > 60$ GeV. Finally, muon tracks must satisfy $|z_0 \cdot \sin \theta| < 0.5$ mm and $|d_0|/\sigma_{d_0} < 3$.

Jets are reconstructed with FASTJET [52] using a particle flow algorithm [53] from noise-suppressed positive-energy topological clusters [54, 55] in the calorimeter using the anti- k_t algorithm [56] with a radius parameter $R = 0.4$. Energy deposited in the calorimeter by charged particles is subtracted and replaced by the momenta of tracks that are matched to those topological clusters. The jet four-momentum is corrected for the non-compensating calorimeter response, signal losses due to noise threshold effects, energy lost in non-instrumented regions, and contributions from the pileup. Jets are required to have $p_T > 25$ GeV and rapidity $|y| < 4.4$. A jet-vertex-tagger (JVT) multivariate discriminant [57] is applied to jets with $p_T < 60$ GeV and $|\eta| < 2.4$, to suppress jets from the pileup.

An overlap removal procedure is performed in order to avoid double-counting objects, with photons given the highest priority. The procedure is as follows: remove electrons overlapping with photons ($\Delta R < 0.4$); remove jets overlapping with photons ($\Delta R < 0.4$) and those closely overlapping with electrons ($\Delta R < 0.2$); remove electrons “close to” the remaining jets ($0.2 < \Delta R < 0.4$); and remove muons overlapping with photons or jets ($\Delta R < 0.4$).

The magnitude of the E_T^{miss} is the absolute value of the negative vector sum of the transverse momenta of the entire event and is calculated via the track-based soft term (TST) approach [58]. It uses selected photon, electron, muon, and jet objects surviving the overlap removal procedure as well as the remaining “soft” tracking terms that were not assigned to any of the remaining physics objects.

5.2 Analysis Regions

Selected events are required to have a candidate PV for the hard scatter, reconstructed from at least two charged tracks, each with $p_T > 500$ MeV. In case of multiple reconstructed vertices, the PV is selected as the one with the largest sum of the p_T^2 values of the associated tracks. No photon pointing information is taken into consideration for PV assignment.

As the primary feature of the signal events is the presence of the DDV, at least two photons are required in all analysis events. Therefore, all events are subject to the offline selection of at least two photons that are matched to the triggers described in Section 3. The leading and subleading photon p_T must be greater than 40 and 30 GeV respectively, and their invariant mass $m_{\gamma\gamma}$ must be > 60 GeV, to ensure the trigger is used in its efficiency plateau. At least one photon must be in the barrel ($|\eta| < 1.37$), while the other must satisfy $|\eta| < 1.37$ or $1.52 < |\eta| < 2.37$. An event cleaning procedure is applied to reject events from calorimeter noise bursts or other non-collision background, which has a negligible impact on the signal efficiency.

The SR is designed to select events that are consistent with the presence of a DDV. As the DDV selections are sufficient to provide essentially background-free signal regions, the other SM boson produced by the NLSP decay is not used in the analysis in order to mitigate model-dependence of the result. The DDV is assumed to come from the two photons that have the highest momenta in the event, whose pointing values are thus used to compute V_R and V_z . The two leading photons must both have $t_\gamma > 0$, for consistency with a delayed signal, as well as $t_\gamma < 12$ ns, to avoid contamination from adjacent bunch crossings. They are additionally required to have an E_{cell} measurement that is read out on HIGH or MEDIUM LAr gain [59], to ensure good performance of the offline calibration. Further, the E_{cell} must be at least 5 GeV, a selection that balances signal acceptance with the rejection of very low-energy deposits that contaminate the timing resolution. Selections on $0 < V_R < 1500$ mm and $|V_z| < 3740$ mm ensure that the DDV is produced within the boundaries of the inner detector. To ensure good resolution on the V_R and V_z reconstruction, $|\Delta\eta|$ between the two photons is required to be greater than 0.1. As the resonance producing the DDV is assumed to be a Higgs or Z boson, $m_{\gamma\gamma} < 135$ GeV is required. The presence of gravitinos in the final state motivates a selection of $E_T^{\text{miss}} > 30$ GeV. Finally, two additional selections are imposed in the SR only, on kinematic variables that were found to help isolate the signal, specifically $p_T^{\gamma\gamma} > 70$ GeV and the azimuthal angle difference $\Delta\phi(\gamma_1, \gamma_2) < 2.4$.

The data-driven background estimation, described in Section 6, is derived from a CR that is orthogonal to the SR by requiring $E_T^{\text{miss}} < 20$ GeV. Due to correlations between the photon times in the data, the timing shapes in the regions where both photons have opposite-sign timing values are slightly narrower than those in the regions with photons of same-sign times. To ensure that the timing correlations and their impact on the analysis variable shapes match what is expected in the SR, the two photons in CR events are required to have same-sign timing values, though both “positive-positive” and “negative-negative” combinations are allowed in order to increase the CR sample size by a factor of two. The selection of $m_{\gamma\gamma} > 135$ GeV in the CR is inverted with respect to the SR requirement. Signal contamination in the control region is calculated to be less than 0.1% for all simulated signal points.

Two VRs, which are defined to be orthogonal to both the SR and CR as well as to each other, are used to validate the background prediction. $\text{VR}(E_T^{\text{miss}})$ is defined in the intermediate region of the E_T^{miss} spectrum, namely $20 \text{ GeV} < E_T^{\text{miss}} < 30 \text{ GeV}$, providing a region of kinematic phase space that is close to that of the SR. The inverted $m_{\gamma\gamma}$ selection used in the CR is kept for this region. $\text{VR}(t)$ uses the same E_T^{miss} and $m_{\gamma\gamma}$ selection as the SR, but inverts the timing selection such that only events that have two photons with negative times are allowed. An additional prompt $Z \rightarrow ee$ -enriched region is defined to study the timing

and vertexing variables, where events have at least two electrons with an invariant mass that satisfies $68 \text{ GeV} < m_{ee} < 108 \text{ GeV}$, and $|\Delta\eta(e_1, e_2)| > 0.1$. As this region is defined with electron objects and the overlap removal procedure prioritizes photons, this selection is orthogonal to all other analysis regions. Signal contamination in the CR is less than 0.1% across all generated signal mass and lifetime hypotheses, and less than 0.2% in both VRs and the $Z \rightarrow ee$ selection.

As both signal and background have a distinct shape in t_{avg} and ρ , a shape fit is performed to exploit the entire spectrum of both variables. The final likelihood fit is performed over the binned t_{avg} distribution, for several categories of ρ . Dedicated optimization studies were used to determine the binning in both variables that maximizes signal exclusion significance, while ensuring sufficient background statistics for all bins. The projected significance of a signal hypothesis incorporating all bins was calculated for each binning considered, and optimization was performed separately for each signal point to ensure that all SR phase space is considered. The final binning was chosen based on the discovery reach across the signal grid and is given in Table 1, along with a summary of all region selections discussed above.

Parameter	Preselection requirements			
Photon multiplicity	> 1			
Photon η	$ \eta < 1.37$ or $1.52 < \eta < 2.37$ (≥ 1 with $ \eta < 1.37$)			
$E_{\text{cell}}(\gamma)$ [GeV]	$E_{\text{cell}}(\gamma_1), E_{\text{cell}}(\gamma_2) > 5$			
$p_T(\gamma)$ [GeV]	$p_T(\gamma_1) > 40, p_T(\gamma_2) > 30$			
$\Delta\eta_{\gamma\gamma}$	> 0.1			
$m_{\gamma\gamma}$ [GeV]	> 60			
V_R [mm]	[0, 1500]			
$ V_z $ [mm]	< 3740			
t_γ [ns]	$t_{\gamma_1}, t_{\gamma_2} \in [-12, 12]$			
Parameter	Analysis region requirements			
	CR	VR(E_T^{miss})	VR(t)	SR
E_T^{miss} [GeV]	< 20	20–30	> 30	
$m_{\gamma\gamma}$ [GeV]	> 135		[60, 135]	
Sign of t_γ	$t_{\gamma_1} \times t_{\gamma_2} > 0$		$t_{\gamma_1}, t_{\gamma_2} < 0$	$t_{\gamma_1}, t_{\gamma_2} > 0$
$p_T^{\gamma\gamma}$ [GeV]	-			> 70
$\Delta\phi(\gamma_1, \gamma_2)$	-			< 2.4
Vertexing and timing bins				
ρ bin edges [mm]	[0, 80, 160, 300, 520, 2000]			
t_{avg} bin edges [ns]	[0, 0.2, 0.4, 0.6, 0.9, 12]			

Table 1: Optimized requirements defining the preselection, SR, CR, and both VRs. Also included are the optimized binnings for the photon vertexing ($\rho = \sqrt{V_R^2 + V_z^2}$) and average timing (t_{avg}) variables.

6 Background estimation

SM processes do not produce a DDV with a significant invariant mass. Background events in the SR are therefore a result of processes with either real photons that are misreconstructed to pass the DDV selection

criteria (including those from satellite collisions), or other objects that fake photons. Due to non-Gaussian tails in the LAr timing distribution, Monte Carlo generators do not give sufficiently good modeling of the data for this variable. Therefore, a fully data-driven background estimation is used to predict the size and shape of these two background sources in the SR.

The low- E_T^{miss} CR is used to extract templates of the t_{avg} shape from data. It is known [27, 29] that the measured pointing and timing distributions of genuine photons are narrower than those of other physics objects (specifically jets) that can be misreconstructed as photons. To capture this shape difference, two templates are defined, one enriched in real photons and the other enriched in fake photons. The real-enhanced photon template is defined by the CR selection given in Table 1, in addition to a requirement that both photons satisfy the Tight identification criteria as discussed in Section 5.1. Similarly, the fake-enhanced photon template is defined as the set of events where at least one photon fails Tight ID.

The background in the high- E_T^{miss} SR is predicted by transforming and mixing these two templates in the following way. The two templates are scaled to match the observed purity in the SR, derived from the f_{TT} value obtained from data events in the SR. The real photon CR template is multiplied by the fraction of SR events where both photons pass Tight (f_{TT}), and the fake photon template is weighted by $1 - f_{TT}$. The observed f_{TT} in the SR ranges from approximately 0.8 in the lowest ρ bin to approximately 0.5 in the highest ρ bin. This is done separately in each ρ category. Prior to purity scaling, the largest deviation in purity across the analysis regions is on the order of 10%, and after scaling the f_{TT} distributions of all regions agree within error. Due to the dependence of calorimeter performance on the magnitude of the energy deposit, the photon timing resolution is correlated with its kinematics, specifically its energy. A reweighting procedure is next applied to the templates that match each photon's E_{cell} distribution to that of the SR, which mitigates this correlation and ensures the validity of extrapolating over E_T^{miss} in the background estimation. E_{cell} -reweighting is done inclusively in timing and exclusively in ρ categories, separately for each template. The E_{cell} shape differences between the CR and SR before reweighting are on the order of 20%, and after reweighting the distributions agree within error. Finally, a mean correction is imposed on all data distributions to correct for small non-zero means ($O(\text{ps})$) introduced by the application of timing corrections derived from electrons to photon objects. The correction is derived and applied separately in each E_{cell} -reweighting region. This procedure requires two features of the SR data events to be unblinded, namely the f_{TT} fraction and the E_{cell} distribution. As neither of these variables discriminates between signal and background in the region of interest and the signal contamination in the CR is below 0.1%, this procedure doesn't affect the potential detection of signal events in the SR. The final background template after these transformations is shown in Figures 4 and 6 as a function of t_{avg} and ρ , respectively.

7 Systematic uncertainties

While the sensitivity of this search is dominated by the statistical uncertainties in the dataset, several sources of systematic uncertainty are considered. These are modeled via dedicated studies and accounted for as nuisance parameters in the final statistical treatment, as described in Section 8. The systematic uncertainties can be either evenly distributed variations that affect only the signal normalization, or uncertainties that impact the distribution shape of the signal and/or the background. Systematic uncertainties are not needed on the background normalization in each ρ category, since these normalizations are implemented as nuisance parameters that are free to float in the fit. As expected given the limited statistical precision of the analysis region, the expected sensitivity with and without systematic uncertainties agrees to within 1% for all mass and lifetime signal points considered.

7.1 Background Shape Uncertainties

Background shape systematic uncertainties are related to the data-driven background estimation, and are assessed through variations on the estimation procedure.

An uncertainty exists on the purity fraction used to weight the real and fake templates to construct an SR prediction. Since the selection criteria of an analysis region require both photons to either pass or fail TIGHT ID selection, a binomial error is assigned to the photon purity fraction. This photon purity fraction error is then used to define maximum deviations in the up and down directions of the photon purity fraction in bins of ρ . These range from $<1\%$ for small t_{avg} and ρ values, and are $<10\%$ at their largest values in the higher bins. A similar uncertainty exists on the E_{cell} -reweighting. The reweights are calculated from the ratio of the two-dimensional histograms between the target and the source photon E_{cell} spectra. Therefore, the error on the reweighting is the statistical error of the ratio of the two histograms, which define the envelope of variation considered. This effect ranges from $O(1)\%$ in the smallest t_{avg} and ρ bins to $O(10)\%$ for the highest.

Finally, a systematic uncertainty is needed to account for the extrapolation from a low- $E_{\text{T}}^{\text{miss}}$ to a high- $E_{\text{T}}^{\text{miss}}$ pileup profile. This is necessary as the timing resolution for photon objects degrades with increasing pileup, due to the increased contribution of jets from pileup interactions. To estimate this effect, the up and down variations are constructed from CR photons based on whether the average number of simultaneous interactions is less than or greater than a specified ρ -dependent threshold value. These threshold values are all approximately 33, which is the average value of pileup for Run 2, and they agree within 10% across the ρ categories. Given the limited background statistics, a smoothing procedure is applied to the pileup variation in the highest ρ category by merging neighboring bins to reduce statistical fluctuations. The size of this uncertainty is $\sim 10\%$ across all five ρ categories.

7.2 Signal Uncertainties

Both normalization and shape uncertainties on the signal prediction are considered. These arise from experimental conditions, theoretical modeling, or analysis methodologies.

The instrumental systematic uncertainties which affect the signal yield are uncertainties on the photon reconstruction efficiencies, reconstruction of $E_{\text{T}}^{\text{miss}}$, trigger object matching, pileup reweighting, and the integrated luminosity measurement. The uncertainty in the integrated luminosity is $\pm 1.7\%$, evaluated using the methodology described in Ref. [37]. The total uncertainty on the signal normalization comes from these instrumental effects and is calculated as the quadrature sum of the detector uncertainties, yielding a value of $2.5\text{--}3\%$ depending on the signal model. The impact of these normalization systematic uncertainties on the CL_s value, with respect to the fit with all background shape systematic uncertainties, is less than 0.2% .

Theoretical uncertainties exist on the choice of the strong coupling constant (α_S), the renormalization and the factorization scale variations, as well as the choice of PDFs. Uncertainties are evaluated by comparing the t_{avg} distribution after varying each of the parameters by a factor of two and taking an envelope of the resulting distributions. An overall $\pm 12.6\%$ normalization uncertainty is applied to all signals as a result of these theoretical modeling effects.

Additional uncertainties are considered that affect the distribution of relative event yields across t_{avg} bins, namely on the timing resolutions in data as compared to simulation. The impact is measured by

implementing an alternate timing smearing, adopting the same procedure of previous non-pointing photon analyses [27]. This procedure has a negligible effect on the results.

8 Statistical analysis

The compatibility of the data with the background-only hypothesis is evaluated with a binned profile likelihood fit of the t_{avg} distribution of the background prediction to that observed in the data, performed simultaneously across all five ρ categories. Similarly, to evaluate the compatibility of the data under the signal presence assumption, a fit of both signal and background templates to data is performed.

The likelihood function is constructed as a product of Poisson probabilities \mathcal{P} for each bin of the average timing distribution for each category. It depends on the signal strength μ , as well as the set of all nuisance parameters (NPs) with Gaussian constraints. The μ parameter multiplies the expected signal cross-section σ and is fully correlated across ρ categories. The normalization factor for the background in each category is modeled as a floating NP that is uncorrelated to other ρ bins.

A profile likelihood ratio was used to perform frequentist hypothesis tests. The p_0 -value, defined as the probability of statistical fluctuations making the background distributions appear to contain at least as much signal as the data distributions, was calculated for different signal models. The statistical fit procedure, as well as the background estimation as derived from the CR, was validated through background-only fits to the data in the two VRs, which each have negligible signal contamination. Figure 7 shows the post-fit t_{avg} distribution of data and background in the five ρ categories for VR(t), showing good agreement between data and background estimation.

The validity of the fit setup and background model was additionally assessed with generated pseudo-datasets. 500 pseudo-datasets were generated by drawing events from the CR, and applying the background estimation transformations described in Section 6 to match the pseudo-dataset timing shape to that of the targeted VR. The number of events for each pseudo-dataset was fixed to the expected yield in the signal region. This process was performed separately for both VR(t) and VR($E_{\text{T}}^{\text{miss}}$), and a background-only fit was performed for each of the 500 pseudo-datasets to obtain a distribution of p_0 values for the background-only hypothesis. The mean of the obtained p_0 distribution was 0.53 and 0.54 for VR(t) and VR($E_{\text{T}}^{\text{miss}}$) respectively, reflecting good behavior of the background model in each fit.

Further validation was achieved via signal-plus-background fits for spurious signal and signal injection tests. The spurious signal was studied via fits of the background expectation to data in the signal-depleted VRs, ensuring that the fit does not find a signal if none is present. A conservative upper bound on the spurious signal was obtained using the signal point in the grid to which the analysis is most sensitive, which is $\tilde{\chi}_1^0$ (135 GeV, 2 ns). The maximum fitted significance of the aforementioned signal point across all three VRs is 0.8σ . In the signal injection tests, the fit was performed to a pseudo-dataset consisting of CR events transformed to match the SR timing distribution shape, to which a signal template was added with varying significance. The fitted signal μ is compared to the injected μ and they are found to be the same within statistical error across the signal grid. The relatively similar shape of the various signal points in both t_{avg} and ρ leads to similar signal-plus-background results across the grid, which also serves as validation that the systematic uncertainties are appropriate for the fit.

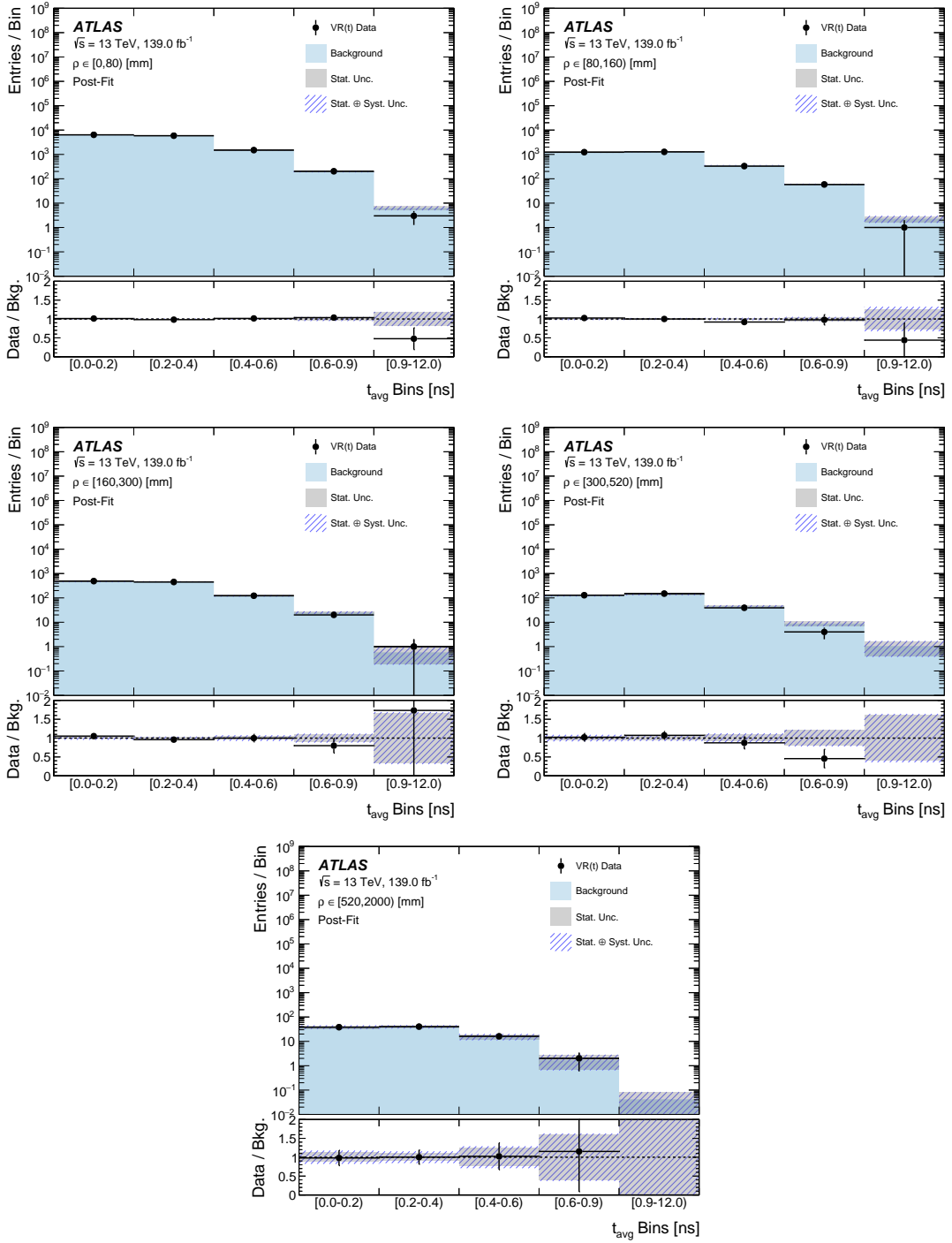


Figure 7: Average timing distributions for VR(t) data and the estimated background as determined by the background-only fit, in each of the five exclusive ρ categories.

9 Results

Figure 8 shows the t_{avg} distributions of SR data and predicted background as determined by a background-only fit with all systematic uncertainties. The observed data are generally found to be in good agreement with the expected background. The largest deviation occurs in the highest ρ category and highest t_{avg} bin, where a single event is observed with $\rho = 560$ mm, a leading photon time of 5.82 ns, and a subleading photon time of 0.45 ns. Such an event is highly incompatible with the signal hypothesis of this search, which should have similarly delayed times for both photons.

The timing of the leading photon around 5 ns and the subleading photon closer to 0 ns makes this event a likely satellite collision candidate, with the leading photon coming from a satellite collision and the second photon arising from an overlaid in-time collision. As a known source of background, events with photons arising from satellite collisions are covered by the data-driven background estimation described in Section 6, and are thus included in the prediction of the event yield in the SR. A simple estimate for the specific contribution of satellite collisions to the total predicted background in the SR is obtained by determining the number of satellite events present in the CR, defined by requiring photon times to be between 4.5 and 6.5 ns inclusively in ρ . Since the presence of satellite collisions is uncorrelated to photon kinematics, a prediction for the SR can be calculated by scaling this number by the ratio of events in the SR to CR. This procedure predicts that 0.5 ± 0.3 satellite events should be observed in the ρ -inclusive SR, where no systematic uncertainties are considered, thus providing further context for the likelihood of this single event observation.

As no significant excess above the background prediction is observed in the SR data, signal-plus-background fits are performed to set upper limits at 95% confidence on the signal production cross-section via the CL_s technique [60, 61] under the asymptotic approximation [62]. Limits are presented as a function of the two parameters of the signal grid, the $\tilde{\chi}_1^0$ mass and lifetime, under the assumption of 100% BR (\mathcal{B}) to either Higgs or Z bosons, as well as the BR of the $\tilde{\chi}_1^0$ to the SM Higgs boson for specific mass and lifetime hypotheses. For the signal points with insufficient statistical precision where the asymptotic approximation breaks down, no limit is provided.

Limits on the cross-section $\sigma(pp \rightarrow \tilde{\chi}_1^0 \tilde{\chi}_1^0)$ in fb are shown in Figure 9, as a function of both $\tilde{\chi}_1^0$ mass and lifetime, for both H and Z decay modes. Figure 10 shows the 95% CL exclusion for the signal hypothesis in the two-dimensional ($m_{\tilde{\chi}_1^0}, \tau_{\tilde{\chi}_1^0}$) plane. In these results, the limits for $Z \rightarrow ee$ decaying signals are more stringent than the $H \rightarrow \gamma\gamma$ decays, as the BR of the Z boson to the dielectron final state is higher than that of the Higgs boson to two photons, so more events are able to pass the analysis selection criteria. $\tilde{\chi}_1^0$ masses up to 369 (704) GeV are excluded for the pure di-Higgs boson (di- Z) decay modes assuming a $\tilde{\chi}_1^0$ lifetime of 2 ns, which corresponds to a production cross-section of 124.5 (6.69) fb.

Limits as a function of the $\tilde{\chi}_1^0$ BR can also be computed by combining samples with both Higgs and Z boson decays of the $\tilde{\chi}_1^0$, as well as the decay of the other $\tilde{\chi}_1^0$ in the event that does not produce the DDV. In these interpretations, the sum of the $\tilde{\chi}_1^0$ BR to the Higgs and Z bosons is assumed to be 1. Figure 11 shows an example of these limits as a function of $\mathcal{B}(\tilde{\chi}_1^0 \rightarrow H + \tilde{G})$ for several mass hypotheses with a fixed $\tilde{\chi}_1^0$ lifetime of 2 ns.

In addition to the signal cross-section limits, an additional test is performed using only the final timing bin ($t_{\text{avg}} > 0.9$ ns) and no vertexing categorization. This region enables a less model-dependent search for generic DDV signatures in data. The results of this model-agnostic test are summarized in Table 2. In this bin, 10.2 ± 3.0 background events are expected and 4 are observed. The compatibility of the observed

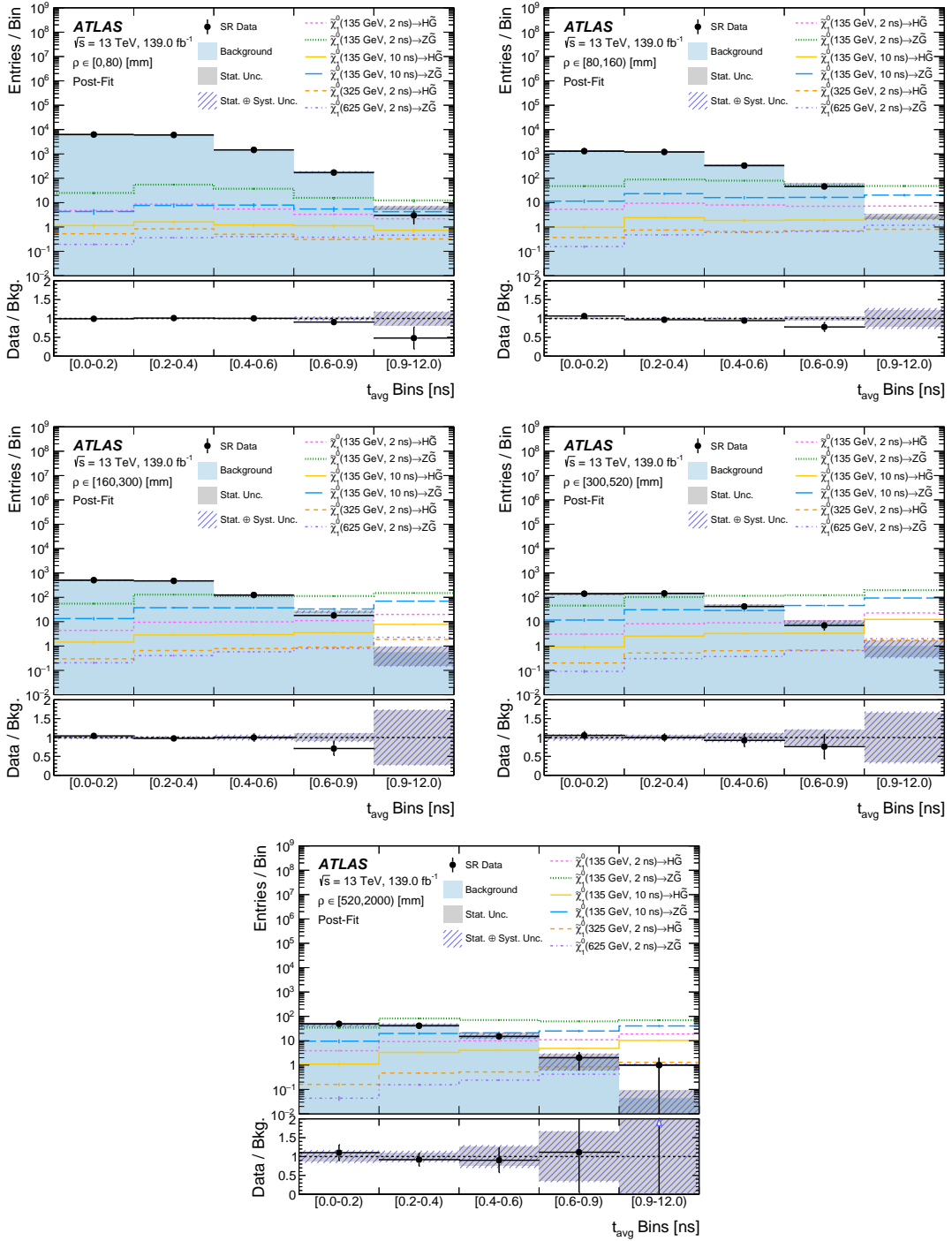


Figure 8: Average timing distributions for SR data and the estimated background as determined by the background-only fit, in each of the five exclusive ρ categories. For comparison, the expected timing shapes for a few different signal models are superimposed, with each model labeled by the values of the $\tilde{\chi}_1^0$ mass and lifetime, as well as decay mode. To provide some indication of the variations in signal yield and shape, three signal models are shown for each of the $\tilde{\chi}_1^0$ decay modes, namely $\tilde{\chi}_1^0 \rightarrow H + \tilde{G}$ and $\tilde{\chi}_1^0 \rightarrow Z + \tilde{G}$. The models shown include a rather low $\tilde{\chi}_1^0$ mass value of 135 GeV for lifetimes of either 2 ns or 10 ns, and a higher $\tilde{\chi}_1^0$ mass value which is near the 95% CL exclusion limit for each decay mode for a lifetime of 2 ns. Each signal model is shown with the signal normalization corresponding to a BR value of unity for the decay mode in question.

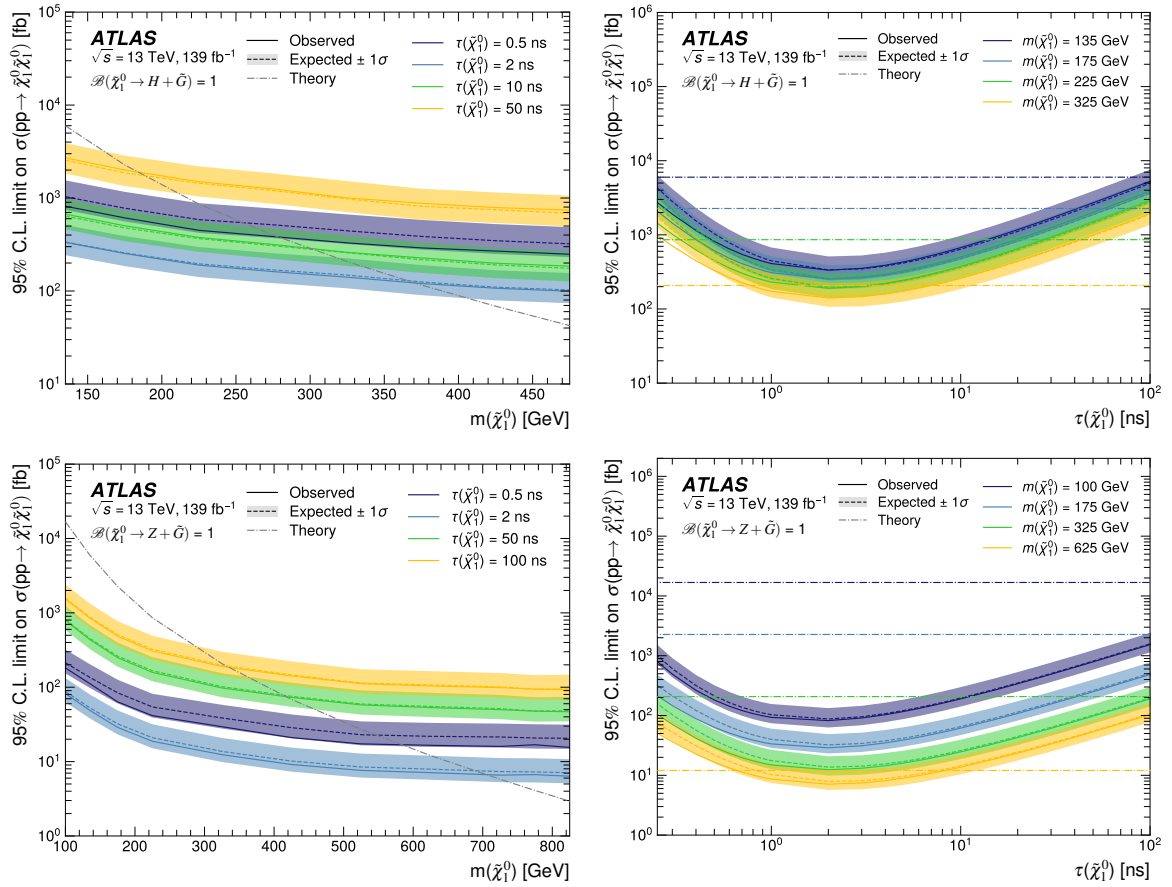


Figure 9: The 95% CL limits on $\sigma(pp \rightarrow \tilde{\chi}_1^0 \tilde{\chi}_1^0)$ in fb as a function of $\tilde{\chi}_1^0$ mass (left) and $\tilde{\chi}_1^0$ lifetime (right), for the different decay modes of $\mathcal{B}(\tilde{\chi}_1^0 \rightarrow H + \tilde{G}) = 1$ (top) and $\mathcal{B}(\tilde{\chi}_1^0 \rightarrow Z + \tilde{G}) = 1$ (bottom). For the limits as a function of mass (lifetime), several signal models with varying lifetime (mass) are overlaid for comparison. Included are the theoretical expectations from higgsino production for each mass hypothesis, calculated from a GMSB SUSY model that assumes nearly degenerate $\tilde{\chi}_1^0$, $\tilde{\chi}_1^\pm$, and $\tilde{\chi}_2^0$.

events under the background-only hypothesis (p_0 -value) and its significance (Z) are calculated. Based on the observed and expected number of events, a 95% CL upper limit on the number of excluded events (N^{excl}) under the background-only hypothesis is calculated.

10 Conclusion

The first search for displaced diphoton vertices originating from the decay of a massive LLP is presented. The data set used was recorded by the ATLAS detector at the LHC and corresponds to an integrated luminosity of 139 fb^{-1} of pp collisions at a center-of-mass energy of $\sqrt{s} = 13 \text{ TeV}$. Precise measurements from the ATLAS LAr calorimeter are used to select these events based on the delayed timing and displaced vertices of the final state photons. No significant deviations are observed in the data with respect to the predicted background. One event is observed in the highest timing bin and highest vertexing category, whose features are consistent with a source of expected background from satellite collisions. Results

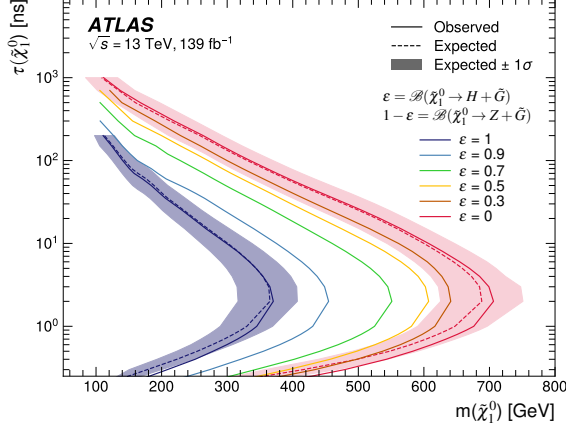


Figure 10: The 95% CL exclusion limits on the target signal hypothesis, for $\tilde{\chi}_1^0$ lifetime in ns as a function of $\tilde{\chi}_1^0$ mass in GeV. The overlaid curves correspond to different decay hypotheses, where the assumed cross-section is for higgsino production, and the $\tilde{\chi}_1^0$ decays to $H + \tilde{G}$ or $Z + \tilde{G}$ such that $\mathcal{B}(H + \tilde{G}) + \mathcal{B}(Z + \tilde{G}) = 100\%$. The curve shown in red represents the decay hypothesis where the $\tilde{\chi}_1^0$ decays to $Z + \tilde{G}$ with 100% branching ratio. The curve shown in blue represents the decay hypothesis where the $\tilde{\chi}_1^0$ decays to $H + \tilde{G}$ with 100% branching ratio.

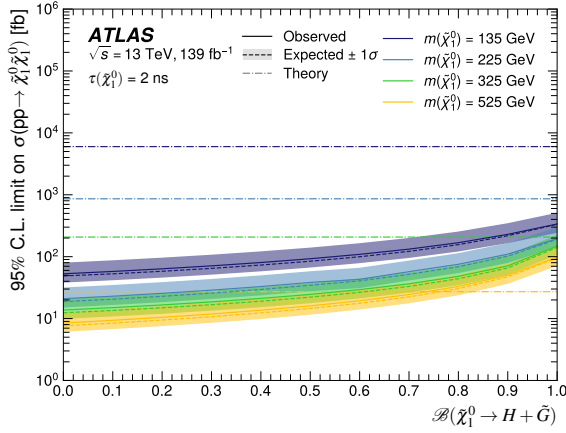


Figure 11: The 95% CL limits on $\sigma(pp \rightarrow \tilde{\chi}_1^0 \tilde{\chi}_1^0)$ in fb as a function of $\tilde{\chi}_1^0$ branching ratio to the SM Higgs boson, where the assumed cross-section is for higgsino production, and $\mathcal{B}(\tilde{\chi}_1^0 \rightarrow Z + \tilde{G}) = 1 - \mathcal{B}(\tilde{\chi}_1^0 \rightarrow H + \tilde{G})$. Several signal hypotheses are overlaid that are labelled by the $\tilde{\chi}_1^0$ mass, all with a fixed $\tilde{\chi}_1^0$ lifetime of 2 ns. Included are the theoretical expectations for each mass hypothesis, calculated from a GMSB SUSY model that assumes nearly degenerate $\tilde{\chi}_1^0$, $\tilde{\chi}_1^\pm$, and $\tilde{\chi}_2^0$.

Selection	Data	Total Background	p_0	Z (σ)	N^{excl} Events
SR, $t_{\text{avg}} > 0.9$ ns	4	10.2 ± 3.0	0.97	-1.96	14.4

Table 2: Results for the model-agnostic test. The expected number of events and the uncertainty on the expected number of events are calculated using a fit to the ρ -inclusive t_{avg} distribution, with $t_{\text{avg}} \in [0.0, 0.9)$ ns and extrapolated to the $t_{\text{avg}} \in [0.9, 12)$ ns bin. The compatibility of the observed events with the background-only expectation is given by the p_0 -value, its corresponding significance Z, and the 95% CL upper limit on the number of excluded events under the background-only hypothesis.

are interpreted in a GMSB SUSY model as 95% CL upper limits on the cross section of di-higgsino production scanning the $\tilde{\chi}_1^0$ mass, lifetime, and branching ratio to the Higgs boson, under the assumption of $\mathcal{B}(\tilde{\chi}_1^0 \rightarrow H + \tilde{G}) + \mathcal{B}(\tilde{\chi}_1^0 \rightarrow Z + \tilde{G}) = 1$ and nearly degenerate $\tilde{\chi}_1^0$, $\tilde{\chi}_1^\pm$, and $\tilde{\chi}_2^0$. Limits are set across the two-dimensional space of $\tilde{\chi}_1^0$ mass and lifetime τ , where the $\tilde{\chi}_1^0$ mass is between 100 and 725 GeV and τ is between 0.25 and 1000 ns. For a branching fraction of 100% of $\tilde{\chi}_1^0$ to H or Z bosons, the highest excluded $\tilde{\chi}_1^0$ masses are 369 GeV for Higgs bosons and 704 GeV for Z bosons. Those limits are obtained for a $\tilde{\chi}_1^0$ lifetime of 2 ns where the analysis is most sensitive.

Acknowledgements

We thank CERN for the very successful operation of the LHC, as well as the support staff from our institutions without whom ATLAS could not be operated efficiently.

We acknowledge the support of ANPCyT, Argentina; YerPhI, Armenia; ARC, Australia; BMWFW and FWF, Austria; ANAS, Azerbaijan; CNPq and FAPESP, Brazil; NSERC, NRC and CFI, Canada; CERN; ANID, Chile; CAS, MOST and NSFC, China; Minciencias, Colombia; MEYS CR, Czech Republic; DNRf and DNSRC, Denmark; IN2P3-CNRS and CEA-DRF/IRFU, France; SRNSFG, Georgia; BMBF, HGF and MPG, Germany; GSRI, Greece; RGC and Hong Kong SAR, China; ISF and Benozzi Center, Israel; INFN, Italy; MEXT and JSPS, Japan; CNRST, Morocco; NWO, Netherlands; RCN, Norway; MEiN, Poland; FCT, Portugal; MNE/IFA, Romania; MESTD, Serbia; MSSR, Slovakia; ARRS and MIZŠ, Slovenia; DSI/NRF, South Africa; MICINN, Spain; SRC and Wallenberg Foundation, Sweden; SERI, SNSF and Cantons of Bern and Geneva, Switzerland; MOST, Taiwan; TENMAK, Türkiye; STFC, United Kingdom; DOE and NSF, United States of America. In addition, individual groups and members have received support from BCKDF, CANARIE, Compute Canada and CRC, Canada; PRIMUS 21/SCI/017 and UNCE SCI/013, Czech Republic; COST, ERC, ERDF, Horizon 2020 and Marie Skłodowska-Curie Actions, European Union; Investissements d’Avenir Labex, Investissements d’Avenir Idex and ANR, France; DFG and AvH Foundation, Germany; Herakleitos, Thales and Aristeia programmes co-financed by EU-ESF and the Greek NSRF, Greece; BSF-NSF and MINERVA, Israel; Norwegian Financial Mechanism 2014-2021, Norway; NCN and NAWA, Poland; La Caixa Banking Foundation, CERCA Programme Generalitat de Catalunya and PROMETEO and GenT Programmes Generalitat Valenciana, Spain; Göran Gustafssons Stiftelse, Sweden; The Royal Society and Leverhulme Trust, United Kingdom.

The crucial computing support from all WLCG partners is acknowledged gratefully, in particular from CERN, the ATLAS Tier-1 facilities at TRIUMF (Canada), NDGF (Denmark, Norway, Sweden), CC-IN2P3 (France), KIT/GridKA (Germany), INFN-CNAF (Italy), NL-T1 (Netherlands), PIC (Spain), ASGC (Taiwan), RAL (UK) and BNL (USA), the Tier-2 facilities worldwide and large non-WLCG resource providers. Major contributors of computing resources are listed in Ref. [63].

References

- [1] ATLAS Collaboration, *Observation of a new particle in the search for the Standard Model Higgs boson with the ATLAS detector at the LHC*, *Phys. Lett. B* **716** (2012) 1, arXiv: [1207.7214 \[hep-ex\]](#).
- [2] CMS Collaboration, *Observation of a new boson at a mass of 125 GeV with the CMS experiment at the LHC*, *Phys. Lett. B* **716** (2012) 30, arXiv: [1207.7235 \[hep-ex\]](#).
- [3] Y. Golfand and E. Likhtman, *Extension of the Algebra of Poincare Group Generators and Violation of P Invariance*, *JETP Lett.* **13** (1971) 323, [*Pisma Zh. Eksp. Teor. Fiz.* **13** (1971) 452].
- [4] A. Neveu and J. H. Schwarz, *Factorizable dual model of pions*, *Nucl. Phys. B* **31** (1971) 86.
- [5] A. Neveu and J. H. Schwarz, *Quark model of dual pions*, *Phys. Rev. D* **4** (1971) 1109.
- [6] P. Ramond, *Dual theory for free fermions*, *Phys. Rev. D* **3** (1971) 2415.
- [7] D. Volkov and V. Akulov, *Is the neutrino a goldstone particle?* *Phys. Lett. B* **46** (1973) 109.
- [8] J. Wess and B. Zumino, *A lagrangian model invariant under supergauge Transformations*, *Phys. Lett. B* **49** (1974) 52.
- [9] J. Wess and B. Zumino, *Supergauge transformations in four dimensions*, *Nucl. Phys. B* **70** (1974) 39.
- [10] P. Fayet, *Supersymmetry and weak, electromagnetic and strong interactions*, *Phys. Lett. B* **64** (1976) 159.
- [11] P. Fayet, *Spontaneously broken supersymmetric theories of weak, electromagnetic and strong interactions*, *Phys. Lett. B* **69** (1977) 489.
- [12] G. R. Farrar and P. Fayet, *Phenomenology of the production, decay, and detection of new hadronic states associated with supersymmetry*, *Phys. Lett. B* **76** (1978) 575.
- [13] P. Fayet, *Relations between the masses of the superpartners of leptons and quarks, the goldstino couplings and the neutral currents*, *Phys. Lett. B* **84** (1979) 416.
- [14] S. Dimopoulos and H. Georgi, *Softly broken supersymmetry and SU(5)*, *Nucl. Phys. B* **193** (1981) 150.
- [15] ATLAS Collaboration, *Search for direct production of electroweakinos in final states with one lepton, missing transverse momentum and a Higgs boson decaying into two b-jets in pp collisions at $\sqrt{s} = 13$ TeV with the ATLAS detector*, *Eur. Phys. J. C* **80** (2020) 691, arXiv: [1909.09226 \[hep-ex\]](#).
- [16] ATLAS Collaboration, *Searches for electroweak production of supersymmetric particles with compressed mass spectra in $\sqrt{s}=13$ TeV pp collisions with the ATLAS detector*, *Physical Review D* **101** (2020), ISSN: 2470-0029, arXiv: [1911.12606 \[hep-ex\]](#).
- [17] ATLAS Collaboration, *Search for long-lived charginos based on a disappearing-track signature using 136 fb^{-1} of pp collisions at $\sqrt{s} = 13$ TeV with the ATLAS detector*, *Eur. Phys. J. C* **82** (2022) 606, arXiv: [2201.02472 \[hep-ex\]](#).
- [18] CMS Collaboration, *Search for electroweak production of charginos and neutralinos in WH events in proton-proton collisions at $\sqrt{s} = 13$ TeV*, *JHEP* **11** (2017) 029, arXiv: [1706.09933 \[hep-ex\]](#).

- [19] CMS Collaboration, *Search for supersymmetry with a compressed mass spectrum in the vector boson fusion topology with 1-lepton and 0-lepton final states in proton-proton collisions at $\sqrt{s} = 13$ TeV*, [JHEP **08** \(2019\) 150](#), arXiv: [1905.13059 \[hep-ex\]](#).
- [20] CMS Collaboration, *Search for disappearing tracks in proton-proton collisions at $\sqrt{s} = 13$ TeV*, [Phys. Lett. B **806** \(2020\) 135502](#), arXiv: [2004.05153 \[hep-ex\]](#).
- [21] M. Dine and W. Fischler, *A phenomenological model of particle physics based on supersymmetry*, [Phys. Lett. B **110** \(1982\) 227](#).
- [22] L. Alvarez-Gaumé, M. Claudson, and M. B. Wise, *Low-energy supersymmetry*, [Nucl. Phys. B **207** \(1982\) 96](#).
- [23] C. R. Nappi and B. A. Ovrut, *Supersymmetric extension of the $SU(3)\times SU(2)\times U(1)$ model*, [Phys. Lett. B **113** \(1982\) 175](#).
- [24] M. Dine and A. Nelson, *Dynamical supersymmetry breaking at low energies*, [Phys. Rev. D **48** \(1993\) 1277](#), eprint: [hep-ph/9303230](#).
- [25] M. Dine, A. Nelson, and Y. Shirman, *Low energy dynamical supersymmetry breaking simplified*, [Phys. Rev. D **51** \(1995\) 1362](#), eprint: [hep-ph/9408384](#).
- [26] M. Dine, A. Nelson, Y.Nir, and Y. Shirman, *New tools for low energy dynamical supersymmetry breaking*, [Phys. Rev. D **53** \(1996\) 2658](#), eprint: [hep-ph/9507378](#).
- [27] ATLAS Collaboration, *Search for displaced photons produced in exotic decays of the Higgs boson using 13 TeV pp collisions with the ATLAS detector*, (2022), arXiv: [2209.01029 \[hep-ex\]](#).
- [28] ATLAS Collaboration, *Search for nonpointing photons in the diphoton and E_T^{miss} final state in $\sqrt{s} = 7$ TeV proton-proton collisions using the ATLAS detector*, [Phys. Rev. D **88** \(2013\) 012001](#), arXiv: [1304.6310 \[hep-ex\]](#).
- [29] ATLAS Collaboration, *Search for nonpointing and delayed photons in the diphoton and missing transverse momentum final state in 8 TeV pp collisions at the LHC using the ATLAS detector*, [Phys. Rev. D **90** \(2014\) 112005](#), arXiv: [1409.5542 \[hep-ex\]](#).
- [30] CMS Collaboration, *Search for long-lived particles using delayed photons in proton-proton collisions at $\sqrt{s} = 13$ TeV*, [Phys. Rev. D **100** \(2019\) 112003](#), arXiv: [1909.06166 \[hep-ex\]](#).
- [31] ATLAS Collaboration, *The ATLAS Experiment at the CERN Large Hadron Collider*, [JINST **3** \(2008\) S08003](#).
- [32] ATLAS Collaboration, *ATLAS Insertable B-Layer: Technical Design Report*, ATLAS-TDR-19; CERN-LHCC-2010-013, 2010, URL: <https://cds.cern.ch/record/1291633>, Addendum: ATLAS-TDR-19-ADD-1; CERN-LHCC-2012-009, 2012, URL: <https://cds.cern.ch/record/1451888>.
- [33] B. Abbott et al., *Production and integration of the ATLAS Insertable B-Layer*, [JINST **13** \(2018\) T05008](#), arXiv: [1803.00844 \[physics.ins-det\]](#).
- [34] ATLAS Collaboration, *Performance of the ATLAS trigger system in 2015*, [Eur. Phys. J. C **77** \(2017\) 317](#), arXiv: [1611.09661 \[hep-ex\]](#).
- [35] ATLAS Collaboration, *The ATLAS Collaboration Software and Firmware*, ATL-SOFT-PUB-2021-001, 2021, URL: <https://cds.cern.ch/record/2767187>.

- [36] ATLAS Collaboration, *ATLAS data quality operations and performance for 2015–2018 data-taking*, [JINST **15** \(2020\) P04003](#), arXiv: [1911.04632 \[physics.ins-det\]](#).
- [37] ATLAS Collaboration, *Luminosity determination in pp collisions at $\sqrt{s} = 8$ TeV using the ATLAS detector at the LHC*, [Eur. Phys. J. C **76** \(2016\) 653](#), arXiv: [1608.03953 \[hep-ex\]](#).
- [38] G. Avoni et al., *The new LUCID-2 detector for luminosity measurement and monitoring in ATLAS*, [JINST **13** \(2018\) P07017](#).
- [39] ATLAS Collaboration, *Performance of electron and photon triggers in ATLAS during LHC Run 2*, [Eur. Phys. J. C **80** \(2020\) 47](#), arXiv: [1909.00761 \[hep-ex\]](#).
- [40] J. Alwall et al., *The automated computation of tree-level and next-to-leading order differential cross sections, and their matching to parton shower simulations*, [JHEP **07** \(2014\) 079](#), arXiv: [1405.0301 \[hep-ph\]](#).
- [41] T. Sjöstrand, S. Mrenna, and P. Skands, *A brief introduction to PYTHIA 8.1*, [Comput. Phys. Commun. **178** \(2008\) 852](#), arXiv: [0710.3820 \[hep-ph\]](#).
- [42] ATLAS Collaboration, *ATLAS Pythia 8 tunes to 7 TeV data*, ATL-PHYS-PUB-2014-021, 2014, URL: <https://cds.cern.ch/record/1966419>.
- [43] R. D. Ball et al., *Parton distributions for the LHC run II*, [JHEP **04** \(2015\) 040](#), arXiv: [1410.8849 \[hep-ph\]](#).
- [44] GEANT4 Collaboration, S. Agostinelli, et al., *GEANT4 – a simulation toolkit*, [Nucl. Instrum. Meth. A **506** \(2003\) 250](#).
- [45] ATLAS Collaboration, *The ATLAS Simulation Infrastructure*, [Eur. Phys. J. C **70** \(2010\) 823](#), arXiv: [1005.4568 \[physics.ins-det\]](#).
- [46] S. Frixione and B. R. Webber, *Matching NLO QCD computations and parton shower simulations*, [JHEP **06** \(2002\) 029](#), arXiv: [hep-ph/0204244](#).
- [47] ATLAS Collaboration, *Example ATLAS tunes of PYTHIA8, PYTHIA6 and POWHEG to an observable sensitive to Z boson transverse momentum*, ATL-PHYS-PUB-2013-017, 2013, URL: <https://cds.cern.ch/record/1629317>.
- [48] J. Pumplin et al., *New Generation of Parton Distributions with Uncertainties from Global QCD Analysis*, [JHEP **07** \(2002\) 012](#), arXiv: [hep-ph/0201195](#).
- [49] W. E. Cleland and E. G. Stern, *Signal processing considerations for liquid ionization calorimeters in a high rate environment*, [Nucl. Instrum. Meth. A **338** \(1994\) 467](#).
- [50] ATLAS Collaboration, *Electron and photon performance measurements with the ATLAS detector using the 2015–2017 LHC proton–proton collision data*, [JINST **14** \(2019\) P12006](#), arXiv: [1908.00005 \[hep-ex\]](#).
- [51] ATLAS Collaboration, *Muon reconstruction and identification efficiency in ATLAS using the full Run 2 pp collision data set at $\sqrt{s} = 13$ TeV*, [Eur. Phys. J. C **81** \(2021\) 578](#), arXiv: [2012.00578 \[hep-ex\]](#).
- [52] M. Cacciari, G. P. Salam, and G. Soyez, *FastJet user manual*, [Eur. Phys. J. C **72** \(2012\) 1896](#), arXiv: [1111.6097 \[hep-ph\]](#).

- [53] ATLAS Collaboration, *Jet reconstruction and performance using particle flow with the ATLAS Detector*, *Eur. Phys. J. C* **77** (2017) 466, arXiv: [1703.10485 \[hep-ex\]](#).
- [54] ATLAS Collaboration, *Topological cell clustering in the ATLAS calorimeters and its performance in LHC Run 1*, *Eur. Phys. J. C* **77** (2017) 490, arXiv: [1603.02934 \[hep-ex\]](#).
- [55] ATLAS Collaboration, *Properties of jets and inputs to jet reconstruction and calibration with the ATLAS detector using proton–proton collisions at $\sqrt{s} = 13$ TeV*, ATL-PHYS-PUB-2015-036, 2015, URL: <https://cds.cern.ch/record/2044564>.
- [56] M. Cacciari, G. P. Salam, and G. Soyez, *The anti- k_t jet clustering algorithm*, *JHEP* **04** (2008) 063, arXiv: [0802.1189 \[hep-ph\]](#).
- [57] ATLAS Collaboration, *Performance of pile-up mitigation techniques for jets in pp collisions at $\sqrt{s} = 8$ TeV using the ATLAS detector*, *Eur. Phys. J. C* **76** (2016) 581, arXiv: [1510.03823 \[hep-ex\]](#).
- [58] ATLAS Collaboration, *Performance of missing transverse momentum reconstruction with the ATLAS detector using proton–proton collisions at $\sqrt{s} = 13$ TeV*, *Eur. Phys. J. C* **78** (2018) 903, arXiv: [1802.08168 \[hep-ex\]](#).
- [59] N. Buchanan et al., *Design and implementation of the Front End Board for the readout of the ATLAS liquid argon calorimeters*, *JINST* **3** (2008) P03004.
- [60] T. Junk, *Confidence level computation for combining searches with small statistics*, *Nucl. Instrum. Meth.* **A434** (1999) 435, arXiv: [hep-ex/9902006 \[hep-ex\]](#).
- [61] A. L. Read, *Presentation of search results: the CL_S technique*, *J. Phys. G* **28** (2002) 2693.
- [62] G. Cowan, K. Cranmer, E. Gross, and O. Vitells, *Asymptotic formulae for likelihood-based tests of new physics*, *Eur. Phys. J. C* **71** (2011) 1554, arXiv: [1007.1727 \[physics.data-an\]](#), Erratum: *Eur. Phys. J. C* **73** (2013) 2501.
- [63] ATLAS Collaboration, *ATLAS Computing Acknowledgements*, ATL-SOFT-PUB-2021-003, 2021, URL: <https://cds.cern.ch/record/2776662>.

The ATLAS Collaboration

G. Aad ¹⁰¹, B. Abbott ¹¹⁹, D.C. Abbott ¹⁰², K. Abeling ⁵⁵, S.H. Abidi ²⁹, A. Aboulhorma ^{35e}, H. Abramowicz ¹⁵⁰, H. Abreu ¹⁴⁹, Y. Abulaiti ¹¹⁶, A.C. Abusleme Hoffman ^{136a}, B.S. Acharya ^{68a,68b,q}, B. Achkar ⁵⁵, C. Adam Bourdarios ⁴, L. Adamczyk ^{84a}, L. Adamek ¹⁵⁴, S.V. Addepalli ²⁶, J. Adelman ¹¹⁴, A. Adiguzel ^{21c}, S. Adorni ⁵⁶, T. Adye ¹³³, A.A. Affolder ¹³⁵, Y. Afik ³⁶, M.N. Agaras ¹³, J. Agarwala ^{72a,72b}, A. Aggarwal ⁹⁹, C. Agheorghiesei ^{27c}, J.A. Aguilar-Saavedra ^{129f}, A. Ahmad ³⁶, F. Ahmadov ^{38,ab}, W.S. Ahmed ¹⁰³, S. Ahuja ⁹⁴, X. Ai ⁴⁸, G. Aielli ^{75a,75b}, I. Aizenberg ¹⁶⁸, M. Akbiyik ⁹⁹, T.P.A. Åkesson ⁹⁷, A.V. Akimov ³⁷, K. Al Khoury ⁴¹, G.L. Alberghi ^{23b}, J. Albert ¹⁶⁴, P. Albicocco ⁵³, S. Alderweireldt ⁵², M. Aleksa ³⁶, I.N. Aleksandrov ³⁸, C. Alexa ^{27b}, T. Alexopoulos ¹⁰, A. Alfonsi ¹¹³, F. Alfonsi ^{23b}, M. Alhroob ¹¹⁹, B. Ali ¹³¹, S. Ali ¹⁴⁷, M. Aliev ³⁷, G. Alimonti ^{70a}, W. Alkahi ⁵⁵, C. Allaire ⁶⁶, B.M.M. Allbrooke ¹⁴⁵, P.P. Allport ²⁰, A. Aloisio ^{71a,71b}, F. Alonso ⁸⁹, C. Alpigiani ¹³⁷, E. Alunno Camelia ^{75a,75b}, M. Alvarez Estevez ⁹⁸, M.G. Alvigi ^{71a,71b}, M. Aly ¹⁰⁰, Y. Amaral Coutinho ^{81b}, A. Ambler ¹⁰³, C. Amelung ³⁶, M. Amerl ¹, C.G. Ames ¹⁰⁸, D. Amidei ¹⁰⁵, S.P. Amor Dos Santos ^{129a}, S. Amoroso ⁴⁸, K.R. Amos ¹⁶², V. Ananiev ¹²⁴, C. Anastopoulos ¹³⁸, T. Andeen ¹¹, J.K. Anders ³⁶, S.Y. Andrean ^{47a,47b}, A. Andreatta ^{70a,70b}, S. Angelidakis ⁹, A. Angerami ^{41,ae}, A.V. Anisenkov ³⁷, A. Annovi ^{73a}, C. Antel ⁵⁶, M.T. Anthony ¹³⁸, E. Antipov ¹²⁰, M. Antonelli ⁵³, D.J.A. Antrim ^{17a}, F. Anulli ^{74a}, M. Aoki ⁸², T. Aoki ¹⁵², J.A. Aparisi Pozo ¹⁶², M.A. Aparo ¹⁴⁵, L. Aperio Bella ⁴⁸, C. Appelt ¹⁸, N. Aranzabal ³⁶, V. Araujo Ferraz ^{81a}, C. Arcangeletti ⁵³, A.T.H. Arce ⁵¹, E. Arena ⁹¹, J-F. Arguin ¹⁰⁷, S. Argyropoulos ⁵⁴, J.-H. Arling ⁴⁸, A.J. Armbruster ³⁶, O. Arnaez ¹⁵⁴, H. Arnold ¹¹³, Z.P. Arrubarrena Tame ¹⁰⁸, G. Artoni ^{74a,74b}, H. Asada ¹¹⁰, K. Asai ¹¹⁷, S. Asai ¹⁵², N.A. Asbah ⁶¹, J. Assahsah ^{35d}, K. Assamagan ²⁹, R. Astalos ^{28a}, R.J. Atkin ^{33a}, M. Atkinson ¹⁶¹, N.B. Atlay ¹⁸, H. Atmani ^{62b}, P.A. Atmasiddha ¹⁰⁵, K. Augsten ¹³¹, S. Auricchio ^{71a,71b}, A.D. Auriol ²⁰, V.A. Austrup ¹⁷⁰, G. Avner ¹⁴⁹, G. Avolio ³⁶, K. Axiotis ⁵⁶, M.K. Ayoub ^{14c}, G. Azuelos ^{107,aj}, D. Babal ^{28a}, H. Bachacou ¹³⁴, K. Bachas ^{151,i}, A. Bachiu ³⁴, F. Backman ^{47a,47b}, A. Badea ⁶¹, P. Bagnaia ^{74a,74b}, M. Bahmani ¹⁸, A.J. Bailey ¹⁶², V.R. Bailey ¹⁶¹, J.T. Baines ¹³³, C. Bakalis ¹⁰, O.K. Baker ¹⁷¹, P.J. Bakker ¹¹³, E. Bakos ¹⁵, D. Bakshi Gupta ⁸, S. Balaji ¹⁴⁶, R. Balasubramanian ¹¹³, E.M. Baldin ³⁷, P. Balek ¹³², E. Ballabene ^{70a,70b}, F. Balli ¹³⁴, L.M. Baltes ^{63a}, W.K. Balunas ³², J. Balz ⁹⁹, E. Banas ⁸⁵, M. Bandieramonte ¹²⁸, A. Bandyopadhyay ²⁴, S. Bansal ²⁴, L. Barak ¹⁵⁰, E.L. Barberio ¹⁰⁴, D. Barberis ^{57b,57a}, M. Barbero ¹⁰¹, G. Barbour ⁹⁵, K.N. Barends ^{33a}, T. Barillari ¹⁰⁹, M-S. Barisits ³⁶, T. Barklow ¹⁴², R.M. Barnett ^{17a}, P. Baron ¹²¹, D.A. Baron Moreno ¹⁰⁰, A. Baroncelli ^{62a}, G. Barone ²⁹, A.J. Barr ¹²⁵, L. Barranco Navarro ^{47a,47b}, F. Barreiro ⁹⁸, J. Barreiro Guimarães da Costa ^{14a}, U. Barron ¹⁵⁰, M.G. Barros Teixeira ^{129a}, S. Barsov ³⁷, F. Bartels ^{63a}, R. Bartoldus ¹⁴², A.E. Barton ⁹⁰, P. Bartos ^{28a}, A. Basalae ⁴⁸, A. Basan ⁹⁹, M. Baselga ⁴⁹, I. Bashta ^{76a,76b}, A. Bassalat ^{66,b}, M.J. Basso ¹⁵⁴, C.R. Basson ¹⁰⁰, R.L. Bates ⁵⁹, S. Batlamous ^{35e}, J.R. Batley ³², B. Batool ¹⁴⁰, M. Battaglia ¹³⁵, D. Battulga ¹⁸, M. Baucé ^{74a,74b}, P. Bauer ²⁴, A. Bayirli ^{21a}, J.B. Beacham ⁵¹, T. Beau ¹²⁶, P.H. Beauchemin ¹⁵⁷, F. Becherer ⁵⁴, P. Bechtel ²⁴, H.P. Beck ^{19,s}, K. Becker ¹⁶⁶, A.J. Beddall ^{21d}, V.A. Bednyakov ³⁸, C.P. Bee ¹⁴⁴, L.J. Beemster ¹⁵, T.A. Beermann ³⁶, M. Begalli ^{81d}, M. Begel ²⁹, A. Behera ¹⁴⁴, J.K. Behr ⁴⁸, C. Beirao Da Cruz E Silva ³⁶, J.F. Beirer ^{55,36}, F. Beisiegel ²⁴, M. Belfkir ¹⁵⁸, G. Bella ¹⁵⁰, L. Bellagamba ^{23b}, A. Bellerive ³⁴, P. Bellos ²⁰, K. Beloborodov ³⁷, K. Belotskiy ³⁷, N.L. Belyaev ³⁷, D. Benckekroun ^{35a}, F. Bendebba ^{35a}, Y. Benhammou ¹⁵⁰, D.P. Benjamin ²⁹,

M. Benoit ²⁹, J.R. Bensinger ²⁶, S. Bentvelsen ¹¹³, L. Beresford ³⁶, M. Beretta ⁵³, D. Berge ¹⁸,
E. Bergeaas Kuutmann ¹⁶⁰, N. Berger ⁴, B. Bergmann ¹³¹, J. Beringer ^{17a}, S. Berlendis ⁷,
G. Bernardi ⁵, C. Bernius ¹⁴², F.U. Bernlochner ²⁴, T. Berry ⁹⁴, P. Berta ¹³², A. Berthold ⁵⁰,
I.A. Bertram ⁹⁰, S. Bethke ¹⁰⁹, A. Betti ^{74a,74b}, A.J. Bevan ⁹³, M. Bhamjee ^{33c}, S. Bhatta ¹⁴⁴,
D.S. Bhattacharya ¹⁶⁵, P. Bhattarai ²⁶, V.S. Bhopatkar ¹²⁰, R. Bi ^{29,am}, R.M. Bianchi ¹²⁸,
O. Biebel ¹⁰⁸, R. Bielski ¹²², M. Biglietti ^{76a}, T.R.V. Billoud ¹³¹, M. Bindi ⁵⁵, A. Bingul ^{21b},
C. Bini ^{74a,74b}, S. Biondi ^{23b,23a}, A. Biondini ⁹¹, C.J. Birch-sykes ¹⁰⁰, G.A. Bird ^{20,133},
M. Birman ¹⁶⁸, T. Bisanz ³⁶, E. Bisceglie ^{43b,43a}, D. Biswas ^{169,m}, A. Bitadze ¹⁰⁰, K. Bjørke ¹²⁴,
I. Bloch ⁴⁸, C. Blocker ²⁶, A. Blue ⁵⁹, U. Blumenschein ⁹³, J. Blumenthal ⁹⁹, G.J. Bobbink ¹¹³,
V.S. Bobrovnikov ³⁷, M. Boehler ⁵⁴, D. Bogavac ³⁶, A.G. Bogdanchikov ³⁷, C. Bohm ^{47a},
V. Boisvert ⁹⁴, P. Bokan ⁴⁸, T. Bold ^{84a}, M. Bomben ⁵, M. Bona ⁹³, M. Boonekamp ¹³⁴,
C.D. Booth ⁹⁴, A.G. Borbély ⁵⁹, H.M. Borecka-Bielska ¹⁰⁷, L.S. Borgna ⁹⁵, G. Borissov ⁹⁰,
D. Bortoletto ¹²⁵, D. Boscherini ^{23b}, M. Bosman ¹³, J.D. Bossio Sola ³⁶, K. Bouaouda ^{35a},
N. Bouchhar ¹⁶², J. Boudreau ¹²⁸, E.V. Bouhova-Thacker ⁹⁰, D. Boumediene ⁴⁰, R. Bouquet ⁵,
A. Boveia ¹¹⁸, J. Boyd ³⁶, D. Boye ²⁹, I.R. Boyko ³⁸, J. Bracinik ²⁰, N. Brahimi ^{62d},
G. Brandt ¹⁷⁰, O. Brandt ³², F. Braren ⁴⁸, B. Brau ¹⁰², J.E. Brau ¹²², K. Brendlinger ⁴⁸,
R. Brenner ¹⁶⁸, L. Brenner ¹¹³, R. Brenner ¹⁶⁰, S. Bressler ¹⁶⁸, B. Brickwedde ⁹⁹, D. Britton ⁵⁹,
D. Britzger ¹⁰⁹, I. Brock ²⁴, G. Brooijmans ⁴¹, W.K. Brooks ^{136f}, E. Brost ²⁹, T.L. Bruckler ¹²⁵,
P.A. Bruckman de Renstrom ⁸⁵, B. Brüers ⁴⁸, D. Bruncko ^{28b,*}, A. Bruni ^{23b}, G. Bruni ^{23b},
M. Bruschi ^{23b}, N. Bruscinò ^{74a,74b}, L. Bryngemark ¹⁴², T. Buanes ¹⁶, Q. Buat ¹³⁷,
P. Buchholz ¹⁴⁰, A.G. Buckley ⁵⁹, I.A. Budagov ^{38,*}, M.K. Bugge ¹²⁴, O. Bulekov ³⁷,
B.A. Bullard ⁶¹, S. Burdin ⁹¹, C.D. Burgard ⁴⁸, A.M. Burger ⁴⁰, B. Burghgrave ⁸, J.T.P. Burr ³²,
C.D. Burton ¹¹, J.C. Burzynski ¹⁴¹, E.L. Busch ⁴¹, V. Büscher ⁹⁹, P.J. Bussey ⁵⁹, J.M. Butler ²⁵,
C.M. Buttar ⁵⁹, J.M. Butterworth ⁹⁵, W. Buttinger ¹³³, C.J. Buxo Vazquez ¹⁰⁶, A.R. Buzykaev ³⁷,
G. Cabras ^{23b}, S. Cabrera Urbán ¹⁶², D. Caforio ⁵⁸, H. Cai ¹²⁸, Y. Cai ^{14a,14d}, V.M.M. Cairo ³⁶,
O. Cakir ^{3a}, N. Calace ³⁶, P. Calafiura ^{17a}, G. Calderini ¹²⁶, P. Calfayan ⁶⁷, G. Callea ⁵⁹,
L.P. Caloba ^{81b}, D. Calvet ⁴⁰, S. Calvet ⁴⁰, T.P. Calvet ¹⁰¹, M. Calvetti ^{73a,73b},
R. Camacho Toro ¹²⁶, S. Camarda ³⁶, D. Camarero Munoz ²⁶, P. Camarri ^{75a,75b},
M.T. Camerlingo ^{76a,76b}, D. Cameron ¹²⁴, C. Camincher ¹⁶⁴, M. Campanelli ⁹⁵, A. Camplani ⁴²,
V. Canale ^{71a,71b}, A. Canesse ¹⁰³, M. Cano Bret ⁷⁹, J. Cantero ¹⁶², Y. Cao ¹⁶¹, F. Capocasa ²⁶,
M. Capua ^{43b,43a}, A. Carbone ^{70a,70b}, R. Cardarelli ^{75a}, J.C.J. Cardenas ⁸, F. Cardillo ¹⁶²,
T. Carli ³⁶, G. Carlino ^{71a}, J.I. Carlotto ¹³, B.T. Carlson ^{128,u}, E.M. Carlson ^{164,155a},
L. Carminati ^{70a,70b}, M. Carnesale ^{74a,74b}, S. Caron ¹¹², E. Carquin ^{136f}, S. Carrá ^{70a,70b},
G. Carratta ^{23b,23a}, F. Carri Argos ^{33g}, J.W.S. Carter ¹⁵⁴, T.M. Carter ⁵², M.P. Casado ^{13j},
A.F. Casha ¹⁵⁴, E.G. Castiglia ¹⁷¹, F.L. Castillo ^{63a}, L. Castillo Garcia ¹³, V. Castillo Gimenez ¹⁶²,
N.F. Castro ^{129a,129e}, A. Catinaccio ³⁶, J.R. Catmore ¹²⁴, V. Cavaliere ²⁹, N. Cavalli ^{23b,23a},
V. Cavasinni ^{73a,73b}, E. Celebi ^{21a}, F. Celli ¹²⁵, M.S. Centonze ^{69a,69b}, K. Cerny ¹²¹,
A.S. Cerqueira ^{81a}, A. Cerri ¹⁴⁵, L. Cerrito ^{75a,75b}, F. Cerutti ^{17a}, A. Cervelli ^{23b}, S.A. Cetin ^{21d},
Z. Chadi ^{35a}, D. Chakraborty ¹¹⁴, M. Chala ^{129f}, J. Chan ¹⁶⁹, W.Y. Chan ¹⁵², J.D. Chapman ³²,
B. Chargeishvili ^{148b}, D.G. Charlton ²⁰, T.P. Charman ⁹³, M. Chatterjee ¹⁹, S. Chekanov ⁶,
S.V. Chekulaev ^{155a}, G.A. Chelkov ^{38,a}, A. Chen ¹⁰⁵, B. Chen ¹⁵⁰, B. Chen ¹⁶⁴, H. Chen ^{14c},
H. Chen ²⁹, J. Chen ^{62c}, J. Chen ²⁶, S. Chen ¹⁵², S.J. Chen ^{14c}, X. Chen ^{62c}, X. Chen ^{14b,ai},
Y. Chen ^{62a}, C.L. Cheng ¹⁶⁹, H.C. Cheng ^{64a}, S. Cheong ¹⁴², A. Cheplakov ³⁸,
E. Cheremushkina ⁴⁸, E. Cherepanova ¹¹³, R. Cherkaoui El Moursli ^{35e}, E. Cheu ⁷, K. Cheung ⁶⁵,
L. Chevalier ¹³⁴, V. Chiarella ⁵³, G. Chiarelli ^{73a}, N. Chiedde ¹⁰¹, G. Chiodini ^{69a},
A.S. Chisholm ²⁰, A. Chitan ^{27b}, M. Chitishvili ¹⁶², Y.H. Chiu ¹⁶⁴, M.V. Chizhov ³⁸, K. Choi ¹¹,
A.R. Chomont ^{74a,74b}, Y. Chou ¹⁰², E.Y.S. Chow ¹¹³, T. Chowdhury ^{33g}, L.D. Christopher ^{33g},

K.L. Chu^{64a}, M.C. Chu^{64a}, X. Chu^{14a,14d}, J. Chudoba¹³⁰, J.J. Chwastowski⁸⁵, D. Cieri¹⁰⁹,
 K.M. Ciesla^{84a}, V. Cindro⁹², A. Ciocio^{17a}, F. Citroto^{71a,71b}, Z.H. Citron^{168,n}, M. Citterio^{70a},
 D.A. Ciubotaru^{27b}, B.M. Ciungu¹⁵⁴, A. Clark⁵⁶, P.J. Clark⁵², J.M. Clavijo Columbie⁴⁸,
 S.E. Clawson¹⁰⁰, C. Clement^{47a,47b}, J. Clercx⁴⁸, L. Clissa^{23b,23a}, Y. Coadou¹⁰¹,
 M. Cobal^{68a,68c}, A. Coccaro^{57b}, R.F. Coelho Barrue^{129a}, R. Coelho Lopes De Sa¹⁰²,
 S. Coelli^{70a}, H. Cohen¹⁵⁰, A.E.C. Coimbra^{70a,70b}, B. Cole⁴¹, J. Collot⁶⁰,
 P. Conde Muiño^{129a,129g}, M.P. Connell^{33c}, S.H. Connell^{33c}, I.A. Connelly⁵⁹, E.I. Conroy¹²⁵,
 F. Conventi^{71a,ak}, H.G. Cooke²⁰, A.M. Cooper-Sarkar¹²⁵, F. Cormier¹⁶³, L.D. Corpe³⁶,
 M. Corradi^{74a,74b}, E.E. Corrigan⁹⁷, F. Corriveau^{103,z}, A. Cortes-Gonzalez¹⁸, M.J. Costa¹⁶²,
 F. Costanza⁴, D. Costanzo¹³⁸, B.M. Cote¹¹⁸, G. Cowan⁹⁴, J.W. Cowley³², K. Cranmer¹¹⁶,
 S. Crépe-Renaudin⁶⁰, F. Crescioli¹²⁶, M. Cristinziani¹⁴⁰, M. Cristoforetti^{77a,77b,d}, V. Croft¹⁵⁷,
 G. Crosetti^{43b,43a}, A. Cueto³⁶, T. Cuhadar Donszelmann¹⁵⁹, H. Cui^{14a,14d}, Z. Cui⁷,
 A.R. Cukierman¹⁴², W.R. Cunningham⁵⁹, F. Curcio^{43b,43a}, P. Czodrowski³⁶, M.M. Czurylo^{63b},
 M.J. Da Cunha Sargedas De Sousa^{62a}, J.V. Da Fonseca Pinto^{81b}, C. Da Via¹⁰⁰, W. Dabrowski^{84a},
 T. Dado⁴⁹, S. Dahbi^{33g}, T. Dai¹⁰⁵, C. Dallapiccola¹⁰², M. Dam⁴², G. D'amen²⁹,
 V. D'Amico¹⁰⁸, J. Damp⁹⁹, J.R. Dandoy¹²⁷, M.F. Daneri³⁰, M. Danninger¹⁴¹, V. Dao³⁶,
 G. Darbo^{57b}, S. Darmora⁶, S.J. Das^{29,am}, S. D'Auria^{70a,70b}, C. David^{155b}, T. Davidek¹³²,
 D.R. Davis⁵¹, B. Davis-Purcell³⁴, I. Dawson⁹³, K. De⁸, R. De Asmundis^{71a},
 M. De Beurs¹¹³, N. De Biase⁴⁸, S. De Castro^{23b,23a}, N. De Groot¹¹², P. de Jong¹¹³,
 H. De la Torre¹⁰⁶, A. De Maria^{14c}, A. De Salvo^{74a}, U. De Sanctis^{75a,75b}, A. De Santo¹⁴⁵,
 J.B. De Vivie De Regie⁶⁰, D.V. Dedovich³⁸, J. Degens¹¹³, A.M. Deiana⁴⁴, F. Del Corso^{23b,23a},
 J. Del Peso⁹⁸, F. Del Rio^{63a}, F. Deliot¹³⁴, C.M. Delitzsch⁴⁹, M. Della Pietra^{71a,71b},
 D. Della Volpe⁵⁶, A. Dell'Acqua³⁶, L. Dell'Asta^{70a,70b}, M. Delmastro⁴, P.A. Delsart⁶⁰,
 S. Demers¹⁷¹, M. Demichev³⁸, S.P. Denisov³⁷, L. D'Eramo¹¹⁴, D. Derendarz⁸⁵,
 F. Derue¹²⁶, P. Dervan⁹¹, K. Desch²⁴, K. Dette¹⁵⁴, C. Deutsch²⁴, P.O. Deviveiros³⁶,
 F.A. Di Bello^{57b,57a}, A. Di Ciaccio^{75a,75b}, L. Di Ciaccio⁴, A. Di Domenico^{74a,74b},
 C. Di Donato^{71a,71b}, A. Di Girolamo³⁶, G. Di Gregorio⁵, A. Di Luca^{77a,77b}, B. Di Micco^{76a,76b},
 R. Di Nardo^{76a,76b}, C. Diaconu¹⁰¹, F.A. Dias¹¹³, T. Dias Do Vale¹⁴¹, M.A. Diaz^{136a,136b},
 F.G. Diaz Capriles²⁴, M. Didenko¹⁶², E.B. Diehl¹⁰⁵, L. Diehl⁵⁴, S. Díez Cornell⁴⁸,
 C. Diez Pardos¹⁴⁰, C. Dimitriadi^{24,160}, A. Dimitrievska^{17a}, W. Ding^{14b}, J. Dingfelder²⁴,
 I-M. Dinu^{27b}, S.J. Dittmeier^{63b}, F. Dittus³⁶, F. Djama¹⁰¹, T. Djobava^{148b}, J.I. Djuvsland¹⁶,
 C. Doglioni^{100,97}, J. Dolejsi¹³², Z. Dolezal¹³², M. Donadelli^{81c}, B. Dong^{62c}, J. Donini⁴⁰,
 A. D'Onofrio^{14c}, M. D'Onofrio⁹¹, J. Dopke¹³³, A. Doria^{71a}, M.T. Dova⁸⁹, A.T. Doyle⁵⁹,
 M.A. Draguet¹²⁵, E. Drechsler¹⁴¹, E. Dreyer¹⁶⁸, I. Drivas-koulouris¹⁰, A.S. Drobac¹⁵⁷,
 M. Drozdova⁵⁶, D. Du^{62a}, T.A. du Pree¹¹³, F. Dubinin³⁷, M. Dubovsky^{28a}, E. Duchovni¹⁶⁸,
 G. Duckeck¹⁰⁸, O.A. Ducu^{27b}, D. Duda¹⁰⁹, A. Dudarev³⁶, M. D'uffizi¹⁰⁰, L. Duflost⁶⁶,
 M. Dührssen³⁶, C. Dülsen¹⁷⁰, A.E. Dumitriu^{27b}, M. Dunford^{63a}, S. Dungs⁴⁹,
 K. Dunne^{47a,47b}, A. Duperrin¹⁰¹, H. Duran Yildiz^{3a}, M. Düren⁵⁸, A. Durglishvili^{148b},
 B.L. Dwyer¹¹⁴, G.I. Dyckes^{17a}, M. Dyndal^{84a}, S. Dysch¹⁰⁰, B.S. Dziedzic⁸⁵,
 Z.O. Earnshaw¹⁴⁵, B. Eckerova^{28a}, M.G. Eggleston⁵¹, E. Egidio Purcino De Souza^{81b},
 L.F. Ehrke⁵⁶, G. Eigen¹⁶, K. Einsweiler^{17a}, T. Ekelof¹⁶⁰, P.A. Ekman⁹⁷, Y. El Ghazali^{35b},
 H. El Jarrari^{35e,147}, A. El Moussaouy^{35a}, V. Ellajosyula¹⁶⁰, M. Ellert¹⁶⁰, F. Ellinghaus¹⁷⁰,
 A.A. Elliot⁹³, N. Ellis³⁶, J. Elmsheuser²⁹, M. Elsing³⁶, D. Emelianov¹³³, A. Emerman⁴¹,
 Y. Enari¹⁵², I. Ene^{17a}, S. Epari¹³, J. Erdmann^{49,ag}, A. Ereditato¹⁹, P.A. Erland⁸⁵,
 M. Errenst¹⁷⁰, M. Escalier⁶⁶, C. Escobar¹⁶², E. Etzion¹⁵⁰, G. Evans^{129a}, H. Evans⁶⁷,
 M.O. Evans¹⁴⁵, A. Ezhilov³⁷, S. Ezzarqtouni^{35a}, F. Fabbri⁵⁹, L. Fabbri^{23b,23a}, G. Facini⁹⁵,
 V. Fadeyev¹³⁵, R.M. Fakhrutdinov³⁷, S. Falciano^{74a}, P.J. Falke²⁴, S. Falke³⁶, J. Faltova¹³²,

Y. Fan [id](#)^{14a}, Y. Fang [id](#)^{14a,14d}, G. Fanourakis [id](#)⁴⁶, M. Fanti [id](#)^{70a,70b}, M. Faraj [id](#)^{68a,68b}, Z. Farazpay⁹⁶,
 A. Farbin [id](#)⁸, A. Farilla [id](#)^{76a}, T. Faroouque [id](#)¹⁰⁶, S.M. Farrington [id](#)⁵², F. Fassi [id](#)^{35e}, D. Fassouliotis [id](#)⁹,
 M. Faucci Giannelli [id](#)^{75a,75b}, W.J. Fawcett [id](#)³², L. Fayard [id](#)⁶⁶, P. Federicova [id](#)¹³⁰, O.L. Fedin [id](#)^{37,a},
 G. Fedotov [id](#)³⁷, M. Feickert [id](#)¹⁶⁹, L. Feligioni [id](#)¹⁰¹, A. Fell [id](#)¹³⁸, D.E. Fellers [id](#)¹²², C. Feng [id](#)^{62b},
 M. Feng [id](#)^{14b}, Z. Feng [id](#)¹¹³, M.J. Fenton [id](#)¹⁵⁹, A.B. Fenyuk³⁷, L. Ferencz [id](#)⁴⁸, S.W. Ferguson [id](#)⁴⁵,
 J. Ferrando [id](#)⁴⁸, A. Ferrari [id](#)¹⁶⁰, P. Ferrari [id](#)^{113,112}, R. Ferrari [id](#)^{72a}, D. Ferrere [id](#)⁵⁶, C. Ferretti [id](#)¹⁰⁵,
 F. Fiedler [id](#)⁹⁹, A. Filipčič [id](#)⁹², E.K. Filmer [id](#)¹, F. Filthaut [id](#)¹¹², M.C.N. Fiolhais [id](#)^{129a,129c,c},
 L. Fiorini [id](#)¹⁶², F. Fischer [id](#)¹⁴⁰, W.C. Fisher [id](#)¹⁰⁶, T. Fitschen [id](#)¹⁰⁰, I. Fleck [id](#)¹⁴⁰, P. Fleischmann [id](#)¹⁰⁵,
 T. Flick [id](#)¹⁷⁰, L. Flores [id](#)¹²⁷, M. Flores [id](#)^{33d,af}, L.R. Flores Castillo [id](#)^{64a}, F.M. Follega [id](#)^{77a,77b},
 N. Fomin [id](#)¹⁶, J.H. Foo [id](#)¹⁵⁴, B.C. Forland⁶⁷, A. Formica [id](#)¹³⁴, A.C. Forti [id](#)¹⁰⁰, E. Fortin [id](#)¹⁰¹,
 A.W. Fortman [id](#)⁶¹, M.G. Foti [id](#)^{17a}, L. Fountas [id](#)^{9,k}, D. Fournier [id](#)⁶⁶, H. Fox [id](#)⁹⁰, P. Francavilla [id](#)^{73a,73b},
 S. Francescato [id](#)⁶¹, S. Franchellucci [id](#)⁵⁶, M. Franchini [id](#)^{23b,23a}, S. Franchino [id](#)^{63a}, D. Francis³⁶,
 L. Franco [id](#)¹¹², L. Franconi [id](#)¹⁹, M. Franklin [id](#)⁶¹, G. Frattari [id](#)²⁶, A.C. Freegard [id](#)⁹³, P.M. Freeman²⁰,
 W.S. Freund [id](#)^{81b}, N. Fritzsche [id](#)⁵⁰, A. Froch [id](#)⁵⁴, D. Froidevaux [id](#)³⁶, J.A. Frost [id](#)¹²⁵, Y. Fu [id](#)^{62a},
 M. Fujimoto [id](#)¹¹⁷, E. Fullana Torregrosa [id](#)^{162,*}, J. Fuster [id](#)¹⁶², A. Gabrielli [id](#)^{23b,23a}, A. Gabrielli [id](#)¹⁵⁴,
 P. Gadow [id](#)⁴⁸, G. Gagliardi [id](#)^{57b,57a}, L.G. Gagnon [id](#)^{17a}, G.E. Gallardo [id](#)¹²⁵, E.J. Gallas [id](#)¹²⁵,
 B.J. Gallop [id](#)¹³³, R. Gamboa Goni [id](#)⁹³, K.K. Gan [id](#)¹¹⁸, S. Ganguly [id](#)¹⁵², J. Gao [id](#)^{62a}, Y. Gao [id](#)⁵²,
 F.M. Garay Walls [id](#)^{136a,136b}, B. Garcia^{29,am}, C. García [id](#)¹⁶², J.E. García Navarro [id](#)¹⁶²,
 J.A. García Pascual [id](#)^{14a}, M. Garcia-Sciveres [id](#)^{17a}, R.W. Gardner [id](#)³⁹, D. Garg [id](#)⁷⁹, R.B. Garg [id](#)^{142,r},
 S. Gargiulo [id](#)⁵⁴, C.A. Garner¹⁵⁴, V. Garonne [id](#)²⁹, S.J. Gasiorowski [id](#)¹³⁷, P. Gaspar [id](#)^{81b}, G. Gaudio [id](#)^{72a},
 V. Gautam¹³, P. Gauzzi [id](#)^{74a,74b}, I.L. Gavrilenko [id](#)³⁷, A. Gavrilyuk [id](#)³⁷, C. Gay [id](#)¹⁶³, G. Gaycken [id](#)⁴⁸,
 E.N. Gazis [id](#)¹⁰, A.A. Geanta [id](#)^{27b,27e}, C.M. Gee [id](#)¹³⁵, J. Geisen [id](#)⁹⁷, M. Geisen [id](#)⁹⁹, C. Gemme [id](#)^{57b},
 M.H. Genest [id](#)⁶⁰, S. Gentile [id](#)^{74a,74b}, S. George [id](#)⁹⁴, W.F. George [id](#)²⁰, T. Geralis [id](#)⁴⁶, L.O. Gerlach⁵⁵,
 P. Gessinger-Befurt [id](#)³⁶, M. Ghasemi Bostanabad [id](#)¹⁶⁴, M. Ghneimat [id](#)¹⁴⁰, K. Ghorbanian [id](#)⁹³,
 A. Ghosal [id](#)¹⁴⁰, A. Ghosh [id](#)¹⁵⁹, A. Ghosh [id](#)⁷, B. Giacobbe [id](#)^{23b}, S. Giagu [id](#)^{74a,74b},
 N. Giangiacomi [id](#)¹⁵⁴, P. Giannetti [id](#)^{73a}, A. Giannini [id](#)^{62a}, S.M. Gibson [id](#)⁹⁴, M. Gignac [id](#)¹³⁵,
 D.T. Gil [id](#)^{84b}, A.K. Gilbert [id](#)^{84a}, B.J. Gilbert [id](#)⁴¹, D. Gillberg [id](#)³⁴, G. Gilles [id](#)¹¹³, N.E.K. Gillwald [id](#)⁴⁸,
 L. Ginabat [id](#)¹²⁶, D.M. Gingrich [id](#)^{2,aj}, M.P. Giordani [id](#)^{68a,68c}, P.F. Giraud [id](#)¹³⁴, G. Giugliarelli [id](#)^{68a,68c},
 D. Giugni [id](#)^{70a}, F. Giuli [id](#)³⁶, I. Gkialas [id](#)^{9,k}, L.K. Gladilin [id](#)³⁷, C. Glasman [id](#)⁹⁸, G.R. Gledhill [id](#)¹²²,
 M. Glisic¹²², I. Gnesi [id](#)^{43b,g}, Y. Go [id](#)^{29,am}, M. Goblirsch-Kolb [id](#)²⁶, B. Gocke [id](#)⁴⁹, D. Godin¹⁰⁷,
 S. Goldfarb [id](#)¹⁰⁴, T. Golling [id](#)⁵⁶, M.G.D. Gololo^{33g}, D. Golubkov [id](#)³⁷, J.P. Gombas [id](#)¹⁰⁶,
 A. Gomes [id](#)^{129a,129b}, G. Gomes Da Silva [id](#)¹⁴⁰, A.J. Gomez Delegido [id](#)¹⁶², R. Goncalves Gama [id](#)⁵⁵,
 R. Gonçalves [id](#)^{129a,129c}, G. Gonella [id](#)¹²², L. Gonella [id](#)²⁰, A. Gongadze [id](#)³⁸, F. Gonnella [id](#)²⁰,
 J.L. Gonski [id](#)⁴¹, R.Y. González Andana [id](#)⁵², S. González de la Hoz [id](#)¹⁶², S. Gonzalez Fernandez [id](#)¹³,
 R. Gonzalez Lopez [id](#)⁹¹, C. Gonzalez Renteria [id](#)^{17a}, R. Gonzalez Suarez [id](#)¹⁶⁰, S. Gonzalez-Sevilla [id](#)⁵⁶,
 G.R. Gonzalvo Rodriguez [id](#)¹⁶², L. Goossens [id](#)³⁶, N.A. Gorasia [id](#)²⁰, P.A. Gorbounov [id](#)³⁷, B. Gorini [id](#)³⁶,
 E. Gorini [id](#)^{69a,69b}, A. Gorišek [id](#)⁹², A.T. Goshaw [id](#)⁵¹, M.I. Gostkin [id](#)³⁸, C.A. Gottardo [id](#)³⁶,
 M. Goughri [id](#)^{35b}, V. Goumarre [id](#)⁴⁸, A.G. Goussiou [id](#)¹³⁷, N. Govender [id](#)^{33c}, C. Goy [id](#)⁴,
 I. Grabowska-Bold [id](#)^{84a}, K. Graham [id](#)³⁴, E. Gramstad [id](#)¹²⁴, S. Grancagnolo [id](#)¹⁸, M. Grandi [id](#)¹⁴⁵,
 V. Gratchev^{37,*}, P.M. Gravila [id](#)^{27f}, F.G. Gravili [id](#)^{69a,69b}, H.M. Gray [id](#)^{17a}, M. Greco [id](#)^{69a,69b},
 C. Grefe [id](#)²⁴, I.M. Gregor [id](#)⁴⁸, P. Grenier [id](#)¹⁴², C. Grieco [id](#)¹³, A.A. Grillo [id](#)¹³⁵, K. Grimm [id](#)^{31,o},
 S. Grinstein [id](#)^{13,w}, J.-F. Grivaz [id](#)⁶⁶, E. Gross [id](#)¹⁶⁸, J. Grosse-Knetter [id](#)⁵⁵, C. Grud¹⁰⁵, A. Grummer [id](#)¹¹¹,
 J.C. Grundy [id](#)¹²⁵, L. Guan [id](#)¹⁰⁵, W. Guan [id](#)¹⁶⁹, C. Gubbels [id](#)¹⁶³, J.G.R. Guerrero Rojas [id](#)¹⁶²,
 G. Guerrieri [id](#)^{68a,68b}, F. Guescini [id](#)¹⁰⁹, R. Gugel [id](#)⁹⁹, J.A.M. Guhit [id](#)¹⁰⁵, A. Guida [id](#)⁴⁸, T. Guillemain [id](#)⁴,
 E. Guilloton [id](#)^{166,133}, S. Guindon [id](#)³⁶, F. Guo [id](#)^{14a,14d}, J. Guo [id](#)^{62c}, L. Guo [id](#)⁶⁶, Y. Guo [id](#)¹⁰⁵,
 R. Gupta [id](#)⁴⁸, S. Gurbuz [id](#)²⁴, S.S. Gurdasani [id](#)⁵⁴, G. Gustavino [id](#)³⁶, M. Guth [id](#)⁵⁶, P. Gutierrez [id](#)¹¹⁹,
 L.F. Gutierrez Zagazeta [id](#)¹²⁷, C. Gutschow [id](#)⁹⁵, C. Guyot [id](#)¹³⁴, C. Gwenlan [id](#)¹²⁵, C.B. Gwilliam [id](#)⁹¹,

E.S. Haaland ¹²⁴, A. Haas ¹¹⁶, M. Habedank ⁴⁸, C. Haber ^{17a}, H.K. Hadavand ⁸, A. Hadeif ⁹⁹,
 S. Hadzic ¹⁰⁹, E.H. Haines ⁹⁵, M. Haleem ¹⁶⁵, J. Haley ¹²⁰, J.J. Hall ¹³⁸, G.D. Hallelwell ¹⁰¹,
 L. Halser ¹⁹, K. Hamano ¹⁶⁴, H. Hamdaoui ^{35e}, M. Hamer ²⁴, G.N. Hamity ⁵², J. Han ^{62b},
 K. Han ^{62a}, L. Han ^{14c}, L. Han ^{62a}, S. Han ^{17a}, Y.F. Han ¹⁵⁴, K. Hanagaki ⁸², M. Hance ¹³⁵,
 D.A. Hangal ^{41,ae}, H. Hanif ¹⁴¹, M.D. Hank ³⁹, R. Hankache ¹⁰⁰, J.B. Hansen ⁴²,
 J.D. Hansen ⁴², P.H. Hansen ⁴², K. Hara ¹⁵⁶, D. Harada ⁵⁶, T. Harenberg ¹⁷⁰, S. Harkusha ³⁷,
 Y.T. Harris ¹²⁵, N.M. Harrison ¹¹⁸, P.F. Harrison ¹⁶⁶, N.M. Hartman ¹⁴², N.M. Hartmann ¹⁰⁸,
 Y. Hasegawa ¹³⁹, A. Hasib ⁵², S. Haug ¹⁹, R. Hauser ¹⁰⁶, M. Havranek ¹³¹, C.M. Hawkes ²⁰,
 R.J. Hawkings ³⁶, S. Hayashida ¹¹⁰, D. Hayden ¹⁰⁶, C. Hayes ¹⁰⁵, R.L. Hayes ¹⁶³, C.P. Hays ¹²⁵,
 J.M. Hays ⁹³, H.S. Hayward ⁹¹, F. He ^{62a}, Y. He ¹⁵³, Y. He ¹²⁶, M.P. Heath ⁵², V. Hedberg ⁹⁷,
 A.L. Heggelund ¹²⁴, N.D. Hehir ⁹³, C. Heidegger ⁵⁴, K.K. Heidegger ⁵⁴, W.D. Heidorn ⁸⁰,
 J. Heilmann ³⁴, S. Heim ⁴⁸, T. Heim ^{17a}, J.G. Heinlein ¹²⁷, J.J. Heinrich ¹²², L. Heinrich ^{109,ah},
 J. Hejbal ¹³⁰, L. Helary ⁴⁸, A. Held ¹⁶⁹, S. Hellesund ¹²⁴, C.M. Helling ¹⁶³, S. Hellman ^{47a,47b},
 C. Helsens ³⁶, R.C.W. Henderson ⁹⁰, L. Henkelmann ³², A.M. Henriques Correia ³⁶, H. Herde ⁹⁷,
 Y. Hernández Jiménez ¹⁴⁴, L.M. Herrmann ²⁴, M.G. Herrmann ¹⁰⁸, T. Herrmann ⁵⁰, G. Herten ⁵⁴,
 R. Hertenberger ¹⁰⁸, L. Hervás ³⁶, N.P. Hesse ^{155a}, H. Hibi ⁸³, E. Higón-Rodríguez ¹⁶²,
 S.J. Hillier ²⁰, I. Hinchliffe ^{17a}, F. Hinterkeuser ²⁴, M. Hirose ¹²³, S. Hirose ¹⁵⁶,
 D. Hirschbuehl ¹⁷⁰, T.G. Hitchings ¹⁰⁰, B. Hiti ⁹², J. Hobbs ¹⁴⁴, R. Hobincu ^{27e}, N. Hod ¹⁶⁸,
 M.C. Hodgkinson ¹³⁸, B.H. Hodgkinson ³², A. Hoecker ³⁶, J. Hofer ⁴⁸, D. Hohn ⁵⁴, T. Holm ²⁴,
 M. Holzbock ¹⁰⁹, L.B.A.H. Hommels ³², B.P. Honan ¹⁰⁰, J. Hong ^{62c}, T.M. Hong ¹²⁸,
 J.C. Honig ⁵⁴, A. Hönle ¹⁰⁹, B.H. Hooberman ¹⁶¹, W.H. Hopkins ⁶, Y. Horii ¹¹⁰, S. Hou ¹⁴⁷,
 A.S. Howard ⁹², J. Howarth ⁵⁹, J. Hoya ⁶, M. Hrabovsky ¹²¹, A. Hrynevich ⁴⁸, T. Hryn'ova ⁴,
 P.J. Hsu ⁶⁵, S.-C. Hsu ¹³⁷, Q. Hu ⁴¹, Y.F. Hu ^{14a,14d,al}, D.P. Huang ⁹⁵, S. Huang ^{64b},
 X. Huang ^{14c}, Y. Huang ^{62a}, Y. Huang ^{14a}, Z. Huang ¹⁰⁰, Z. Hubacek ¹³¹, M. Huebner ²⁴,
 F. Huegging ²⁴, T.B. Huffman ¹²⁵, M. Huhtinen ³⁶, S.K. Huiberts ¹⁶, R. Hulskén ¹⁰³,
 N. Huseynov ^{12,a}, J. Huston ¹⁰⁶, J. Huth ⁶¹, R. Hyneman ¹⁴², S. Hyrych ^{28a}, G. Iacobucci ⁵⁶,
 G. Iakovidis ²⁹, I. Ibragimov ¹⁴⁰, L. Iconomidou-Fayard ⁶⁶, P. Iengo ^{71a,71b}, R. Iguchi ¹⁵²,
 T. Iizawa ⁵⁶, Y. Ikegami ⁸², A. Ilg ¹⁹, N. Ilic ¹⁵⁴, H. Imam ^{35a}, T. Ingebretsen Carlson ^{47a,47b},
 G. Introzzi ^{72a,72b}, M. Iodice ^{76a}, V. Ippolito ^{74a,74b}, M. Ishino ¹⁵², W. Islam ¹⁶⁹, C. Issever ^{18,48},
 S. Istin ^{21a,ao}, H. Ito ¹⁶⁷, J.M. Iturbe Ponce ^{64a}, R. Iuppa ^{77a,77b}, A. Ivina ¹⁶⁸, J.M. Izen ⁴⁵,
 V. Izzo ^{71a}, P. Jacka ^{130,131}, P. Jackson ¹, R.M. Jacobs ⁴⁸, B.P. Jaeger ¹⁴¹, C.S. Jagfeld ¹⁰⁸,
 G. Jäkel ¹⁷⁰, K. Jakobs ⁵⁴, T. Jakoubek ¹⁶⁸, J. Jamieson ⁵⁹, K.W. Janas ^{84a}, G. Jarlskog ⁹⁷,
 A.E. Jaspan ⁹¹, M. Javurkova ¹⁰², F. Jeanneau ¹³⁴, L. Jeanty ¹²², J. Jejelava ^{148a,ac}, P. Jenni ^{54,h},
 C.E. Jessiman ³⁴, S. Jézéquel ⁴, J. Jia ¹⁴⁴, X. Jia ⁶¹, X. Jia ^{14a,14d}, Z. Jia ^{14c}, Y. Jiang ^{62a},
 S. Jiggins ⁵², J. Jimenez Pena ¹⁰⁹, S. Jin ^{14c}, A. Jinaru ^{27b}, O. Jinnouchi ¹⁵³, P. Johansson ¹³⁸,
 K.A. Johns ⁷, D.M. Jones ³², E. Jones ¹⁶⁶, P. Jones ³², R.W.L. Jones ⁹⁰, T.J. Jones ⁹¹,
 R. Joshi ¹¹⁸, J. Jovicevic ¹⁵, X. Ju ^{17a}, J.J. Junggeburth ³⁶, A. Juste Rozas ^{13,w}, S. Kabana ^{136e},
 A. Kaczmarska ⁸⁵, M. Kado ^{74a,74b}, H. Kagan ¹¹⁸, M. Kagan ¹⁴², A. Kahn ⁴¹, A. Kahn ¹²⁷,
 C. Kahra ⁹⁹, T. Kaji ¹⁶⁷, E. Kajomovitz ¹⁴⁹, N. Kakati ¹⁶⁸, C.W. Kalderon ²⁹,
 A. Kamenshchikov ¹⁵⁴, S. Kanayama ¹⁵³, N.J. Kang ¹³⁵, Y. Kano ¹¹⁰, D. Kar ^{33g}, K. Karava ¹²⁵,
 M.J. Kareem ^{155b}, E. Karentzos ⁵⁴, I. Karkanas ^{151,f}, S.N. Karpov ³⁸, Z.M. Karpova ³⁸,
 V. Kartvelishvili ⁹⁰, A.N. Karyukhin ³⁷, E. Kasimi ^{151,f}, C. Kato ^{62d}, J. Katzy ⁴⁸, S. Kaur ³⁴,
 K. Kawade ¹³⁹, K. Kawagoe ⁸⁸, T. Kawamoto ¹³⁴, G. Kawamura ⁵⁵, E.F. Kay ¹⁶⁴, F.I. Kaya ¹⁵⁷,
 S. Kazakos ¹³, V.F. Kazanin ³⁷, Y. Ke ¹⁴⁴, J.M. Keaveney ^{33a}, R. Keeler ¹⁶⁴, G.V. Kehris ⁶¹,
 J.S. Keller ³⁴, A.S. Kelly ⁹⁵, D. Kelsey ¹⁴⁵, J.J. Kempster ²⁰, K.E. Kennedy ⁴¹, P.D. Kennedy ⁹⁹,
 O. Kepka ¹³⁰, B.P. Kerridge ¹⁶⁶, S. Kersten ¹⁷⁰, B.P. Kerševan ⁹², S. Keshri ⁶⁶,
 L. Keszeghova ^{28a}, S. Ketabchi Haghghat ¹⁵⁴, M. Khandoga ¹²⁶, A. Khanov ¹²⁰,

A.G. Kharlamov ³⁷, T. Kharlamova ³⁷, E.E. Khoda ¹³⁷, T.J. Khoo ¹⁸, G. Khorauli ¹⁶⁵,
 J. Khubua ^{148b}, Y.A.R. Khwaira ⁶⁶, M. Kiehn ³⁶, A. Kilgallon ¹²², D.W. Kim ^{47a,47b},
 E. Kim ¹⁵³, Y.K. Kim ³⁹, N. Kimura ⁹⁵, A. Kirchhoff ⁵⁵, D. Kirchmeier ⁵⁰, C. Kirfel ²⁴,
 J. Kirk ¹³³, A.E. Kiryunin ¹⁰⁹, T. Kishimoto ¹⁵², D.P. Kisliuk ¹⁵⁴, C. Kitsaki ¹⁰, O. Kivernyk ²⁴,
 M. Klassen ^{63a}, C. Klein ³⁴, L. Klein ¹⁶⁵, M.H. Klein ¹⁰⁵, M. Klein ⁹¹, S.B. Klein ⁵⁶,
 U. Klein ⁹¹, P. Klimek ³⁶, A. Klimentov ²⁹, F. Klimpel ¹⁰⁹, T. Klingl ²⁴, T. Klioutchnikova ³⁶,
 F.F. Klitzner ¹⁰⁸, P. Kluit ¹¹³, S. Kluth ¹⁰⁹, E. Kneringer ⁷⁸, T.M. Knight ¹⁵⁴, A. Knue ⁵⁴,
 D. Kobayashi ⁸⁸, R. Kobayashi ⁸⁶, M. Kocian ¹⁴², P. Kodyš ¹³², D.M. Koeck ¹⁴⁵, P.T. Koenig ²⁴,
 T. Koffas ³⁴, M. Kolb ¹³⁴, I. Koletsou ⁴, T. Komarek ¹²¹, K. Köneke ⁵⁴, A.X.Y. Kong ¹,
 T. Kono ¹¹⁷, N. Konstantinidis ⁹⁵, B. Konya ⁹⁷, R. Kopeliansky ⁶⁷, S. Koperny ^{84a}, K. Korcyl ⁸⁵,
 K. Kordas ^{151,f}, G. Koren ¹⁵⁰, A. Korn ⁹⁵, S. Korn ⁵⁵, I. Korolkov ¹³, N. Korotkova ³⁷,
 B. Kortman ¹¹³, O. Kortner ¹⁰⁹, S. Kortner ¹⁰⁹, W.H. Kostecka ¹¹⁴, V.V. Kostyukhin ¹⁴⁰,
 A. Kotsokechagia ¹³⁴, A. Kotwal ⁵¹, A. Koulouris ³⁶, A. Kourkoumeli-Charalampidi ^{72a,72b},
 C. Kourkoumelis ⁹, E. Kourlitis ⁶, O. Kovanda ¹⁴⁵, R. Kowalewski ¹⁶⁴, W. Kozanecki ¹³⁴,
 A.S. Kozhin ³⁷, V.A. Kramarenko ³⁷, G. Kramberger ⁹², P. Kramer ⁹⁹, M.W. Krasny ¹²⁶,
 A. Krasznahorkay ³⁶, J.A. Kremer ⁹⁹, T. Kresse ⁵⁰, J. Kretzschmar ⁹¹, K. Kreul ¹⁸,
 P. Krieger ¹⁵⁴, F. Krieter ¹⁰⁸, S. Krishnamurthy ¹⁰², A. Krishnan ^{63b}, M. Krivos ¹³²,
 K. Krizka ^{17a}, K. Kroeninger ⁴⁹, H. Kroha ¹⁰⁹, J. Kroll ¹³⁰, J. Kroll ¹²⁷, K.S. Krowpman ¹⁰⁶,
 U. Kruchonak ³⁸, H. Krüger ²⁴, N. Krumnack ⁸⁰, M.C. Kruse ⁵¹, J.A. Krzysiak ⁸⁵,
 O. Kuchinskaia ³⁷, S. Kuday ^{3a}, D. Kuechler ⁴⁸, J.T. Kuechler ⁴⁸, S. Kuehn ³⁶, T. Kuhl ⁴⁸,
 V. Kukhtin ³⁸, Y. Kulchitsky ^{37,a}, S. Kuleshov ^{136d,136b}, M. Kumar ^{33g}, N. Kumari ¹⁰¹,
 A. Kupco ¹³⁰, T. Kupfer ⁴⁹, A. Kupich ³⁷, O. Kuprash ⁵⁴, H. Kurashige ⁸³, L.L. Kurchaninov ^{155a},
 Y.A. Kurochkin ³⁷, A. Kurova ³⁷, M. Kuze ¹⁵³, A.K. Kvam ¹⁰², J. Kvita ¹²¹, T. Kwan ¹⁰³,
 K.W. Kwok ^{64a}, N.G. Kyriacou ¹⁰⁵, L.A.O. Laatu ¹⁰¹, C. Lacasta ¹⁶², F. Lacava ^{74a,74b},
 H. Lacker ¹⁸, D. Lacour ¹²⁶, N.N. Lad ⁹⁵, E. Ladygin ³⁸, B. Laforge ¹²⁶, T. Lagouri ^{136e},
 S. Lai ⁵⁵, I.K. Lakomic ^{84a}, N. Lalloue ⁶⁰, J.E. Lambert ¹¹⁹, S. Lammers ⁶⁷, W. Lampl ⁷,
 C. Lampoudis ^{151,f}, A.N. Lancaster ¹¹⁴, E. Lançon ²⁹, U. Landgraf ⁵⁴, M.P.J. Landon ⁹³,
 V.S. Lang ⁵⁴, R.J. Langenberg ¹⁰², A.J. Lankford ¹⁵⁹, F. Lanni ³⁶, K. Lantzsch ²⁴, A. Lanza ^{72a},
 A. Lapertosa ^{57b,57a}, J.F. Laporte ¹³⁴, T. Lari ^{70a}, F. Lasagni Manghi ^{23b}, M. Lassnig ³⁶,
 V. Latonova ¹³⁰, T.S. Lau ^{64a}, A. Laudrain ⁹⁹, A. Laurier ³⁴, S.D. Lawlor ⁹⁴, Z. Lawrence ¹⁰⁰,
 M. Lazzaroni ^{70a,70b}, B. Le ¹⁰⁰, B. Leban ⁹², A. Lebedev ⁸⁰, M. LeBlanc ³⁶, T. LeCompte ⁶,
 F. Ledroit-Guillon ⁶⁰, A.C.A. Lee ⁹⁵, G.R. Lee ¹⁶, L. Lee ⁶¹, S.C. Lee ¹⁴⁷, S. Lee ^{47a,47b},
 T.F. Lee ⁹¹, L.L. Leeuw ^{33c}, H.P. Lefebvre ⁹⁴, M. Lefebvre ¹⁶⁴, C. Leggett ^{17a}, K. Lehmann ¹⁴¹,
 G. Lehmann Miotto ³⁶, M. Leigh ⁵⁶, W.A. Leight ¹⁰², A. Leisos ^{151,v}, M.A.L. Leite ^{81c},
 C.E. Leitgeb ⁴⁸, R. Leitner ¹³², K.J.C. Leney ⁴⁴, T. Lenz ²⁴, S. Leone ^{73a}, C. Leonidopoulos ⁵²,
 A. Leopold ¹⁴³, C. Leroy ¹⁰⁷, R. Les ¹⁰⁶, C.G. Lester ³², M. Levchenko ³⁷, J. Levêque ⁴,
 D. Levin ¹⁰⁵, L.J. Levinson ¹⁶⁸, M.P. Lewicki ⁸⁵, D.J. Lewis ⁴, A. Li ⁵, B. Li ^{14b}, B. Li ^{62b},
 C. Li ^{62a}, C-Q. Li ^{62c}, H. Li ^{62a}, H. Li ^{62b}, H. Li ^{14c}, H. Li ^{62b}, J. Li ^{62c}, K. Li ¹³⁷, L. Li ^{62c},
 M. Li ^{14a,14d}, Q.Y. Li ^{62a}, S. Li ^{14a,14d}, S. Li ^{62d,62c,e}, T. Li ^{62b}, X. Li ¹⁰³, Z. Li ^{62b}, Z. Li ¹²⁵,
 Z. Li ¹⁰³, Z. Li ⁹¹, Z. Li ^{14a,14d}, Z. Liang ^{14a}, M. Liberatore ⁴⁸, B. Liberti ^{75a}, K. Lie ^{64c},
 J. Lieber Marin ^{81b}, K. Lin ¹⁰⁶, R.A. Linck ⁶⁷, R.E. Lindley ⁷, J.H. Lindon ², A. Linss ⁴⁸,
 E. Lipeles ¹²⁷, A. Lipniacka ¹⁶, A. Lister ¹⁶³, J.D. Little ⁴, B. Liu ^{14a}, B.X. Liu ¹⁴¹,
 D. Liu ^{62d,62c}, J.B. Liu ^{62a}, J.K.K. Liu ³², K. Liu ^{62d,62c}, M. Liu ^{62a}, M.Y. Liu ^{62a}, P. Liu ^{14a},
 Q. Liu ^{62d,137,62c}, X. Liu ^{62a}, Y. Liu ⁴⁸, Y. Liu ^{14c,14d}, Y.L. Liu ¹⁰⁵, Y.W. Liu ^{62a},
 M. Livan ^{72a,72b}, J. Llorente Merino ¹⁴¹, S.L. Lloyd ⁹³, E.M. Lobodzinska ⁴⁸, P. Loch ⁷,
 S. Loffredo ^{75a,75b}, T. Lohse ¹⁸, K. Lohwasser ¹³⁸, M. Lokajicek ^{130,*}, J.D. Long ¹⁶¹,
 I. Longarini ^{74a,74b}, L. Longo ^{69a,69b}, R. Longo ¹⁶¹, I. Lopez Paz ³⁶, A. Lopez Solis ⁴⁸,





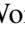

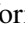


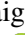
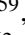


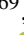

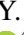
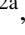






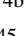


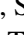

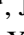

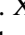
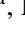


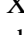
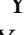





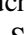

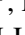

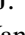


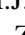

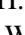

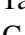

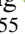





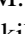




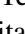




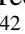

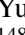


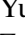

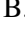
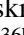
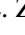


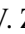


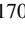

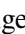
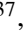

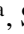


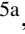




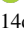
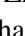
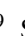

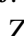





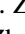

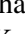


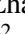
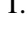

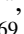
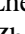
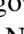


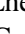
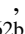

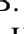
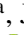


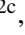



J. Lorenz ^{id108}, N. Lorenzo Martinez ^{id4}, A.M. Lory ^{id108}, A. Lösle ^{id54}, X. Lou ^{id47a,47b}, X. Lou ^{id14a,14d},
 A. Lounis ^{id66}, J. Love ^{id6}, P.A. Love ^{id90}, J.J. Lozano Bahilo ^{id162}, G. Lu ^{id14a,14d}, M. Lu ^{id79},
 S. Lu ^{id127}, Y.J. Lu ^{id65}, H.J. Lubatti ^{id137}, C. Luci ^{id74a,74b}, F.L. Lucio Alves ^{id14c}, A. Lucotte ^{id60},
 F. Luehring ^{id67}, I. Luise ^{id144}, O. Lukianchuk ^{id66}, O. Lundberg ^{id143}, B. Lund-Jensen ^{id143},
 N.A. Luongo ^{id122}, M.S. Lutz ^{id150}, D. Lynn ^{id29}, H. Lyons⁹¹, R. Lysak ^{id130}, E. Lytken ^{id97}, F. Lyu ^{id14a},
 V. Lyubushkin ^{id38}, T. Lyubushkina ^{id38}, H. Ma ^{id29}, L.L. Ma ^{id62b}, Y. Ma ^{id95}, D.M. Mac Donell ^{id164},
 G. Maccarrone ^{id53}, J.C. MacDonald ^{id138}, R. Madar ^{id40}, W.F. Mader ^{id50}, J. Maeda ^{id83}, T. Maeno ^{id29},
 M. Maerker ^{id50}, V. Magerl ^{id54}, H. Maguire ^{id138}, D.J. Mahon ^{id41}, C. Maidantchik ^{id81b},
 A. Maio ^{id129a,129b,129d}, K. Maj ^{id84a}, O. Majersky ^{id28a}, S. Majewski ^{id122}, N. Makovec ^{id66},
 V. Maksimovic ^{id15}, B. Malaescu ^{id126}, Pa. Malecki ^{id85}, V.P. Maleev ^{id37}, F. Malek ^{id60},
 D. Malito ^{id43b,43a}, U. Mallik ^{id79}, C. Malone ^{id32}, S. Maltezos¹⁰, S. Malyukov³⁸, J. Mamuzic ^{id13},
 G. Mancini ^{id53}, G. Manco ^{id72a,72b}, J.P. Mandalia ^{id93}, I. Mandić ^{id92},
 L. Manhaes de Andrade Filho ^{id81a}, I.M. Maniatis ^{id151,f}, M. Manisha ^{id134}, J. Manjarres Ramos ^{id50},
 D.C. Mankad ^{id168}, A. Mann ^{id108}, B. Mansoulie ^{id134}, S. Manzoni ^{id36}, A. Marantis ^{id151,v},
 G. Marchiori ^{id5}, M. Marcisovsky ^{id130}, L. Marcoccia ^{id75a,75b}, C. Marcon ^{id70a,70b}, M. Marinescu ^{id20},
 M. Marjanovic ^{id119}, E.J. Marshall ^{id90}, Z. Marshall ^{id17a}, S. Marti-Garcia ^{id162}, T.A. Martin ^{id166},
 V.J. Martin ^{id52}, B. Martin dit Latour ^{id16}, L. Martinelli ^{id74a,74b}, M. Martinez ^{id13,w},
 P. Martinez Agullo ^{id162}, V.I. Martinez Outschoorn ^{id102}, P. Martinez Suarez ^{id13}, S. Martin-Haugh ^{id133},
 V.S. Martoiu ^{id27b}, A.C. Martyniuk ^{id95}, A. Marzin ^{id36}, S.R. Maschek ^{id109}, L. Masetti ^{id99},
 T. Mashimo ^{id152}, J. Masik ^{id100}, A.L. Maslennikov ^{id37}, L. Massa ^{id23b}, P. Massarotti ^{id71a,71b},
 P. Mastrandrea ^{id73a,73b}, A. Mastroberardino ^{id43b,43a}, T. Masubuchi ^{id152}, T. Mathisen ^{id160},
 N. Matsuzawa¹⁵², J. Maurer ^{id27b}, B. Maček ^{id92}, D.A. Maximov ^{id37}, R. Mazini ^{id147}, I. Maznas ^{id151,f},
 M. Mazza ^{id106}, S.M. Mazza ^{id135}, C. Mc Ginn ^{id29}, J.P. Mc Gowan ^{id103}, S.P. Mc Kee ^{id105},
 W.P. McCormack ^{id17a}, E.F. McDonald ^{id104}, A.E. McDougall ^{id113}, J.A. Mcfayden ^{id145},
 G. Mchedlidze ^{id148b}, R.P. Mckenzie ^{id33g}, T.C. Mclachlan ^{id48}, D.J. Mclaughlin ^{id95}, K.D. McLean ^{id164},
 S.J. McMahan ^{id133}, P.C. McNamara ^{id104}, C.M. Mccpartland ^{id91}, R.A. McPherson ^{id164,z}, T. Megy ^{id40},
 S. Mehlhase ^{id108}, A. Mehta ^{id91}, B. Meirose ^{id45}, D. Melini ^{id149}, B.R. Mellado Garcia ^{id33g},
 A.H. Melo ^{id55}, F. Meloni ^{id48}, E.D. Mendes Gouveia ^{id129a}, A.M. Mendes Jacques Da Costa ^{id20},
 H.Y. Meng ^{id154}, L. Meng ^{id90}, S. Menke ^{id109}, M. Mentink ^{id36}, E. Meoni ^{id43b,43a}, C. Merlassino ^{id125},
 L. Merola ^{id71a,71b}, C. Meroni ^{id70a}, G. Merz¹⁰⁵, O. Meshkov ^{id37}, J.K.R. Meshreki ^{id140}, J. Metcalfe ^{id6},
 A.S. Mete ^{id6}, C. Meyer ^{id67}, J-P. Meyer ^{id134}, M. Michetti ^{id18}, R.P. Middleton ^{id133}, L. Mijović ^{id52},
 G. Mikenberg ^{id168}, M. Mikesikova ^{id130}, M. Mikuž ^{id92}, H. Mildner ^{id138}, A. Milic ^{id36},
 C.D. Milke ^{id44}, D.W. Miller ^{id39}, L.S. Miller ^{id34}, A. Milov ^{id168}, D.A. Milstead^{47a,47b}, T. Min^{14c},
 A.A. Minaenko ^{id37}, I.A. Minashvili ^{id148b}, L. Mince ^{id59}, A.I. Mincer ^{id116}, B. Mindur ^{id84a},
 M. Mineev ^{id38}, Y. Mino ^{id86}, L.M. Mir ^{id13}, M. Miralles Lopez ^{id162}, M. Mironova ^{id125},
 M.C. Missio ^{id112}, T. Mitani ^{id167}, A. Mitra ^{id166}, V.A. Mitsou ^{id162}, O. Miu ^{id154}, P.S. Miyagawa ^{id93},
 Y. Miyazaki⁸⁸, A. Mizukami ^{id82}, J.U. Mjörnmark ^{id97}, T. Mkrtchyan ^{id63a}, T. Mlinarevic ^{id95},
 M. Mlynarikova ^{id36}, T. Moa ^{id47a,47b}, S. Mobius ^{id55}, K. Mochizuki ^{id107}, P. Moder ^{id48}, P. Mogg ^{id108},
 A.F. Mohammed ^{id14a,14d}, S. Mohapatra ^{id41}, G. Mokgatitwane ^{id33g}, B. Mondal ^{id140}, S. Mondal ^{id131},
 K. Mönig ^{id48}, E. Monnier ^{id101}, L. Monsonis Romero¹⁶², J. Montejo Berlingen ^{id36}, M. Montella ^{id118},
 F. Monticelli ^{id89}, N. Morange ^{id66}, A.L. Moreira De Carvalho ^{id129a}, M. Moreno Llácer ^{id162},
 C. Moreno Martinez ^{id56}, P. Morettini ^{id57b}, S. Morgenstern ^{id166}, M. Morii ^{id61}, M. Morinaga ^{id152},
 A.K. Morley ^{id36}, F. Morodei ^{id74a,74b}, L. Morvaj ^{id36}, P. Moschovakos ^{id36}, B. Moser ^{id36},
 M. Mosidze^{148b}, T. Moskalets ^{id54}, P. Moskvitina ^{id112}, J. Moss ^{id31,p}, E.J.W. Moyse ^{id102},
 O. Mtintsilana ^{id33g}, S. Muanza ^{id101}, J. Mueller ^{id128}, D. Muenstermann ^{id90}, R. Müller ^{id19},
 G.A. Mullier ^{id160}, J.J. Mullin¹²⁷, D.P. Mungo ^{id154}, J.L. Munoz Martinez ^{id13}, D. Munoz Perez ^{id162},
 F.J. Munoz Sanchez ^{id100}, M. Murin ^{id100}, W.J. Murray ^{id166,133}, A. Murrone ^{id70a,70b}, J.M. Muse ^{id119},

M. Muškinja ^{17a}, C. Mwewa ²⁹, A.G. Myagkov ^{37,a}, A.J. Myers ⁸, A.A. Myers ¹²⁸, G. Myers ⁶⁷,
M. Myska ¹³¹, B.P. Nachman ^{17a}, O. Nackenhorst ⁴⁹, A. Nag ⁵⁰, K. Nagai ¹²⁵, K. Nagano ⁸²,
J.L. Nagle ^{29,am}, E. Nagy ¹⁰¹, A.M. Nairz ³⁶, Y. Nakahama ⁸², K. Nakamura ⁸², H. Nanjo ¹²³,
R. Narayan ⁴⁴, E.A. Narayanan ¹¹¹, I. Naryshkin ³⁷, M. Naseri ³⁴, C. Nass ²⁴, G. Navarro ^{22a},
J. Navarro-Gonzalez ¹⁶², R. Nayak ¹⁵⁰, A. Nayaz ¹⁸, P.Y. Nechaeva ³⁷, F. Nechansky ⁴⁸,
L. Nedic ¹²⁵, T.J. Neep ²⁰, A. Negri ^{72a,72b}, M. Negrini ^{23b}, C. Nellist ¹¹², C. Nelson ¹⁰³,
K. Nelson ¹⁰⁵, S. Nemecek ¹³⁰, M. Nessi ^{36,i}, M.S. Neubauer ¹⁶¹, F. Neuhaus ⁹⁹, J. Neundorf ⁴⁸,
R. Newhouse ¹⁶³, P.R. Newman ²⁰, C.W. Ng ¹²⁸, Y.S. Ng ¹⁸, Y.W.Y. Ng ⁴⁸, B. Ngair ^{35e},
H.D.N. Nguyen ¹⁰⁷, R.B. Nickerson ¹²⁵, R. Nicolaidou ¹³⁴, J. Nielsen ¹³⁵, M. Niemeyer ⁵⁵,
N. Nikiforou ³⁶, V. Nikolaenko ^{37,a}, I. Nikolic-Audit ¹²⁶, K. Nikolopoulos ²⁰, P. Nilsson ²⁹,
H.R. Nindhito ⁵⁶, A. Nisati ^{74a}, N. Nishu ², R. Nisius ¹⁰⁹, J-E. Nitschke ⁵⁰,
E.K. Nkadimeng ^{33g}, S.J. Noacco Rosende ⁸⁹, T. Nobe ¹⁵², D.L. Noel ³², Y. Noguchi ⁸⁶,
T. Nommensen ¹⁴⁶, M.A. Nomura ²⁹, M.B. Norfolk ¹³⁸, R.R.B. Norisam ⁹⁵, B.J. Norman ³⁴,
J. Novak ⁹², T. Novak ⁴⁸, O. Novgorodova ⁵⁰, L. Novotny ¹³¹, R. Novotny ¹¹¹, L. Nozka ¹²¹,
K. Ntekas ¹⁵⁹, N.M.J. Nunes De Moura Junior ^{81b}, E. Nurse ⁹⁵, F.G. Oakham ^{34,aj}, J. Ocariz ¹²⁶,
A. Ochi ⁸³, I. Ochoa ^{129a}, S. Oerdek ¹⁶⁰, A. Ogrodnik ^{84a}, A. Oh ¹⁰⁰, C.C. Ohm ¹⁴³,
H. Oide ⁸², R. Oishi ¹⁵², M.L. Ojeda ⁴⁸, Y. Okazaki ⁸⁶, M.W. O'Keefe ⁹¹, Y. Okumura ¹⁵²,
A. Olariu ^{27b}, L.F. Oleiro Seabra ^{129a}, S.A. Olivares Pino ^{136e}, D. Oliveira Damazio ²⁹,
D. Oliveira Goncalves ^{81a}, J.L. Oliver ¹⁵⁹, M.J.R. Olsson ¹⁵⁹, A. Olszewski ⁸⁵, J. Olszowska ^{85,*},
Ö.O. Öncel ⁵⁴, D.C. O'Neil ¹⁴¹, A.P. O'Neill ¹⁹, A. Onofre ^{129a,129e}, P.U.E. Onyisi ¹¹,
M.J. Oreglia ³⁹, G.E. Orellana ⁸⁹, D. Orestano ^{76a,76b}, N. Orlando ¹³, R.S. Orr ¹⁵⁴, V. O'Shea ⁵⁹,
R. Ospanov ^{62a}, G. Otero y Garzon ³⁰, H. Otono ⁸⁸, P.S. Ott ^{63a}, G.J. Ottino ^{17a}, M. Ouchrif ^{35d},
J. Ouellette ^{29,am}, F. Ould-Saada ¹²⁴, M. Owen ⁵⁹, R.E. Owen ¹³³, K.Y. Oyulmaz ^{21a},
V.E. Ozcan ^{21a}, N. Ozturk ⁸, S. Ozturk ^{21d}, J. Pacalt ¹²¹, H.A. Pacey ³², K. Pachal ⁵¹,
A. Pacheco Pages ¹³, C. Padilla Aranda ¹³, G. Padovano ^{74a,74b}, S. Pagan Griso ^{17a}, G. Palacino ⁶⁷,
A. Palazzo ^{69a,69b}, S. Palestini ³⁶, M. Palka ^{84b}, J. Pan ¹⁷¹, T. Pan ^{64a}, D.K. Panchal ¹¹,
C.E. Pandini ¹¹³, J.G. Panduro Vazquez ⁹⁴, H. Pang ^{14b}, P. Pani ⁴⁸, G. Panizzo ^{68a,68c},
L. Paolozzi ⁵⁶, C. Papadatos ¹⁰⁷, S. Parajuli ⁴⁴, A. Paramonov ⁶, C. Paraskevopoulos ¹⁰,
D. Paredes Hernandez ^{64b}, T.H. Park ¹⁵⁴, M.A. Parker ³², F. Parodi ^{57b,57a}, E.W. Parrish ¹¹⁴,
V.A. Parrish ⁵², J.A. Parsons ⁴¹, U. Parzefall ⁵⁴, B. Pascual Dias ¹⁰⁷, L. Pascual Dominguez ¹⁵⁰,
V.R. Pascuzzi ^{17a}, F. Pasquali ¹¹³, E. Pasqualucci ^{74a}, S. Passaggio ^{57b}, F. Pastore ⁹⁴,
P. Pasuwan ^{47a,47b}, P. Patel ⁸⁵, J.R. Pater ¹⁰⁰, T. Pauly ³⁶, J. Pearkes ¹⁴², M. Pedersen ¹²⁴,
R. Pedro ^{129a}, S.V. Peleganchuk ³⁷, O. Penc ³⁶, E.A. Pender ⁵², C. Peng ^{64b}, H. Peng ^{62a},
K.E. Pensi ¹⁰⁸, M. Penzin ³⁷, B.S. Peralva ^{81d}, A.P. Pereira Peixoto ⁶⁰, L. Pereira Sanchez ^{47a,47b},
D.V. Perepelitsa ^{29,am}, E. Perez Codina ^{155a}, M. Perganti ¹⁰, L. Perini ^{70a,70b,*}, H. Pernegger ³⁶,
S. Perrella ³⁶, A. Perrevoort ¹¹², O. Perrin ⁴⁰, K. Peters ⁴⁸, R.F.Y. Peters ¹⁰⁰, B.A. Petersen ³⁶,
T.C. Petersen ⁴², E. Petit ¹⁰¹, V. Petousis ¹³¹, C. Petridou ^{151,f}, A. Petrukhin ¹⁴⁰, M. Pettee ^{17a},
N.E. Pettersson ³⁶, A. Petukhov ³⁷, K. Petukhova ¹³², A. Peyaud ¹³⁴, R. Pezoa ^{136f},
L. Pezzotti ³⁶, G. Pezzullo ¹⁷¹, T.M. Pham ¹⁶⁹, T. Pham ¹⁰⁴, P.W. Phillips ¹³³, M.W. Phipps ¹⁶¹,
G. Piacquadio ¹⁴⁴, E. Pianori ^{17a}, F. Piazza ^{70a,70b}, R. Piegaia ³⁰, D. Pietreanu ^{27b},
A.D. Pilkington ¹⁰⁰, M. Pinamonti ^{68a,68c}, J.L. Pinfeld ², B.C. Pinheiro Pereira ^{129a},
C. Pitman Donaldson ⁹⁵, D.A. Pizzi ³⁴, L. Pizzimento ^{75a,75b}, A. Pizzini ¹¹³, M.-A. Pleier ²⁹,
V. Plesanovs ⁵⁴, V. Pleskot ¹³², E. Plotnikova ³⁸, G. Poddar ⁴, R. Poettgen ⁹⁷, L. Poggioli ¹²⁶,
I. Pogrebnyak ¹⁰⁶, D. Pohl ²⁴, I. Pokharel ⁵⁵, S. Polacek ¹³², G. Polesello ^{72a}, A. Poley ^{141,155a},
R. Polifka ¹³¹, A. Polini ^{23b}, C.S. Pollard ¹²⁵, Z.B. Pollock ¹¹⁸, V. Polychronakos ²⁹,
E. Pompa Pacchi ^{74a,74b}, D. Ponomarenko ³⁷, L. Pontecorvo ³⁶, S. Popa ^{27a}, G.A. Popeneciu ^{27d},
D.M. Portillo Quintero ^{155a}, S. Pospisil ¹³¹, P. Postolache ^{27c}, K. Potamianos ¹²⁵, I.N. Potrap ³⁸,

C.J. Potter ³², H. Potti ¹, T. Poulsen ⁴⁸, J. Poveda ¹⁶², M.E. Pozo Astigarraga ³⁶,
 A. Prades Ibanez ¹⁶², M.M. Prapa ⁴⁶, J. Pretel ⁵⁴, D. Price ¹⁰⁰, M. Primavera ^{69a},
 M.A. Principe Martin ⁹⁸, R. Privara ¹²¹, M.L. Proffitt ¹³⁷, N. Proklova ¹²⁷, K. Prokofiev ^{64c},
 G. Proto ^{75a,75b}, S. Protopopescu ²⁹, J. Proudfoot ⁶, M. Przybycien ^{84a}, J.E. Puddefoot ¹³⁸,
 D. Pudzha ³⁷, P. Puzo ⁶⁶, D. Pyatiizbyantseva ³⁷, J. Qian ¹⁰⁵, D. Qichen ¹⁰⁰, Y. Qin ¹⁰⁰,
 T. Qiu ⁹³, A. Quadt ⁵⁵, M. Queitsch-Maitland ¹⁰⁰, G. Quetant ⁵⁶, G. Rabanal Bolanos ⁶¹,
 D. Rafanoharana ⁵⁴, F. Ragusa ^{70a,70b}, J.L. Rainbolt ³⁹, J.A. Raine ⁵⁶, S. Rajagopalan ²⁹,
 E. Ramakoti ³⁷, K. Ran ^{48,14d}, N.P. Rapheeha ^{33g}, V. Raskina ¹²⁶, D.F. Rassloff ^{63a}, S. Rave ⁹⁹,
 B. Ravina ⁵⁵, I. Ravinovich ¹⁶⁸, M. Raymond ³⁶, A.L. Read ¹²⁴, N.P. Readioff ¹³⁸,
 D.M. Rebuzzi ^{72a,72b}, G. Redlinger ²⁹, K. Reeves ⁴⁵, J.A. Reidelsturz ¹⁷⁰, D. Reikher ¹⁵⁰,
 A. Reiss ⁹⁹, A. Rej ¹⁴⁰, C. Rembser ³⁶, A. Renardi ⁴⁸, M. Renda ^{27b}, M.B. Rendel ¹⁰⁹, F. Renner ⁴⁸,
 A.G. Rennie ⁵⁹, S. Resconi ^{70a}, M. Ressegotti ^{57b,57a}, E.D. Resseguie ^{17a}, S. Rettie ³⁶,
 J.G. Reyes Rivera ¹⁰⁶, B. Reynolds ¹¹⁸, E. Reynolds ^{17a}, M. Rezaei Estabragh ¹⁷⁰, O.L. Rezanova ³⁷,
 P. Reznicek ¹³², E. Ricci ^{77a,77b}, R. Richter ¹⁰⁹, S. Richter ^{47a,47b}, E. Richter-Was ^{84b},
 M. Ridel ¹²⁶, P. Rieck ¹¹⁶, P. Riedler ³⁶, M. Rijssenbeek ¹⁴⁴, A. Rimoldi ^{72a,72b}, M. Rimoldi ⁴⁸,
 L. Rinaldi ^{23b,23a}, T.T. Rinn ²⁹, M.P. Rinnagel ¹⁰⁸, G. Ripellino ¹⁴³, I. Riu ¹³, P. Rivadeneira ⁴⁸,
 J.C. Rivera Vergara ¹⁶⁴, F. Rizatdinova ¹²⁰, E. Rizvi ⁹³, C. Rizzi ⁵⁶, B.A. Roberts ¹⁶⁶,
 B.R. Roberts ^{17a}, S.H. Robertson ^{103,z}, M. Robin ⁴⁸, D. Robinson ³², C.M. Robles Gajardo ^{136f},
 M. Robles Manzano ⁹⁹, A. Robson ⁵⁹, A. Rocchi ^{75a,75b}, C. Roda ^{73a,73b}, S. Rodriguez Bosca ^{63a},
 Y. Rodriguez Garcia ^{22a}, A. Rodriguez Rodriguez ⁵⁴, A.M. Rodríguez Vera ^{155b}, S. Roe ³⁶,
 J.T. Roemer ¹⁵⁹, A.R. Roepe-Gier ¹¹⁹, J. Roggel ¹⁷⁰, O. Røhne ¹²⁴, R.A. Rojas ¹⁶⁴, B. Roland ⁵⁴,
 C.P.A. Roland ⁶⁷, J. Roloff ²⁹, A. Romaniouk ³⁷, E. Romano ^{72a,72b}, M. Romano ^{23b},
 A.C. Romero Hernandez ¹⁶¹, N. Rompotis ⁹¹, L. Roos ¹²⁶, S. Rosati ^{74a}, B.J. Rosser ³⁹,
 E. Rossi ⁴, E. Rossi ^{71a,71b}, L.P. Rossi ^{57b}, L. Rossini ⁴⁸, R. Rosten ¹¹⁸, M. Rotaru ^{27b},
 B. Rottler ⁵⁴, D. Rousseau ⁶⁶, D. Rousso ³², G. Rovelli ^{72a,72b}, A. Roy ¹⁶¹, A. Rozanov ¹⁰¹,
 Y. Rozen ¹⁴⁹, X. Ruan ^{33g}, A. Rubio Jimenez ¹⁶², A.J. Ruby ⁹¹, V.H. Ruelas Rivera ¹⁸,
 T.A. Ruggeri ¹, F. Rühr ⁵⁴, A. Ruiz-Martinez ¹⁶², A. Rummler ³⁶, Z. Rurikova ⁵⁴,
 N.A. Rusakovich ³⁸, H.L. Russell ¹⁶⁴, J.P. Rutherford ⁷, K. Rybacki ⁹⁰, M. Rybar ¹³²,
 E.B. Rye ¹²⁴, A. Ryzhov ³⁷, J.A. Sabater Iglesias ⁵⁶, P. Sabatini ¹⁶², L. Sabetta ^{74a,74b},
 H.F-W. Sadrozinski ¹³⁵, F. Safai Tehrani ^{74a}, B. Safarzadeh Samani ¹⁴⁵, M. Safdari ¹⁴²,
 S. Saha ¹⁰³, M. Sahinsoy ¹⁰⁹, M. Saimpert ¹³⁴, M. Saito ¹⁵², T. Saito ¹⁵², D. Salamani ³⁶,
 G. Salamanna ^{76a,76b}, A. Salnikov ¹⁴², J. Salt ¹⁶², A. Salvador Salas ¹³, D. Salvatore ^{43b,43a},
 F. Salvatore ¹⁴⁵, A. Salzburger ³⁶, D. Sammel ⁵⁴, D. Sampsonidis ^{151,f}, D. Sampsonidou ^{62d,62c},
 J. Sánchez ¹⁶², A. Sanchez Pineda ⁴, V. Sanchez Sebastian ¹⁶², H. Sandaker ¹²⁴, C.O. Sander ⁴⁸,
 J.A. Sandesara ¹⁰², M. Sandhoff ¹⁷⁰, C. Sandoval ^{22b}, D.P.C. Sankey ¹³³, A. Sansoni ⁵³,
 L. Santi ^{74a,74b}, C. Santoni ⁴⁰, H. Santos ^{129a,129b}, S.N. Santpur ^{17a}, A. Santra ¹⁶⁸,
 K.A. Saoucha ¹³⁸, J.G. Saraiva ^{129a,129d}, J. Sardain ⁷, O. Sasaki ⁸², K. Sato ¹⁵⁶, C. Sauer ^{63b},
 F. Sauerburger ⁵⁴, E. Sauvan ⁴, P. Savard ^{154,aj}, R. Sawada ¹⁵², C. Sawyer ¹³³, L. Sawyer ⁹⁶,
 I. Sayago Galvan ¹⁶², C. Sbarra ^{23b}, A. Sbrizzi ^{23b,23a}, T. Scanlon ⁹⁵, J. Schaarschmidt ¹³⁷,
 P. Schacht ¹⁰⁹, D. Schaefer ³⁹, U. Schäfer ⁹⁹, A.C. Schaffer ⁶⁶, D. Schaile ¹⁰⁸,
 R.D. Schamberger ¹⁴⁴, E. Schanet ¹⁰⁸, C. Scharf ¹⁸, M.M. Schefer ¹⁹, V.A. Schegelsky ³⁷,
 D. Scheirich ¹³², F. Schenck ¹⁸, M. Schernau ¹⁵⁹, C. Scheulen ⁵⁵, C. Schiavi ^{57b,57a},
 Z.M. Schillaci ²⁶, E.J. Schioppa ^{69a,69b}, M. Schioppa ^{43b,43a}, B. Schlag ⁹⁹, K.E. Schleicher ⁵⁴,
 S. Schlenker ³⁶, J. Schmeing ¹⁷⁰, M.A. Schmidt ¹⁷⁰, K. Schmieden ⁹⁹, C. Schmitt ⁹⁹,
 S. Schmitt ⁴⁸, L. Schoeffel ¹³⁴, A. Schoening ^{63b}, P.G. Scholer ⁵⁴, E. Schopf ¹²⁵, M. Schott ⁹⁹,
 J. Schovancova ³⁶, S. Schramm ⁵⁶, F. Schroeder ¹⁷⁰, H-C. Schultz-Coulon ^{63a}, M. Schumacher ⁵⁴,
 B.A. Schumm ¹³⁵, Ph. Schune ¹³⁴, A. Schwartzman ¹⁴², T.A. Schwarz ¹⁰⁵, Ph. Schwemling ¹³⁴,

R. Schwienhorst ¹⁰⁶, A. Sciandra ¹³⁵, G. Sciolla ²⁶, F. Scuri ^{73a}, F. Scutti ¹⁰⁴, C.D. Sebastiani ⁹¹, K. Sedlaczek ⁴⁹, P. Seema ¹⁸, S.C. Seidel ¹¹¹, A. Seiden ¹³⁵, B.D. Seidlitz ⁴¹, T. Seiss ³⁹, C. Seitz ⁴⁸, J.M. Seixas ^{81b}, G. Sekhniaidze ^{71a}, S.J. Sekula ⁴⁴, L. Selem ⁴, N. Semprini-Cesari ^{23b,23a}, S. Sen ⁵¹, D. Sengupta ⁵⁶, V. Senthilkumar ¹⁶², L. Serin ⁶⁶, L. Serkin ^{68a,68b}, M. Sessa ^{76a,76b}, H. Severini ¹¹⁹, S. Sevova ¹⁴², F. Sforza ^{57b,57a}, A. Sfyrla ⁵⁶, E. Shabalina ⁵⁵, R. Shaheen ¹⁴³, J.D. Shahinian ¹²⁷, D. Shaked Renous ¹⁶⁸, L.Y. Shan ^{14a}, M. Shapiro ^{17a}, A. Sharma ³⁶, A.S. Sharma ¹⁶³, P. Sharma ⁷⁹, S. Sharma ⁴⁸, P.B. Shatalov ³⁷, K. Shaw ¹⁴⁵, S.M. Shaw ¹⁰⁰, Q. Shen ^{62c,5}, P. Sherwood ⁹⁵, L. Shi ⁹⁵, C.O. Shimmin ¹⁷¹, Y. Shimogama ¹⁶⁷, J.D. Shinner ⁹⁴, I.P.J. Shipsey ¹²⁵, S. Shirabe ⁶⁰, M. Shiyakova ^{38,y}, J. Shlomi ¹⁶⁸, M.J. Shochet ³⁹, J. Shojaii ¹⁰⁴, D.R. Shope ¹²⁴, S. Shrestha ^{118,an}, E.M. Shrif ^{33g}, M.J. Shroff ¹⁶⁴, P. Sicho ¹³⁰, A.M. Sickles ¹⁶¹, E. Sideras Haddad ^{33g}, A. Sidoti ^{23b}, F. Siegert ⁵⁰, Dj. Sijacki ¹⁵, R. Sikora ^{84a}, F. Sili ⁸⁹, J.M. Silva ²⁰, M.V. Silva Oliveira ³⁶, S.B. Silverstein ^{47a}, S. Simion ⁶⁶, R. Simoniello ³⁶, E.L. Simpson ⁵⁹, N.D. Simpson ⁹⁷, S. Simsek ^{21d}, S. Sindhu ⁵⁵, P. Sinervo ¹⁵⁴, V. Sinetckii ³⁷, S. Singh ¹⁴¹, S. Singh ¹⁵⁴, S. Sinha ⁴⁸, S. Sinha ^{33g}, M. Sioli ^{23b,23a}, I. Siral ³⁶, S.Yu. Sivoklokov ^{37,*}, J. Sjölin ^{47a,47b}, A. Skaf ⁵⁵, E. Skorda ⁹⁷, P. Skubic ¹¹⁹, M. Slawinska ⁸⁵, V. Smakhtin ¹⁶⁸, B.H. Smart ¹³³, J. Smiesko ³⁶, S.Yu. Smirnov ³⁷, Y. Smirnov ³⁷, L.N. Smirnova ^{37,a}, O. Smirnova ⁹⁷, A.C. Smith ⁴¹, E.A. Smith ³⁹, H.A. Smith ¹²⁵, J.L. Smith ⁹¹, R. Smith ¹⁴², M. Smizanska ⁹⁰, K. Smolek ¹³¹, A. Smykiewicz ⁸⁵, A.A. Snesarev ³⁷, H.L. Snoek ¹¹³, S. Snyder ²⁹, R. Sobie ^{164,z}, A. Soffer ¹⁵⁰, C.A. Solans Sanchez ³⁶, E.Yu. Soldatov ³⁷, U. Soldevila ¹⁶², A.A. Solodkov ³⁷, S. Solomon ⁵⁴, A. Soloshenko ³⁸, K. Solovieva ⁵⁴, O.V. Solovyanov ³⁷, V. Solovyev ³⁷, P. Sommer ³⁶, A. Sonay ¹³, W.Y. Song ^{155b}, A. Sopczak ¹³¹, A.L. Soppio ⁹⁵, F. Sopkova ^{28b}, V. Sothilingam ^{63a}, S. Sottocornola ^{72a,72b}, R. Soualah ^{115b}, Z. Soumami ^{35e}, D. South ⁴⁸, S. Spagnolo ^{69a,69b}, M. Spalla ¹⁰⁹, F. Spanò ⁹⁴, D. Sperlich ⁵⁴, G. Spigo ³⁶, M. Spina ¹⁴⁵, S. Spinali ⁹⁰, D.P. Spiteri ⁵⁹, M. Spousta ¹³², E.J. Staats ³⁴, A. Stabile ^{70a,70b}, R. Stamen ^{63a}, M. Stamenkovic ¹¹³, A. Stampekis ²⁰, M. Standke ²⁴, E. Stanecka ⁸⁵, M.V. Stange ⁵⁰, B. Stanislaus ^{17a}, M.M. Stanitzki ⁴⁸, M. Stankaityte ¹²⁵, B. Stapf ⁴⁸, E.A. Starchenko ³⁷, G.H. Stark ¹³⁵, J. Stark ^{101,ad}, D.M. Starko ^{155b}, P. Staroba ¹³⁰, P. Starovoitov ^{63a}, S. Stärz ¹⁰³, R. Staszewski ⁸⁵, G. Stavropoulos ⁴⁶, J. Steentoft ¹⁶⁰, P. Steinberg ²⁹, A.L. Steinhebel ¹²², B. Stelzer ^{141,155a}, H.J. Stelzer ¹²⁸, O. Stelzer-Chilton ^{155a}, H. Stenzel ⁵⁸, T.J. Stevenson ¹⁴⁵, G.A. Stewart ³⁶, M.C. Stockton ³⁶, G. Stoicea ^{27b}, M. Stolarski ^{129a}, S. Stonjek ¹⁰⁹, A. Straessner ⁵⁰, J. Strandberg ¹⁴³, S. Strandberg ^{47a,47b}, M. Strauss ¹¹⁹, T. Strebler ¹⁰¹, P. Strizenec ^{28b}, R. Ströhmer ¹⁶⁵, D.M. Strom ¹²², L.R. Strom ⁴⁸, R. Stroynowski ⁴⁴, A. Strubig ^{47a,47b}, S.A. Stucci ²⁹, B. Stugu ¹⁶, J. Stupak ¹¹⁹, N.A. Styles ⁴⁸, D. Su ¹⁴², S. Su ^{62a}, W. Su ^{62d,137,62c}, X. Su ^{62a,66}, K. Sugizaki ¹⁵², V.V. Sulin ³⁷, M.J. Sullivan ⁹¹, D.M.S. Sultan ^{77a,77b}, L. Sultanaliyeva ³⁷, S. Sultansoy ^{3b}, T. Sumida ⁸⁶, S. Sun ¹⁰⁵, S. Sun ¹⁶⁹, O. Sunneborn Gudnadottir ¹⁶⁰, M.R. Sutton ¹⁴⁵, M. Svatos ¹³⁰, M. Swiatlowski ^{155a}, T. Swirski ¹⁶⁵, I. Sykora ^{28a}, M. Sykora ¹³², T. Sykora ¹³², D. Ta ⁹⁹, K. Tackmann ^{48,x}, A. Taffard ¹⁵⁹, R. Tafirout ^{155a}, J.S. Tafoya Vargas ⁶⁶, R.H.M. Taibah ¹²⁶, R. Takashima ⁸⁷, K. Takeda ⁸³, E.P. Takeva ⁵², Y. Takubo ⁸², M. Talby ¹⁰¹, A.A. Talyshv ³⁷, K.C. Tam ^{64b}, N.M. Tamir ¹⁵⁰, A. Tanaka ¹⁵², J. Tanaka ¹⁵², R. Tanaka ⁶⁶, M. Tanasini ^{57b,57a}, J. Tang ^{62c}, Z. Tao ¹⁶³, S. Tapia Araya ⁸⁰, S. Tapprogge ⁹⁹, A. Tarek Abouelfadl Mohamed ¹⁰⁶, S. Tarem ¹⁴⁹, K. Tariq ^{62b}, G. Tarna ^{101,27b}, G.F. Tartarelli ^{70a}, P. Tas ¹³², M. Tasevsky ¹³⁰, E. Tassi ^{43b,43a}, A.C. Tate ¹⁶¹, G. Tateno ¹⁵², Y. Tayalati ^{35e}, G.N. Taylor ¹⁰⁴, W. Taylor ^{155b}, H. Teagle ⁹¹, A.S. Tee ¹⁶⁹, R. Teixeira De Lima ¹⁴², P. Teixeira-Dias ⁹⁴, J.J. Teoh ¹⁵⁴, K. Terashi ¹⁵², J. Terron ⁹⁸, S. Terzo ¹³, M. Testa ⁵³, R.J. Teuscher ^{154,z}, A. Thaler ⁷⁸, O. Theiner ⁵⁶, N. Themistokleous ⁵², T. Thevenaux-Pelzer ¹⁸, O. Thielmann ¹⁷⁰, D.W. Thomas ⁹⁴,

J.P. Thomas ²⁰, E.A. Thompson ⁴⁸, P.D. Thompson ²⁰, E. Thomson ¹²⁷, E.J. Thorpe ⁹³,
Y. Tian ⁵⁵, V. Tikhomirov ^{37,a}, Yu.A. Tikhonov ³⁷, S. Timoshenko ³⁷, E.X.L. Ting ¹, P. Tipton ¹⁷¹,
S. Tisserant ¹⁰¹, S.H. Tlou ^{33g}, A. Tnourji ⁴⁰, K. Todome ^{23b,23a}, S. Todorova-Nova ¹³², S. Todt ⁵⁰,
M. Togawa ⁸², J. Tojo ⁸⁸, S. Tokár ^{28a}, K. Tokushuku ⁸², R. Tombs ³², M. Tomoto ^{82,110},
L. Tompkins ^{142,r}, K.W. Topolnicki ^{84b}, P. Tornambe ¹⁰², E. Torrence ¹²², H. Torres ⁵⁰,
E. Torró Pastor ¹⁶², M. Toscani ³⁰, C. Tosciri ³⁹, M. Tost ¹¹, D.R. Tovey ¹³⁸, A. Traeet ¹⁶,
I.S. Trandafir ^{27b}, T. Trefzger ¹⁶⁵, A. Tricoli ²⁹, I.M. Trigger ^{155a}, S. Trincaz-Duvoid ¹²⁶,
D.A. Trischuk ²⁶, B. Trocmé ⁶⁰, A. Trofymov ⁶⁶, C. Troncon ^{70a}, L. Truong ^{33c},
M. Trzebinski ⁸⁵, A. Trzupiek ⁸⁵, F. Tsai ¹⁴⁴, M. Tsai ¹⁰⁵, A. Tsiamis ^{151,f}, P.V. Tsiareshka ³⁷,
S. Tsigaridas ^{155a}, A. Tsirigotis ^{151,v}, V. Tsiskaridze ¹⁴⁴, E.G. Tskhadadze ^{148a}, M. Tsopoulou ^{151,f},
Y. Tsujikawa ⁸⁶, I.I. Tsukerman ³⁷, V. Tsulaia ^{17a}, S. Tsuno ⁸², O. Tsur ¹⁴⁹, D. Tsybychev ¹⁴⁴,
Y. Tu ^{64b}, A. Tudorache ^{27b}, V. Tudorache ^{27b}, A.N. Tuna ³⁶, S. Turchikhin ³⁸, I. Turk Cakir ^{3a},
R. Turra ^{70a}, T. Turtuvshin ^{38,aa}, P.M. Tuts ⁴¹, S. Tzamarias ^{151,f}, P. Tzanis ¹⁰, E. Tzovara ⁹⁹,
K. Uchida ¹⁵², F. Ukegawa ¹⁵⁶, P.A. Ulloa Poblete ^{136c}, E.N. Umaka ⁸⁰, G. Unal ³⁶, M. Unal ¹¹,
A. Undrus ²⁹, G. Unel ¹⁵⁹, J. Urban ^{28b}, P. Urquijo ¹⁰⁴, G. Usai ⁸, R. Ushioda ¹⁵³,
M. Usman ¹⁰⁷, Z. Uysal ^{21b}, L. Vacavant ¹⁰¹, V. Vacek ¹³¹, B. Vachon ¹⁰³, K.O.H. Vadla ¹²⁴,
T. Vafeiadis ³⁶, A. Vaitkus ⁹⁵, C. Valderanis ¹⁰⁸, E. Valdes Santurio ^{47a,47b}, M. Valente ^{155a},
S. Valentinetti ^{23b,23a}, A. Valero ¹⁶², A. Vallier ^{101,ad}, J.A. Valls Ferrer ¹⁶², T.R. Van Daalen ¹³⁷,
P. Van Gemmeren ⁶, M. Van Rijnbach ^{124,36}, S. Van Stroud ⁹⁵, I. Van Vulpen ¹¹³,
M. Vanadia ^{75a,75b}, W. Vandelli ³⁶, M. Vandembroucke ¹³⁴, E.R. Vandewall ¹²⁰, D. Vannicola ¹⁵⁰,
L. Vannoli ^{57b,57a}, R. Vari ^{74a}, E.W. Varnes ⁷, C. Varni ^{17a}, T. Varol ¹⁴⁷, D. Varouchas ⁶⁶,
L. Varriale ¹⁶², K.E. Varvell ¹⁴⁶, M.E. Vasile ^{27b}, L. Vaslin ⁴⁰, G.A. Vasquez ¹⁶⁴, F. Vazeille ⁴⁰,
T. Vazquez Schroeder ³⁶, J. Veatch ³¹, V. Vecchio ¹⁰⁰, M.J. Veen ¹⁰², I. Veliscek ¹²⁵,
L.M. Veloce ¹⁵⁴, F. Veloso ^{129a,129c}, S. Veneziano ^{74a}, A. Ventura ^{69a,69b}, A. Verbytskyi ¹⁰⁹,
M. Verducci ^{73a,73b}, C. Vergis ²⁴, M. Verissimo De Araujo ^{81b}, W. Verkerke ¹¹³,
J.C. Vermeulen ¹¹³, C. Vernieri ¹⁴², P.J. Verschuuren ⁹⁴, M. Vessella ¹⁰², M.C. Vetterli ^{141,aj},
A. Vgenopoulos ^{151,f}, N. Viaux Maira ^{136f}, T. Vickey ¹³⁸, O.E. Vickey Boeriu ¹³⁸,
G.H.A. Viehhauser ¹²⁵, L. Vigani ^{63b}, M. Villa ^{23b,23a}, M. Villaplana Perez ¹⁶², E.M. Villhauer ⁵²,
E. Vilucchi ⁵³, M.G. Vincter ³⁴, G.S. Virdee ²⁰, A. Vishwakarma ⁵², C. Vittori ^{23b,23a},
I. Vivarelli ¹⁴⁵, V. Vladimirov ¹⁶⁶, E. Voevodina ¹⁰⁹, F. Vogel ¹⁰⁸, P. Vokac ¹³¹, J. Von Ahnen ⁴⁸,
E. Von Toerne ²⁴, B. Vormwald ³⁶, V. Vorobel ¹³², K. Vorobev ³⁷, M. Vos ¹⁶²,
J.H. Vossebeld ⁹¹, M. Vozak ¹¹³, L. Vozdecky ⁹³, N. Vranjes ¹⁵, M. Vranjes Milosavljevic ¹⁵,
M. Vreeswijk ¹¹³, R. Vuillermet ³⁶, O. Vujanovic ⁹⁹, I. Vukotic ³⁹, S. Wada ¹⁵⁶, C. Wagner ¹⁰²,
W. Wagner ¹⁷⁰, S. Wahdan ¹⁷⁰, H. Wahlberg ⁸⁹, R. Wakasa ¹⁵⁶, M. Wakida ¹¹⁰,
V.M. Walbrecht ¹⁰⁹, J. Walder ¹³³, R. Walker ¹⁰⁸, W. Walkowiak ¹⁴⁰, A.M. Wang ⁶¹,
A.Z. Wang ¹⁶⁹, C. Wang ^{62a}, C. Wang ^{62c}, H. Wang ^{17a}, J. Wang ^{64a}, R.-J. Wang ⁹⁹,
R. Wang ⁶¹, R. Wang ⁶, S.M. Wang ¹⁴⁷, S. Wang ^{62b}, T. Wang ^{62a}, W.T. Wang ⁷⁹,
X. Wang ^{14c}, X. Wang ¹⁶¹, X. Wang ^{62c}, Y. Wang ^{62d}, Y. Wang ^{14c}, Z. Wang ¹⁰⁵,
Z. Wang ^{62d,51,62c}, Z. Wang ¹⁰⁵, A. Warburton ¹⁰³, R.J. Ward ²⁰, N. Warrack ⁵⁹, A.T. Watson ²⁰,
H. Watson ⁵⁹, M.F. Watson ²⁰, G. Watts ¹³⁷, B.M. Waugh ⁹⁵, A.F. Webb ¹¹, C. Weber ²⁹,
H.A. Weber ¹⁸, M.S. Weber ¹⁹, S.M. Weber ^{63a}, C. Wei ^{62a}, Y. Wei ¹²⁵, A.R. Weidberg ¹²⁵,
J. Weingarten ⁴⁹, M. Weirich ⁹⁹, C. Weiser ⁵⁴, C.J. Wells ⁴⁸, T. Wenaus ²⁹, B. Wendland ⁴⁹,
T. Wengler ³⁶, N.S. Wenke ¹⁰⁹, N. Wermes ²⁴, M. Wessels ^{63a}, K. Whalen ¹²², A.M. Wharton ⁹⁰,
A.S. White ⁶¹, A. White ⁸, M.J. White ¹, D. Whiteson ¹⁵⁹, L. Wickremasinghe ¹²³,
W. Wiedenmann ¹⁶⁹, C. Wiel ⁵⁰, M. Wielers ¹³³, N. Wieseotte ⁹⁹, C. Wiglesworth ⁴²,
L.A.M. Wiik-Fuchs ⁵⁴, D.J. Wilbern ¹¹⁹, H.G. Wilkens ³⁶, D.M. Williams ⁴¹, H.H. Williams ¹²⁷,
S. Williams ³², S. Willocq ¹⁰², P.J. Windischhofer ¹²⁵, F. Winklmeier ¹²², B.T. Winter ⁵⁴,

J.K. Winter ¹⁰⁰, M. Wittgen¹⁴², M. Wobisch ⁹⁶, R. Wölker ¹²⁵, J. Wollrath¹⁵⁹, M.W. Wolter ⁸⁵, H. Wolters ^{129a,129c}, V.W.S. Wong ¹⁶³, A.F. Wongel ⁴⁸, E.L. Woodward ⁴¹, S.D. Worm ⁴⁸, B.K. Wosiek ⁸⁵, K.W. Woźniak ⁸⁵, K. Wraight ⁵⁹, J. Wu ^{14a,14d}, M. Wu ^{64a}, M. Wu ¹¹², S.L. Wu ¹⁶⁹, X. Wu ⁵⁶, Y. Wu ^{62a}, Z. Wu ^{134,62a}, J. Wuerzinger ¹²⁵, T.R. Wyatt ¹⁰⁰, B.M. Wynne ⁵², S. Xella ⁴², L. Xia ^{14c}, M. Xia ^{14b}, J. Xiang ^{64c}, X. Xiao ¹⁰⁵, M. Xie ^{62a}, X. Xie ^{62a}, S. Xin ^{14a,14d}, J. Xiong ^{17a}, I. Xiotidis¹⁴⁵, D. Xu ^{14a}, H. Xu^{62a}, H. Xu ^{62a}, L. Xu ^{62a}, R. Xu ¹²⁷, T. Xu ¹⁰⁵, W. Xu ¹⁰⁵, Y. Xu ^{14b}, Z. Xu ^{62b}, Z. Xu ^{14a}, B. Yabsley ¹⁴⁶, S. Yacoob ^{33a}, N. Yamaguchi ⁸⁸, Y. Yamaguchi ¹⁵³, H. Yamauchi ¹⁵⁶, T. Yamazaki ^{17a}, Y. Yamazaki ⁸³, J. Yan^{62c}, S. Yan ¹²⁵, Z. Yan ²⁵, H.J. Yang ^{62c,62d}, H.T. Yang ^{62a}, S. Yang ^{62a}, T. Yang ^{64c}, X. Yang ^{62a}, X. Yang ^{14a}, Y. Yang ⁴⁴, Z. Yang ^{62a,105}, W-M. Yao ^{17a}, Y.C. Yap ⁴⁸, H. Ye ^{14c}, H. Ye ⁵⁵, J. Ye ⁴⁴, S. Ye ²⁹, X. Ye ^{62a}, Y. Yeh ⁹⁵, I. Yeletsikh ³⁸, B.K. Yeo ^{17a}, M.R. Yexley ⁹⁰, P. Yin ⁴¹, K. Yorita ¹⁶⁷, S. Younas ^{27b}, C.J.S. Young ⁵⁴, C. Young ¹⁴², M. Yuan ¹⁰⁵, R. Yuan ^{62b,1}, L. Yue ⁹⁵, X. Yue ^{63a}, M. Zaazoua ^{35e}, B. Zabinski ⁸⁵, E. Zaid⁵², T. Zakareishvili ^{148b}, N. Zakharchuk ³⁴, S. Zambito ⁵⁶, J.A. Zamora Saa ^{136d,136b}, J. Zang ¹⁵², D. Zanzi ⁵⁴, O. Zaplatilek ¹³¹, S.V. Zeibner ⁴⁹, C. Zeitnitz ¹⁷⁰, J.C. Zeng ¹⁶¹, D.T. Zenger Jr ²⁶, O. Zenin ³⁷, T. Ženiš ^{28a}, S. Zenz ⁹³, S. Zerradi ^{35a}, D. Zerwas ⁶⁶, B. Zhang ^{14c}, D.F. Zhang ¹³⁸, G. Zhang ^{14b}, J. Zhang ^{62b}, J. Zhang ⁶, K. Zhang ^{14a,14d}, L. Zhang ^{14c}, P. Zhang^{14a,14d}, R. Zhang ¹⁶⁹, S. Zhang ¹⁰⁵, T. Zhang ¹⁵², X. Zhang ^{62c}, X. Zhang ^{62b}, Y. Zhang ^{62c,5}, Z. Zhang ^{17a}, Z. Zhang ⁶⁶, H. Zhao ¹³⁷, P. Zhao ⁵¹, T. Zhao ^{62b}, Y. Zhao ¹³⁵, Z. Zhao ^{62a}, A. Zhemchugov ³⁸, X. Zheng ^{62a}, Z. Zheng ¹⁴², D. Zhong ¹⁶¹, B. Zhou¹⁰⁵, C. Zhou ¹⁶⁹, H. Zhou ⁷, N. Zhou ^{62c}, Y. Zhou⁷, C.G. Zhu ^{62b}, C. Zhu ^{14a,14d}, H.L. Zhu ^{62a}, H. Zhu ^{14a}, J. Zhu ¹⁰⁵, Y. Zhu ^{62c}, Y. Zhu ^{62a}, X. Zhuang ^{14a}, K. Zhukov ³⁷, V. Zhulanov ³⁷, N.I. Zimine ³⁸, J. Zinsser ^{63b}, M. Ziolkowski ¹⁴⁰, L. Živković ¹⁵, A. Zoccoli ^{23b,23a}, K. Zoch ⁵⁶, T.G. Zorbas ¹³⁸, O. Zormpa ⁴⁶, W. Zou ⁴¹, L. Zwalinski ³⁶.

¹Department of Physics, University of Adelaide, Adelaide; Australia.

²Department of Physics, University of Alberta, Edmonton AB; Canada.

³(^a)Department of Physics, Ankara University, Ankara; (^b)Division of Physics, TOBB University of Economics and Technology, Ankara; Türkiye.

⁴LAPP, Université Savoie Mont Blanc, CNRS/IN2P3, Annecy; France.

⁵APC, Université Paris Cité, CNRS/IN2P3, Paris; France.

⁶High Energy Physics Division, Argonne National Laboratory, Argonne IL; United States of America.

⁷Department of Physics, University of Arizona, Tucson AZ; United States of America.

⁸Department of Physics, University of Texas at Arlington, Arlington TX; United States of America.

⁹Physics Department, National and Kapodistrian University of Athens, Athens; Greece.

¹⁰Physics Department, National Technical University of Athens, Zografou; Greece.

¹¹Department of Physics, University of Texas at Austin, Austin TX; United States of America.

¹²Institute of Physics, Azerbaijan Academy of Sciences, Baku; Azerbaijan.

¹³Institut de Física d'Altes Energies (IFAE), Barcelona Institute of Science and Technology, Barcelona; Spain.

¹⁴(^a)Institute of High Energy Physics, Chinese Academy of Sciences, Beijing; (^b)Physics Department, Tsinghua University, Beijing; (^c)Department of Physics, Nanjing University, Nanjing; (^d)University of Chinese Academy of Science (UCAS), Beijing; China.

¹⁵Institute of Physics, University of Belgrade, Belgrade; Serbia.

¹⁶Department for Physics and Technology, University of Bergen, Bergen; Norway.

¹⁷(^a)Physics Division, Lawrence Berkeley National Laboratory, Berkeley CA; (^b)University of California, Berkeley CA; United States of America.

- ¹⁸Institut für Physik, Humboldt Universität zu Berlin, Berlin; Germany.
- ¹⁹Albert Einstein Center for Fundamental Physics and Laboratory for High Energy Physics, University of Bern, Bern; Switzerland.
- ²⁰School of Physics and Astronomy, University of Birmingham, Birmingham; United Kingdom.
- ²¹(^a) Department of Physics, Bogazici University, Istanbul; (^b) Department of Physics Engineering, Gaziantep University, Gaziantep; (^c) Department of Physics, Istanbul University, Istanbul; (^d) Istinye University, Sariyer, Istanbul; Türkiye.
- ²²(^a) Facultad de Ciencias y Centro de Investigaciones, Universidad Antonio Nariño, Bogotá; (^b) Departamento de Física, Universidad Nacional de Colombia, Bogotá; Colombia.
- ²³(^a) Dipartimento di Fisica e Astronomia A. Righi, Università di Bologna, Bologna; (^b) INFN Sezione di Bologna; Italy.
- ²⁴Physikalisches Institut, Universität Bonn, Bonn; Germany.
- ²⁵Department of Physics, Boston University, Boston MA; United States of America.
- ²⁶Department of Physics, Brandeis University, Waltham MA; United States of America.
- ²⁷(^a) Transilvania University of Brasov, Brasov; (^b) Horia Hulubei National Institute of Physics and Nuclear Engineering, Bucharest; (^c) Department of Physics, Alexandru Ioan Cuza University of Iasi, Iasi; (^d) National Institute for Research and Development of Isotopic and Molecular Technologies, Physics Department, Cluj-Napoca; (^e) University Politehnica Bucharest, Bucharest; (^f) West University in Timisoara, Timisoara; (^g) Faculty of Physics, University of Bucharest, Bucharest; Romania.
- ²⁸(^a) Faculty of Mathematics, Physics and Informatics, Comenius University, Bratislava; (^b) Department of Subnuclear Physics, Institute of Experimental Physics of the Slovak Academy of Sciences, Kosice; Slovak Republic.
- ²⁹Physics Department, Brookhaven National Laboratory, Upton NY; United States of America.
- ³⁰Universidad de Buenos Aires, Facultad de Ciencias Exactas y Naturales, Departamento de Física, y CONICET, Instituto de Física de Buenos Aires (IFIBA), Buenos Aires; Argentina.
- ³¹California State University, CA; United States of America.
- ³²Cavendish Laboratory, University of Cambridge, Cambridge; United Kingdom.
- ³³(^a) Department of Physics, University of Cape Town, Cape Town; (^b) iThemba Labs, Western Cape; (^c) Department of Mechanical Engineering Science, University of Johannesburg, Johannesburg; (^d) National Institute of Physics, University of the Philippines Diliman (Philippines); (^e) University of South Africa, Department of Physics, Pretoria; (^f) University of Zululand, KwaDlangezwa; (^g) School of Physics, University of the Witwatersrand, Johannesburg; South Africa.
- ³⁴Department of Physics, Carleton University, Ottawa ON; Canada.
- ³⁵(^a) Faculté des Sciences Ain Chock, Réseau Universitaire de Physique des Hautes Energies - Université Hassan II, Casablanca; (^b) Faculté des Sciences, Université Ibn-Tofail, Kénitra; (^c) Faculté des Sciences Semlalia, Université Cadi Ayyad, LPHEA-Marrakech; (^d) LPMR, Faculté des Sciences, Université Mohamed Premier, Oujda; (^e) Faculté des sciences, Université Mohammed V, Rabat; (^f) Institute of Applied Physics, Mohammed VI Polytechnic University, Ben Guerir; Morocco.
- ³⁶CERN, Geneva; Switzerland.
- ³⁷Affiliated with an institute covered by a cooperation agreement with CERN.
- ³⁸Affiliated with an international laboratory covered by a cooperation agreement with CERN.
- ³⁹Enrico Fermi Institute, University of Chicago, Chicago IL; United States of America.
- ⁴⁰LPC, Université Clermont Auvergne, CNRS/IN2P3, Clermont-Ferrand; France.
- ⁴¹Nevis Laboratory, Columbia University, Irvington NY; United States of America.
- ⁴²Niels Bohr Institute, University of Copenhagen, Copenhagen; Denmark.
- ⁴³(^a) Dipartimento di Fisica, Università della Calabria, Rende; (^b) INFN Gruppo Collegato di Cosenza, Laboratori Nazionali di Frascati; Italy.

- ⁴⁴Physics Department, Southern Methodist University, Dallas TX; United States of America.
- ⁴⁵Physics Department, University of Texas at Dallas, Richardson TX; United States of America.
- ⁴⁶National Centre for Scientific Research "Demokritos", Agia Paraskevi; Greece.
- ⁴⁷(^a) Department of Physics, Stockholm University; (^b) Oskar Klein Centre, Stockholm; Sweden.
- ⁴⁸Deutsches Elektronen-Synchrotron DESY, Hamburg and Zeuthen; Germany.
- ⁴⁹Fakultät Physik, Technische Universität Dortmund, Dortmund; Germany.
- ⁵⁰Institut für Kern- und Teilchenphysik, Technische Universität Dresden, Dresden; Germany.
- ⁵¹Department of Physics, Duke University, Durham NC; United States of America.
- ⁵²SUPA - School of Physics and Astronomy, University of Edinburgh, Edinburgh; United Kingdom.
- ⁵³INFN e Laboratori Nazionali di Frascati, Frascati; Italy.
- ⁵⁴Physikalisches Institut, Albert-Ludwigs-Universität Freiburg, Freiburg; Germany.
- ⁵⁵II. Physikalisches Institut, Georg-August-Universität Göttingen, Göttingen; Germany.
- ⁵⁶Département de Physique Nucléaire et Corpusculaire, Université de Genève, Genève; Switzerland.
- ⁵⁷(^a) Dipartimento di Fisica, Università di Genova, Genova; (^b) INFN Sezione di Genova; Italy.
- ⁵⁸II. Physikalisches Institut, Justus-Liebig-Universität Giessen, Giessen; Germany.
- ⁵⁹SUPA - School of Physics and Astronomy, University of Glasgow, Glasgow; United Kingdom.
- ⁶⁰LPSC, Université Grenoble Alpes, CNRS/IN2P3, Grenoble INP, Grenoble; France.
- ⁶¹Laboratory for Particle Physics and Cosmology, Harvard University, Cambridge MA; United States of America.
- ⁶²(^a) Department of Modern Physics and State Key Laboratory of Particle Detection and Electronics, University of Science and Technology of China, Hefei; (^b) Institute of Frontier and Interdisciplinary Science and Key Laboratory of Particle Physics and Particle Irradiation (MOE), Shandong University, Qingdao; (^c) School of Physics and Astronomy, Shanghai Jiao Tong University, Key Laboratory for Particle Astrophysics and Cosmology (MOE), SKLPPC, Shanghai; (^d) Tsung-Dao Lee Institute, Shanghai; China.
- ⁶³(^a) Kirchhoff-Institut für Physik, Ruprecht-Karls-Universität Heidelberg, Heidelberg; (^b) Physikalisches Institut, Ruprecht-Karls-Universität Heidelberg, Heidelberg; Germany.
- ⁶⁴(^a) Department of Physics, Chinese University of Hong Kong, Shatin, N.T., Hong Kong; (^b) Department of Physics, University of Hong Kong, Hong Kong; (^c) Department of Physics and Institute for Advanced Study, Hong Kong University of Science and Technology, Clear Water Bay, Kowloon, Hong Kong; China.
- ⁶⁵Department of Physics, National Tsing Hua University, Hsinchu; Taiwan.
- ⁶⁶IJCLab, Université Paris-Saclay, CNRS/IN2P3, 91405, Orsay; France.
- ⁶⁷Department of Physics, Indiana University, Bloomington IN; United States of America.
- ⁶⁸(^a) INFN Gruppo Collegato di Udine, Sezione di Trieste, Udine; (^b) ICTP, Trieste; (^c) Dipartimento Politecnico di Ingegneria e Architettura, Università di Udine, Udine; Italy.
- ⁶⁹(^a) INFN Sezione di Lecce; (^b) Dipartimento di Matematica e Fisica, Università del Salento, Lecce; Italy.
- ⁷⁰(^a) INFN Sezione di Milano; (^b) Dipartimento di Fisica, Università di Milano, Milano; Italy.
- ⁷¹(^a) INFN Sezione di Napoli; (^b) Dipartimento di Fisica, Università di Napoli, Napoli; Italy.
- ⁷²(^a) INFN Sezione di Pavia; (^b) Dipartimento di Fisica, Università di Pavia, Pavia; Italy.
- ⁷³(^a) INFN Sezione di Pisa; (^b) Dipartimento di Fisica E. Fermi, Università di Pisa, Pisa; Italy.
- ⁷⁴(^a) INFN Sezione di Roma; (^b) Dipartimento di Fisica, Sapienza Università di Roma, Roma; Italy.
- ⁷⁵(^a) INFN Sezione di Roma Tor Vergata; (^b) Dipartimento di Fisica, Università di Roma Tor Vergata, Roma; Italy.
- ⁷⁶(^a) INFN Sezione di Roma Tre; (^b) Dipartimento di Matematica e Fisica, Università Roma Tre, Roma; Italy.
- ⁷⁷(^a) INFN-TIFPA; (^b) Università degli Studi di Trento, Trento; Italy.
- ⁷⁸Universität Innsbruck, Department of Astro and Particle Physics, Innsbruck; Austria.
- ⁷⁹University of Iowa, Iowa City IA; United States of America.

- ⁸⁰Department of Physics and Astronomy, Iowa State University, Ames IA; United States of America.
- ⁸¹(^a) Departamento de Engenharia Elétrica, Universidade Federal de Juiz de Fora (UFJF), Juiz de Fora; (^b) Universidade Federal do Rio De Janeiro COPPE/EE/IF, Rio de Janeiro; (^c) Instituto de Física, Universidade de São Paulo, São Paulo; (^d) Rio de Janeiro State University, Rio de Janeiro; Brazil.
- ⁸²KEK, High Energy Accelerator Research Organization, Tsukuba; Japan.
- ⁸³Graduate School of Science, Kobe University, Kobe; Japan.
- ⁸⁴(^a) AGH University of Krakow, Faculty of Physics and Applied Computer Science, Krakow; (^b) Marian Smoluchowski Institute of Physics, Jagiellonian University, Krakow; Poland.
- ⁸⁵Institute of Nuclear Physics Polish Academy of Sciences, Krakow; Poland.
- ⁸⁶Faculty of Science, Kyoto University, Kyoto; Japan.
- ⁸⁷Kyoto University of Education, Kyoto; Japan.
- ⁸⁸Research Center for Advanced Particle Physics and Department of Physics, Kyushu University, Fukuoka ; Japan.
- ⁸⁹Instituto de Física La Plata, Universidad Nacional de La Plata and CONICET, La Plata; Argentina.
- ⁹⁰Physics Department, Lancaster University, Lancaster; United Kingdom.
- ⁹¹Oliver Lodge Laboratory, University of Liverpool, Liverpool; United Kingdom.
- ⁹²Department of Experimental Particle Physics, Jožef Stefan Institute and Department of Physics, University of Ljubljana, Ljubljana; Slovenia.
- ⁹³School of Physics and Astronomy, Queen Mary University of London, London; United Kingdom.
- ⁹⁴Department of Physics, Royal Holloway University of London, Egham; United Kingdom.
- ⁹⁵Department of Physics and Astronomy, University College London, London; United Kingdom.
- ⁹⁶Louisiana Tech University, Ruston LA; United States of America.
- ⁹⁷Fysiska institutionen, Lunds universitet, Lund; Sweden.
- ⁹⁸Departamento de Física Teórica C-15 and CIAFF, Universidad Autónoma de Madrid, Madrid; Spain.
- ⁹⁹Institut für Physik, Universität Mainz, Mainz; Germany.
- ¹⁰⁰School of Physics and Astronomy, University of Manchester, Manchester; United Kingdom.
- ¹⁰¹CPPM, Aix-Marseille Université, CNRS/IN2P3, Marseille; France.
- ¹⁰²Department of Physics, University of Massachusetts, Amherst MA; United States of America.
- ¹⁰³Department of Physics, McGill University, Montreal QC; Canada.
- ¹⁰⁴School of Physics, University of Melbourne, Victoria; Australia.
- ¹⁰⁵Department of Physics, University of Michigan, Ann Arbor MI; United States of America.
- ¹⁰⁶Department of Physics and Astronomy, Michigan State University, East Lansing MI; United States of America.
- ¹⁰⁷Group of Particle Physics, University of Montreal, Montreal QC; Canada.
- ¹⁰⁸Fakultät für Physik, Ludwig-Maximilians-Universität München, München; Germany.
- ¹⁰⁹Max-Planck-Institut für Physik (Werner-Heisenberg-Institut), München; Germany.
- ¹¹⁰Graduate School of Science and Kobayashi-Maskawa Institute, Nagoya University, Nagoya; Japan.
- ¹¹¹Department of Physics and Astronomy, University of New Mexico, Albuquerque NM; United States of America.
- ¹¹²Institute for Mathematics, Astrophysics and Particle Physics, Radboud University/Nikhef, Nijmegen; Netherlands.
- ¹¹³Nikhef National Institute for Subatomic Physics and University of Amsterdam, Amsterdam; Netherlands.
- ¹¹⁴Department of Physics, Northern Illinois University, DeKalb IL; United States of America.
- ¹¹⁵(^a) New York University Abu Dhabi, Abu Dhabi; (^b) University of Sharjah, Sharjah; United Arab Emirates.
- ¹¹⁶Department of Physics, New York University, New York NY; United States of America.

- ¹¹⁷Ochanomizu University, Otsuka, Bunkyo-ku, Tokyo; Japan.
- ¹¹⁸Ohio State University, Columbus OH; United States of America.
- ¹¹⁹Homer L. Dodge Department of Physics and Astronomy, University of Oklahoma, Norman OK; United States of America.
- ¹²⁰Department of Physics, Oklahoma State University, Stillwater OK; United States of America.
- ¹²¹Palacký University, Joint Laboratory of Optics, Olomouc; Czech Republic.
- ¹²²Institute for Fundamental Science, University of Oregon, Eugene, OR; United States of America.
- ¹²³Graduate School of Science, Osaka University, Osaka; Japan.
- ¹²⁴Department of Physics, University of Oslo, Oslo; Norway.
- ¹²⁵Department of Physics, Oxford University, Oxford; United Kingdom.
- ¹²⁶LPNHE, Sorbonne Université, Université Paris Cité, CNRS/IN2P3, Paris; France.
- ¹²⁷Department of Physics, University of Pennsylvania, Philadelphia PA; United States of America.
- ¹²⁸Department of Physics and Astronomy, University of Pittsburgh, Pittsburgh PA; United States of America.
- ¹²⁹^(a)Laboratório de Instrumentação e Física Experimental de Partículas - LIP, Lisboa;^(b)Departamento de Física, Faculdade de Ciências, Universidade de Lisboa, Lisboa;^(c)Departamento de Física, Universidade de Coimbra, Coimbra;^(d)Centro de Física Nuclear da Universidade de Lisboa, Lisboa;^(e)Departamento de Física, Universidade do Minho, Braga;^(f)Departamento de Física Teórica y del Cosmos, Universidad de Granada, Granada (Spain);^(g)Departamento de Física, Instituto Superior Técnico, Universidade de Lisboa, Lisboa; Portugal.
- ¹³⁰Institute of Physics of the Czech Academy of Sciences, Prague; Czech Republic.
- ¹³¹Czech Technical University in Prague, Prague; Czech Republic.
- ¹³²Charles University, Faculty of Mathematics and Physics, Prague; Czech Republic.
- ¹³³Particle Physics Department, Rutherford Appleton Laboratory, Didcot; United Kingdom.
- ¹³⁴IRFU, CEA, Université Paris-Saclay, Gif-sur-Yvette; France.
- ¹³⁵Santa Cruz Institute for Particle Physics, University of California Santa Cruz, Santa Cruz CA; United States of America.
- ¹³⁶^(a)Departamento de Física, Pontificia Universidad Católica de Chile, Santiago;^(b)Millennium Institute for Subatomic physics at high energy frontier (SAPHIR), Santiago;^(c)Instituto de Investigación Multidisciplinario en Ciencia y Tecnología, y Departamento de Física, Universidad de La Serena;^(d)Universidad Andres Bello, Department of Physics, Santiago;^(e)Instituto de Alta Investigación, Universidad de Tarapacá, Arica;^(f)Departamento de Física, Universidad Técnica Federico Santa María, Valparaíso; Chile.
- ¹³⁷Department of Physics, University of Washington, Seattle WA; United States of America.
- ¹³⁸Department of Physics and Astronomy, University of Sheffield, Sheffield; United Kingdom.
- ¹³⁹Department of Physics, Shinshu University, Nagano; Japan.
- ¹⁴⁰Department Physik, Universität Siegen, Siegen; Germany.
- ¹⁴¹Department of Physics, Simon Fraser University, Burnaby BC; Canada.
- ¹⁴²SLAC National Accelerator Laboratory, Stanford CA; United States of America.
- ¹⁴³Department of Physics, Royal Institute of Technology, Stockholm; Sweden.
- ¹⁴⁴Departments of Physics and Astronomy, Stony Brook University, Stony Brook NY; United States of America.
- ¹⁴⁵Department of Physics and Astronomy, University of Sussex, Brighton; United Kingdom.
- ¹⁴⁶School of Physics, University of Sydney, Sydney; Australia.
- ¹⁴⁷Institute of Physics, Academia Sinica, Taipei; Taiwan.
- ¹⁴⁸^(a)E. Andronikashvili Institute of Physics, Iv. Javakhishvili Tbilisi State University, Tbilisi;^(b)High Energy Physics Institute, Tbilisi State University, Tbilisi;^(c)University of Georgia, Tbilisi; Georgia.

- ¹⁴⁹Department of Physics, Technion, Israel Institute of Technology, Haifa; Israel.
- ¹⁵⁰Raymond and Beverly Sackler School of Physics and Astronomy, Tel Aviv University, Tel Aviv; Israel.
- ¹⁵¹Department of Physics, Aristotle University of Thessaloniki, Thessaloniki; Greece.
- ¹⁵²International Center for Elementary Particle Physics and Department of Physics, University of Tokyo, Tokyo; Japan.
- ¹⁵³Department of Physics, Tokyo Institute of Technology, Tokyo; Japan.
- ¹⁵⁴Department of Physics, University of Toronto, Toronto ON; Canada.
- ¹⁵⁵(^a) TRIUMF, Vancouver BC; (^b) Department of Physics and Astronomy, York University, Toronto ON; Canada.
- ¹⁵⁶Division of Physics and Tomonaga Center for the History of the Universe, Faculty of Pure and Applied Sciences, University of Tsukuba, Tsukuba; Japan.
- ¹⁵⁷Department of Physics and Astronomy, Tufts University, Medford MA; United States of America.
- ¹⁵⁸United Arab Emirates University, Al Ain; United Arab Emirates.
- ¹⁵⁹Department of Physics and Astronomy, University of California Irvine, Irvine CA; United States of America.
- ¹⁶⁰Department of Physics and Astronomy, University of Uppsala, Uppsala; Sweden.
- ¹⁶¹Department of Physics, University of Illinois, Urbana IL; United States of America.
- ¹⁶²Instituto de Física Corpuscular (IFIC), Centro Mixto Universidad de Valencia - CSIC, Valencia; Spain.
- ¹⁶³Department of Physics, University of British Columbia, Vancouver BC; Canada.
- ¹⁶⁴Department of Physics and Astronomy, University of Victoria, Victoria BC; Canada.
- ¹⁶⁵Fakultät für Physik und Astronomie, Julius-Maximilians-Universität Würzburg, Würzburg; Germany.
- ¹⁶⁶Department of Physics, University of Warwick, Coventry; United Kingdom.
- ¹⁶⁷Waseda University, Tokyo; Japan.
- ¹⁶⁸Department of Particle Physics and Astrophysics, Weizmann Institute of Science, Rehovot; Israel.
- ¹⁶⁹Department of Physics, University of Wisconsin, Madison WI; United States of America.
- ¹⁷⁰Fakultät für Mathematik und Naturwissenschaften, Fachgruppe Physik, Bergische Universität Wuppertal, Wuppertal; Germany.
- ¹⁷¹Department of Physics, Yale University, New Haven CT; United States of America.
- ^a Also Affiliated with an institute covered by a cooperation agreement with CERN.
- ^b Also at An-Najah National University, Nablus; Palestine.
- ^c Also at Borough of Manhattan Community College, City University of New York, New York NY; United States of America.
- ^d Also at Bruno Kessler Foundation, Trento; Italy.
- ^e Also at Center for High Energy Physics, Peking University; China.
- ^f Also at Center for Interdisciplinary Research and Innovation (CIRI-AUTH), Thessaloniki ; Greece.
- ^g Also at Centro Studi e Ricerche Enrico Fermi; Italy.
- ^h Also at CERN, Geneva; Switzerland.
- ⁱ Also at Département de Physique Nucléaire et Corpusculaire, Université de Genève, Genève; Switzerland.
- ^j Also at Departament de Física de la Universitat Autònoma de Barcelona, Barcelona; Spain.
- ^k Also at Department of Financial and Management Engineering, University of the Aegean, Chios; Greece.
- ^l Also at Department of Physics and Astronomy, Michigan State University, East Lansing MI; United States of America.
- ^m Also at Department of Physics and Astronomy, University of Louisville, Louisville, KY; United States of America.
- ⁿ Also at Department of Physics, Ben Gurion University of the Negev, Beer Sheva; Israel.
- ^o Also at Department of Physics, California State University, East Bay; United States of America.
- ^p Also at Department of Physics, California State University, Sacramento; United States of America.

- ^q Also at Department of Physics, King's College London, London; United Kingdom.
- ^r Also at Department of Physics, Stanford University, Stanford CA; United States of America.
- ^s Also at Department of Physics, University of Fribourg, Fribourg; Switzerland.
- ^t Also at Department of Physics, University of Thessaly; Greece.
- ^u Also at Department of Physics, Westmont College, Santa Barbara; United States of America.
- ^v Also at Hellenic Open University, Patras; Greece.
- ^w Also at Institutio Catalana de Recerca i Estudis Avancats, ICREA, Barcelona; Spain.
- ^x Also at Institut für Experimentalphysik, Universität Hamburg, Hamburg; Germany.
- ^y Also at Institute for Nuclear Research and Nuclear Energy (INRNE) of the Bulgarian Academy of Sciences, Sofia; Bulgaria.
- ^z Also at Institute of Particle Physics (IPP); Canada.
- ^{aa} Also at Institute of Physics and Technology, Ulaanbaatar; Mongolia.
- ^{ab} Also at Institute of Physics, Azerbaijan Academy of Sciences, Baku; Azerbaijan.
- ^{ac} Also at Institute of Theoretical Physics, Ilia State University, Tbilisi; Georgia.
- ^{ad} Also at L2IT, Université de Toulouse, CNRS/IN2P3, UPS, Toulouse; France.
- ^{ae} Also at Lawrence Livermore National Laboratory, Livermore; United States of America.
- ^{af} Also at National Institute of Physics, University of the Philippines Diliman (Philippines); Philippines.
- ^{ag} Also at RWTH Aachen University, III. Physikalisches Institut A, Aachen; Germany.
- ^{ah} Also at Technical University of Munich, Munich; Germany.
- ^{ai} Also at The Collaborative Innovation Center of Quantum Matter (CICQM), Beijing; China.
- ^{aj} Also at TRIUMF, Vancouver BC; Canada.
- ^{ak} Also at Università di Napoli Parthenope, Napoli; Italy.
- ^{al} Also at University of Chinese Academy of Sciences (UCAS), Beijing; China.
- ^{am} Also at University of Colorado Boulder, Department of Physics, Colorado; United States of America.
- ^{an} Also at Washington College, Maryland; United States of America.
- ^{ao} Also at Yeditepe University, Physics Department, Istanbul; Türkiye.
- * Deceased